

FORCED CONVECTION HEAT TRANSFER TO A TWO-PHASE
MIXTURE OF WATER AND STEAM IN A HELICAL COIL

By

BERRY CRAIN, JR.

Bachelor of Science
Mississippi State University
State College, Mississippi
1963

Master of Science
Oklahoma State University
Stillwater, Oklahoma
1965

Submitted to the Faculty of the Graduate College
of the Oklahoma State University
in partial fulfillment of the requirements
for the Degree of
DOCTOR OF PHILOSOPHY
December 28, 1973

THESIS
1973D
C887f
cop. 2

© 1975

BERRY CRAIN, JR.

ALL RIGHTS RESERVED

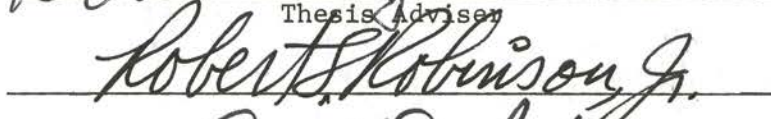
MAY 6 1975

FORCED CONVECTION HEAT TRANSFER TO A TWO-PHASE
MIXTURE OF WATER AND STEAM IN A HELICAL COIL

Thesis Approved:



Thesis Adviser









Dean of the Graduate School

907119

PREFACE

Forced convection heat transfer to high-quality two-phase mixtures in helically coiled tubes was studied. Circumferential average and local heat transfer coefficients were correlated as a function of the Lockhart-Martinelli parameter. A visual flow study and a study of system stability were also performed.

The author is deeply indebted to Dr. Kenneth J. Bell for his guidance and many helpful suggestions. The encouragement offered by members of the Advisory Committee is also acknowledged.

Gratitude is expressed for the financial support provided by Oklahoma State University and by the National Aeronautics and Space Administration during the period in which the author was a NASA Trainee.

The sacrifices and encouragement of my wife, Diane, were instrumental in making this undertaking possible.

TABLE OF CONTENTS

Chapter	Page
I. INTRODUCTION	1
II. LITERATURE SURVEY	4
Single-Phase Heat Transfer in Curved Channels	4
Two-Phase Heat Transfer in Curved Channels	6
Related Studies	9
III. EXPERIMENTAL APPARATUS	11
The Coils	11
Temperature Measurement Devices	14
Auxiliary Equipment	17
IV. EXPERIMENTAL PROCEDURE	20
Calibration of Thermocouples	20
Calibration of Coil Heat Loss	20
Rotameter Calibration	21
Execution of Single-Phase Runs	22
Execution of Two-Phase Runs	22
V. EXPERIMENTAL RESULTS	24
Single-Phase Heat Transfer	24
Two-Phase Heat Transfer	30
Two-Phase Pressure Drop	57
Stability	59
VI. CORRELATION AND DISCUSSION OF RESULTS	64
VII. CONCLUSIONS AND RECOMMENDATIONS	80
SELECTED BIBLIOGRAPHY	82
APPENDIX A - NUMERICAL SOLUTION OF WALL TEMPERATURE GRADIENT FOR A COILED TUBE WITH INTERNAL HEAT GENERATION IN THE WALL	85
Heat Balance on Incremental Element	87
Heat Conduction Distances and Areas for Adjacent Elements	92

Chapter	Page
Distance and Area for Electrical Conduction	95
Results of Solution	96
APPENDIX B - VISUAL FLOW OBSERVATIONS	100
APPENDIX C - SAMPLE CALCULATIONS	105
APPENDIX D - HEAT TRANSFER DATA FOR SMALL COIL	118
APPENDIX E - HEAT TRANSFER DATA FOR LARGE COIL	139
APPENDIX F - ERROR ANALYSIS	145
APPENDIX G - CALIBRATION OF THERMOCOUPLES, ROTAMETERS, AND COIL HEAT LOSS	149
NOMENCLATURE	156

LIST OF TABLES

Table	Page
I. Coil Dimensions	13
II. Placement of Thermocouples	15
III. Measured and Calculated Heat Transfer Coefficients	28
IV. Experimental Conditions for Two-Phase Runs	31
V. Local Conditions for Secondary Flow Effect	57
VI. Two-Phase Pressure Drop	58
VII. Local Conditions for Oscillatory Behavior	62
VIII. Variations in Outside Diameter of the Coils	87
IX. Raw Data for Run 109	106
X. Run 101, Single-Phase, Laminar Flow	119
XI. Run 102, Single-Phase, Laminar Flow	120
XII. Run 103, Single-Phase, Turbulent Flow	121
XIII. Run 104, Two-Phase	122
XIV. Run 105, Two-Phase	123
XV. Run 106, Two-Phase	124
XVI. Run 107, Two-Phase	125
XVII. Run 108, Two-Phase	126
XVIII. Run 109, Two-Phase	127
XIX. Run 110, Two-Phase	128
XX. Run 111, Two-Phase	129
XXI. Run 113, Two-Phase	130
XXII. Run 114, Two-Phase	131

Table	Page
XXIII. Run 116, Two Phase	132
XXIV. Run 117, Two-Phase	133
XXV. Run 118, Two-Phase	134
XXVI. Run 119, Two-Phase	135
XXVII. Run 120, Two-Phase	136
XXVIII. Run 121, Two-Phase	137
XXIX. Run 122, Two-Phase	138
XXX. Run 201, Two-Phase	140
XXXI. Run 202, Two-Phase	141
XXXII. Run 203, Two-Phase	142
XXXIII. Run 205, Two-Phase	143
XXXIV. Run 206, Two-Phase	144
XXXV. Calibration of Thermocouples for Small Coil	150
XXXVI. Calibration of Thermocouples for Large Coil	151
XXXVII. Calibration of Rotameter No. 3	152
XXXVIII. Calibration of Rotameter No. 4	153
XXXIX. Calibration of Heat Loss for Small Coil	154
XL. Calibration of Heat Loss for Large Coil	155

LIST OF FIGURES

Figure	Page
1. Secondary Flow in a Coil	3
2. Schematic Diagram of Experimental Apparatus	12
3. Circumferential Location of Thermocouples at Longitudinal Stations 1, 3, 4, 5, 6, 7, 8, 10	16
4. Circumferential Location of Thermocouples at Longitudinal Stations 2 and 9	16
5. Single-Phase Heat Transfer, Small Coil, Run 101	25
6. Single-Phase Heat Transfer, Small Coil, Run 102	26
7. Single-Phase Heat Transfer, Small Coil, Run 103	29
8. Two-Phase Heat Transfer, Small Coil, Run 104	32
9. Two-Phase Heat Transfer, Small Coil, Run 105	33
10. Two-Phase Heat Transfer, Small Coil, Run 106	34
11. Two-Phase Heat Transfer, Small Coil, Run 107	35
12. Two-Phase Heat Transfer, Small Coil, Run 108	36
13. Two-Phase Heat Transfer, Small Coil, Run 109	37
14. Two-Phase Heat Transfer, Small Coil, Run 110	38
15. Two-Phase Heat Transfer, Small Coil, Run 111	39
16. Two-Phase Heat Transfer, Small Coil, Run 113	40
17. Two-Phase Heat Transfer, Small Coil, Run 114	41
18. Two-Phase Heat Transfer, Small Coil, Run 116	42
19. Two-Phase Heat Transfer, Small Coil, Run 117	43
20. Two-Phase Heat Transfer, Small Coil, Run 118	44

Figure	Page
21. Two-Phase Heat Transfer, Small Coil, Run 119	45
22. Two-Phase Heat Transfer, Small Coil, Run 120	46
23. Two-Phase Heat Transfer, Small Coil, Run 121	47
24. Two-Phase Heat Transfer, Small Coil, Run 122	48
25. Two-Phase Heat Transfer, Large Coil, Run 201	49
26. Two-Phase Heat Transfer, Large Coil, Run 202	50
27. Two-Phase Heat Transfer, Large Coil, Run 203	51
28. Two-Phase Heat Transfer, Large Coil, Run 205	52
29. Two-Phase Heat Transfer, Large Coil, Run 206	53
30. Oscillations	60
31. Comparison of Stability of Small and Large Coils	63
32. Correlation of Circumferential Average Heat Transfer Coefficients, Small Coil	67
33. Correlation of Local Heat Transfer Coefficients, 0° Position, Small Coil	68
34. Correlation of Local Heat Transfer Coefficients, 90° Position, Small Coil	69
35. Correlation of Local Heat Transfer Coefficients, 180° Position, Small Coil	70
36. Correlation of Local Heat Transfer Coefficients, 270° Position, Small Coil	71
37. Correlation of Circumferential Average Heat Transfer Coefficients, Large Coil	73
38. Correlation of Local Heat Transfer Coefficients, 0° Position, Large Coil	74
39. Correlation of Local Heat Transfer Coefficients, 90° Position, Large Coil	75
40. Correlation of Local Heat Transfer Coefficients, 180° Position, Large Coil	76
41. Correlation of Local Heat Transfer Coefficients, 270° Position, Large Coil	77

Figure	Page
42. Comparison of Results With Results of Owhadi and de La Harpe, et al.	78
43. Effect of Bending on Tube Wall	88
44. Tube Cross-Sections	90
45. Angular Position of Incremental Element	93
46. Temperature Profiles for Run 104, Station 2	97
47. Temperature Profiles for Run 117, Station 9	98
48. Temperature Profiles for Run 118, Station 10	99
49. Visual Flow Apparatus	102
50. Flow Pattern on Inside Tube Wall	102
51. Flow Pattern at Higher Air Velocity and Liquid Rate	104
52. Close-Up of Outer Tube Wall	104

CHAPTER I

INTRODUCTION

The effect of helical geometry on single-phase convection heat transfer has been studied by investigators since 1925, using both analytical and experimental techniques. However, only a limited number of studies on two-phase forced convection heat transfer in helical coils has been reported. In these, there is considerable scatter in the experimental data points for the high quality regime (greater than 50% steam by weight). The purpose of the study reported herein was to provide insight on the mechanism of two-phase forced convection heat transfer in a helical coil and to obtain additional, more accurate experimental data in the high quality regime.

In a straight-tube boiling system with net steam production, several different flow regimes may exist within the tube. For a sub-cooled water feed with superheated steam effluent the following flow regimes are present:

- 1) single-phase water
- 2) bubble or froth flow
- 3) slug flow
- 4) annular flow
- 5) mist flow, and
- 6) single-phase steam.

However, for steam qualities of greater than 50%, the void fraction

(vapor volume fraction) is generally well above 90% and only the mist and the annular-mist flow regimes are possible. These flow regimes are characterized by small liquid droplets which are carried along by the vapor flow.

Coil geometry can modify the mist flow patterns that would exist in a straight tube. The radial velocity component produced by the centrifugal force results in a secondary flow pattern superimposed on the main flow pattern (See Figure 1). Liquid particles are flung onto the outer wall of the tube and spiral back to the inner wall as they move along the tube, due to drag forces exerted by the secondary flow pattern in the vapor core. From this point they are re-entrained by the main stream and flung onto the outer wall again. Thus the secondary flow, by causing the mist to form a continuous liquid phase on the heated surface, causes the heat to be transferred from the wall directly to the liquid and thus improves the heat transfer.

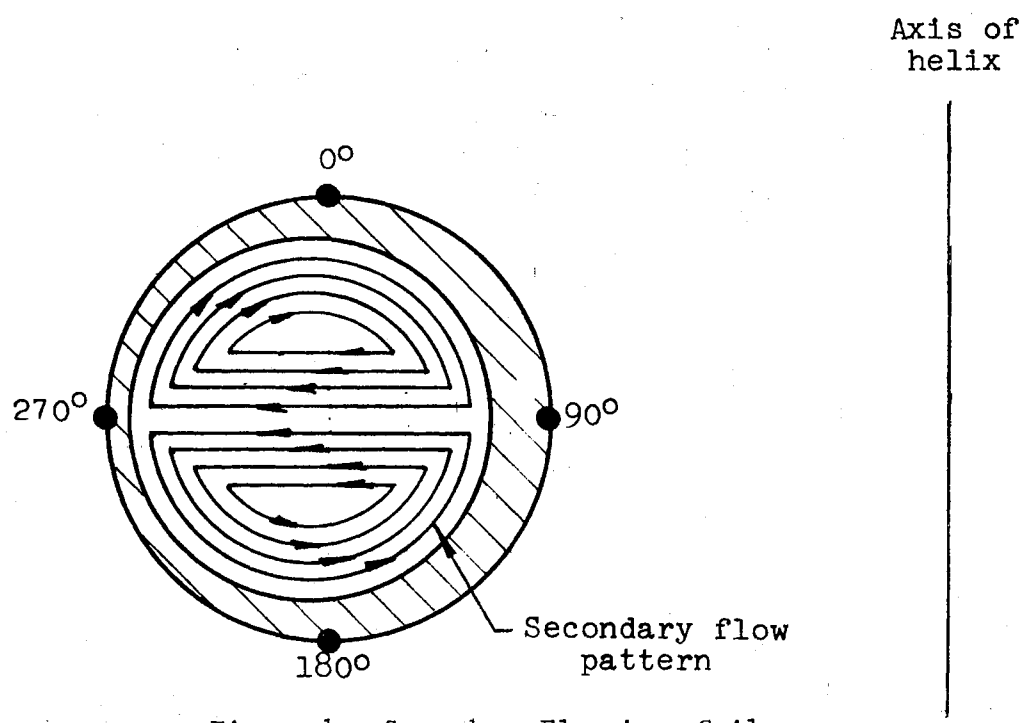


Figure 1. Secondary Flow in a Coil

CHAPTER II

LITERATURE SURVEY

Single-Phase Heat Transfer in Curved Channels

Kreith (13) performed an analytical study of the influences of curvature on heat transfer to incompressible fluids. Using the analogy between momentum transfer and heat transfer and experimental results of wall shear stress and velocity distribution obtained by Wattendorf (30), Nusselt numbers were calculated for concave and convex heating surfaces. The calculations were performed for Reynolds numbers ranging from 0.01 to 100, and for radii of curvature ranging from 0.12 to 1.2 feet. It was found that the heat transfer coefficient for a heating surface with a concave curvature is considerably higher than for a heating surface with a convex curvature under similar flow conditions.

An experimental investigation of heat transfer in coiled tubes during laminar and turbulent flow was performed by Seban and McLaughlin (29). The authors measured heat transfer coefficients in coiled tubes with ratios of coil to tube diameter of 17 and 104 for Reynolds numbers from 12 to 6.5×10^4 . Circumferential average heat transfer coefficients were correlated with Reynolds number for both laminar and turbulent flow.

Rogers and Mayhew (27) experimentally determined heat transfer coefficients for turbulent flow in helically coiled tubes. Three

coils with ratios of coil to tube diameter of 10.8, 13.3, and 20.1 were heated in a steam jacket with water flowing in the coil. The range of Reynolds numbers covered was 3×10^3 to 5×10^4 . The heat transfer coefficients were correlated with Reynolds number.

Mori and Nakayama (20, 21) conducted theoretical and experimental studies of laminar and turbulent flow in a curved pipe. Laminar flow results showed that the Nusselt number could be correlated as a function of the Dean number and the Prandtl number. Nusselt numbers calculated from experimental data using air as a test fluid agreed with theoretical predictions. Turbulent flow Nusselt numbers were also correlated with the Dean and Prandtl numbers and comparison of theoretical and experimental results again showed good agreement.

An experimental investigation of heat transfer to aqueous solutions of glycerol in laminar flow in helical and spiral coils was performed by Kubair and Kuloor (14). The authors obtained experimental measurements over a Reynolds number range of 60 through 6000. Nusselt numbers were correlated as a function of the Graetz number and of the ratio of the tubing inside diameter to the coil diameter. The maximum deviation between observed and calculated values was ± 10 percent and the average deviation was less than 5 percent. An analogy between momentum and heat transfer was performed using equations modified for coil geometry. The modified equations satisfactorily predicted heat transfer rates from rates of momentum transfer.

Miropolskiy, et al (17) carried out an experimental investigation of heat transfer and pressure drop in the heating and cooling of water flowing in coils of various dimensions. The authors found that the heat transfer coefficients increase during heating and decrease during

cooling as the ratio of the tube diameter to the coil diameter increases. They also found that the length of the preliminary heat transfer section in a coil, beyond which the heat transfer coefficients reach stable values, is approximately proportional to the diameter of curvature of the coil and to the square root of the tube inside diameter.

David et al. (9) studied the effect of secondary fluid motion on laminar flow heat transfer in helically coiled tubes. The authors obtained a numerical solution of the differential equations for heat transport for the laminar flow regime and for Dean numbers above 100. Experimental data, obtained with five different test fluids, showed that the Nusselt number could be correlated as a function of the Dean and Prandtl numbers.

Two-Phase Heat Transfer in Curved Channels

An experimental study by Hendricks and Simon (10) was one of the first investigations of two-phase heat transfer in curved channels. The authors collected data and calculated heat transfer coefficients for forced convection heat transfer to subcritical (two-phase), supercritical, and gaseous hydrogen flowing through tube bends. The bend angle of the tubes ranged from 26 to 75 degrees and the radii of curvature from 2 to 7.5 inches. System pressures were varied from 100 to 600 psia and the heat flux range investigated was from 5.18×10^5 to 1.81×10^6 Btu/(hr) (sq. ft.). The authors concluded that heat transfer coefficients on the concave surface (outside of curve as seen by fluid) could be as much as three times greater than those on the convex

surface. The coefficients on the convex surface generally agreed with straight tube data taken at similar conditions.

Carver et al. (5) investigated the effect of curvature of a tube on the departure from nucleate boiling (DNB). Experiments were performed in helical coils with boiling water at 2600 psia. The coils were 16 and 65 inches in radius and had a nominal inside diameter of 0.42 inch. The heat flux was varied from 5.0×10^4 to 2.2×10^5 Btu/(hr)(sq. ft.). The authors concluded that (1) DNB in coiled tubes occurs at different steam qualities for different positions around the circumference of the tube, whereas, for a straight vertical tube, DNB occurs around the complete circumference of the tube at one steam quality; (2) coiled tubes have higher average DNB steam qualities than do straight vertical tubes; (3) surface temperature fluctuations at the DNB transition point are much lower than those in a straight vertical tube; (4) DNB steam quality was higher for the small coil than for the large coil; and (5) an increase in mass velocity resulted in an increase in average DNB steam quality.

Yudovich (32) performed an experimental study on the boiling of water and n-hexane in a helical coil heated in a steam bath. The heated section was fabricated by winding a 1/2-inch OD copper tube into a helix seven inches in diameter. At low flows in the range of 3380 to 11,600 lb/(hr)(sq. ft.) all of the feed was vaporized and the temperature of the superheated vapor leaving the coil increased with flow rate. At higher flows only partial vaporization of the feed occurred and the coil average heat flux increased from 4660 Btu/(hr)(sq. ft.) at 2.28×10^4 lb/(hr)(sq. ft.) to 6400 Btu/(hr)(sq. ft.) at 4.17×10^4

lb/(hr)(sq. ft.) and then decreased to 4360 Btu/(hr)(sq. ft.) at 7.52×10^4 lb/(hr)(sq. ft.).

Owhadi et al. (2, 22, 23, 24) investigated forced convection boiling inside helically coiled tubes. Owhadi (22) studied two-phase heat transfer at pressures near atmospheric in two helical coils 9.86 and 20.5 inches in diameter. The tubing inside diameter was 0.492 inch. The range of flows investigated was 5.83×10^4 to 2.32×10^5 lb/(hr)(sq. ft.) and the heat flux range was 1.9×10^4 to 8.1×10^4 Btu/(hr)(sq. ft.). The exit quality varied from 1.4 percent vapor to 50 °F. superheated steam. Temperature measurements were made at four points around the tube at each of nine stations along the tube. The circumferential average heat transfer coefficient was correlated as a function of the Lockhart-Martinelli parameter. The experimental results were also reported elsewhere (23, 24) and were later recorrelated on a local basis rather than on a circumferential average basis (2).

Miropolskiy et al. (19) studied heat transfer to single-phase water and steam and to two-phase water-steam mixtures in 90° and 360° pipe bends. The flow rate was varied from 7.37×10^4 to 1.47×10^6 lb/(hr)(sq. ft.) and the pressure range was 305 to 4300 psia. The authors found that the critical heat flux in bends is less than in straight pipes at low qualities and is greater than in straight pipes at high qualities.

An experimental study of boiling heat transfer and pressure drop of liquid helium-I under forced circulation in a helically coiled tube was performed by de La Harpe et al. (7). The test section was a helix 4.33 inches in diameter formed from a piece of 0.118 inch ID, 0.138 inch OD monel tubing sixteen feet long. Pressures were near

atmospheric and the maximum flow and heat flux were 94,500 lb/(hr) (sq. ft.) and 190 Btu/(hr)(sq. ft.), respectively. The authors successfully correlated the heat transfer data with the Martinelli-Nelson correlating parameter, X_{tt} (16).

A recent study by Miropolskiy and Pikus (18) reports critical heat fluxes and heat transfer coefficients for film boiling of water in electrically heated pipe bends. The range of pressures investigated was 1420-3120 psia and the flow was varied from 7.37×10^4 to 1.47×10^6 lb/(hr)(sq. ft.). It was found that the heat transfer coefficients for the pipe bends were higher than heat transfer coefficients for straight tubes under similar conditions, apparently due to the effect of secondary flow on transfer of liquid droplets to the tube wall.

Related Studies

Rippel et al. (26) performed an experimental investigation of pressure drop, holdup, and axial mixing for two-phase flow in a helical coil. Experimental data were obtained for flow of air-water, helium-water, Freon 12-water, and air-2-propanol. The helical coil was constructed by winding 1/2-inch OD 18 gauge tubing around a cylinder eight inches in diameter. The length of tubing was 88.3 feet. Liquid holdup was measured by trapping and by use of a tracer material. The two-phase pressure drop was correlated successfully using the Lockhart-Martinelli method. The authors found that the experimental liquid holdups were less than holdups for a straight horizontal pipe, a fact that may be caused by the secondary flow pattern of a helical coil.

A study by Banerjee et al. (1) reported experimental determination of the effects of tube diameter, coil diameter, coil pitch, and liquid

viscosity on pressure drop and liquid holdup for two-phase flow in helically coiled tubes. Ten different coils were used. Nine of these were made of 5/8-inch ID tubing and one of two-inch ID tubing. Coil diameters of six, nine, and twelve inches and coil pitches of two, five, and eight degrees were investigated. The effect of liquid viscosity was studied using air-water and air-oil mixtures. The authors found that the pressure drop and holdup data were suitably correlated by the Lockhart-Martinelli method. They found no effect of coil pitch on pressure drop and holdup for the range of pitches investigated. High-speed movies of the flow patterns in the coils showed that, for certain combinations of gas and liquid flow rate, the liquid formed a film on the tube wall closest to the coil axis. They termed this behavior "film inversion."

CHAPTER III

EXPERIMENTAL APPARATUS

The apparatus used in these experiments consisted of a feed stream preparation and metering system, the test section in which heat was generated and transferred to the test fluid, a power generation system, and instrumentation. The system is diagrammed schematically in Figure 2.

The Coils

Experiments were performed using two different helical coils, both of which were made from Type 304 stainless steel seamless tubing. The tubing before coiling was 5/8-inch OD with a wall thickness of 0.065 inch. The helix diameters of the small coil and the large coil were 9.99 and 20.64 inches respectively. The heated length of tubing in both coils was 10 feet and the axis of the helix was vertical in both cases. Some flattening of the tubing occurred during formation of the coils. The major and minor diameters of the tubing after bending as well as the other dimensions are shown in Table I.

Heat was generated in the coils with a DC current obtained from a Lincolnweld SA-750 electric welder. The current was introduced into the coils through electrodes made of copper bars silver-soldered to the tubing. Electrical insulation of the coils from the rest of the system was provided by a short length of silicone rubber tubing at each end of

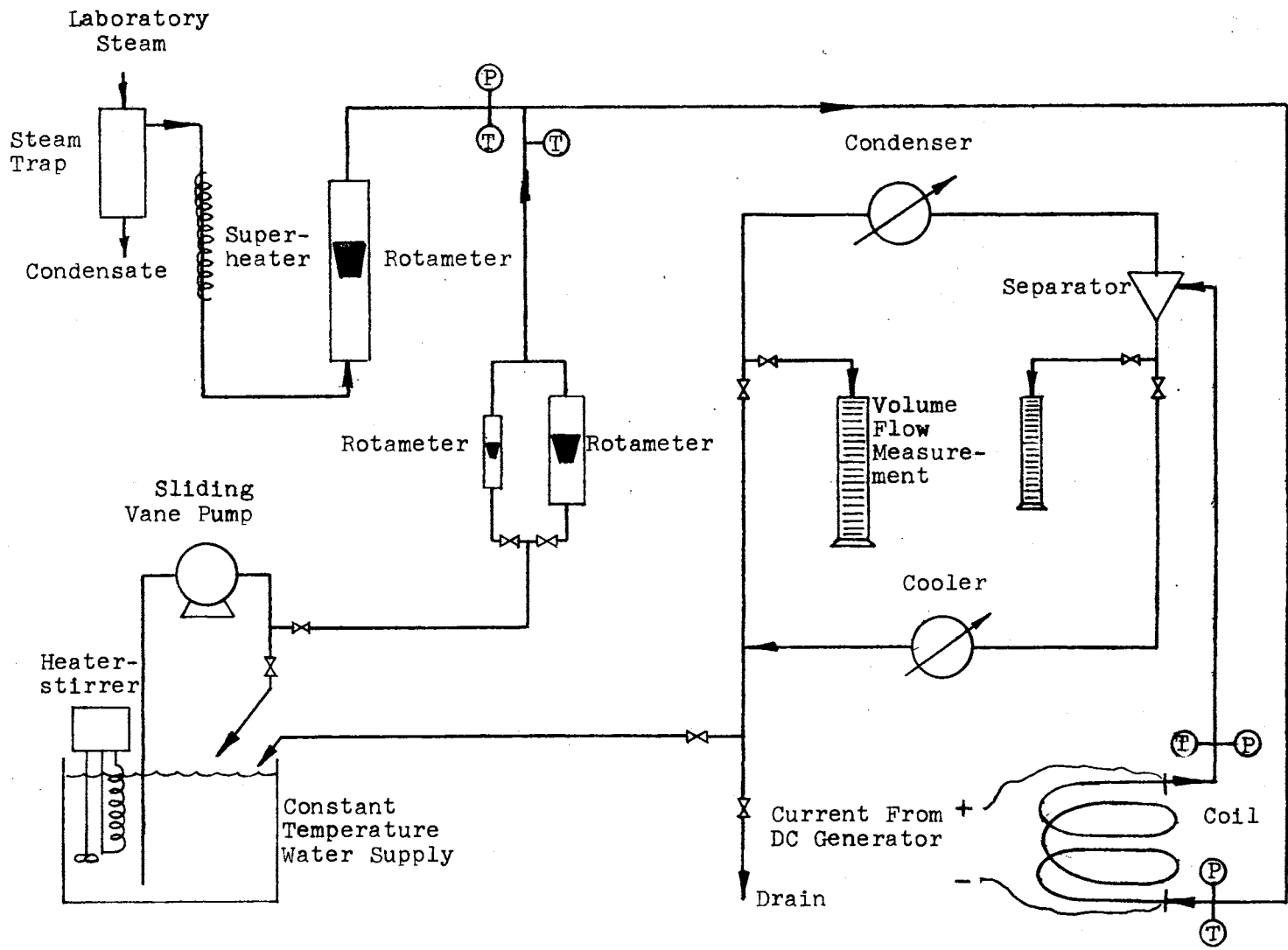


Figure 2. Schematic Diagram of Experimental Apparatus

the coil. The coils were thermally insulated by wrapping them with several layers of bonded fiberglass insulation.

TABLE I
COIL DIMENSIONS

Dimension	Small Coil	Large Coil
Coil diameter, inches center-to-center	9.99	20.64
Straight tube outside diameter, inch	0.625	0.625
Straight tube inside diameter, inch	0.495	0.495
Coiled tube major outside diameter, inch	0.636	0.630
Coiled tube minor outside diameter, inch	0.616	0.625
Distance between turns, inches center-to-center	4.26	4.48
Ratio of coil diameter to straight tube inside diameter	20.2	41.7
Heated length of coil, feet	10.0	10.0
Length of straight tube before inlet electrode, inches	12.0	11.0
Length of straight tube after exit electrode, inches	3.0	4.0
Approximate number of turns in coil	3.8	1.8

Temperature Measurement Devices

Iron-constantan thermocouples were used to measure the outside wall temperature of the tubing. The thermocouple wires were 30 B and S gauge and fiberglass-insulated. The thermocouples were fastened to the tubing with Sauereisen cement by first applying a very thin spot of cement to the tubing and then cementing the thermocouple bead upon this spot. The thermocouples were then clamped into place with worm clamps to insure good contact with the tube surface in case of loosening of the cement during heating. The thermocouple wires were led along the tube surface for a distance of about two inches to minimize heat conduction through the wire away from the thermocouple junction.

There were ten thermocouple stations along the length of the coil. The first thermocouple station was one foot from the inlet electrode and the next eight stations were at intervals of one foot. The tenth station was three inches from the exit electrode and thus nine inches from the ninth thermocouple station. There were four thermocouples at stations 1, 3 through 8, and 10 and eight thermocouples at stations 2 and 9. Placements of the thermocouples on the surfaces of the coils are summarized in Table II.

The circumferential arrangement of the thermocouples at each station are shown in Figures 3 and 4. At the stations where four thermocouples were used the junctions were placed 90 degrees apart, at the top, bottom and both sides of the tube. In the case where eight thermocouples were used the junctions were 45 degrees apart. The numbering system of the thermocouples was as follows: Stations along the coil were numbered from one through ten starting from the coil inlet. Each

thermocouple was numbered individually, thermocouple number one always being at the top of the tube. Where four thermocouples were used, number two was located on the inside of the helix, three at the bottom, and four on the outside of the helix. Where eight thermocouples were used, the thermocouples were numbered in the same direction, number three being at the inside of the helix, five at the bottom, and seven at the outside. Thermocouple number 25, for example, would be located two feet from the inlet electrode and at the bottom of the tube. Thermocouple number 102 would be 9-3/4 feet from the inlet electrode and at the inside of the helix.

TABLE II
PLACEMENT OF THERMOCOUPLES*

Station	No. of Thermocouples	Distance from Inlet Electrode, ft.
1	4	1
2	8	2
3	4	3
4	4	4
5	4	5
6	4	6
7	4	7
8	4	8
9	8	9
10	4	9.75

*Thermocouple placements were identical on small and large coils.

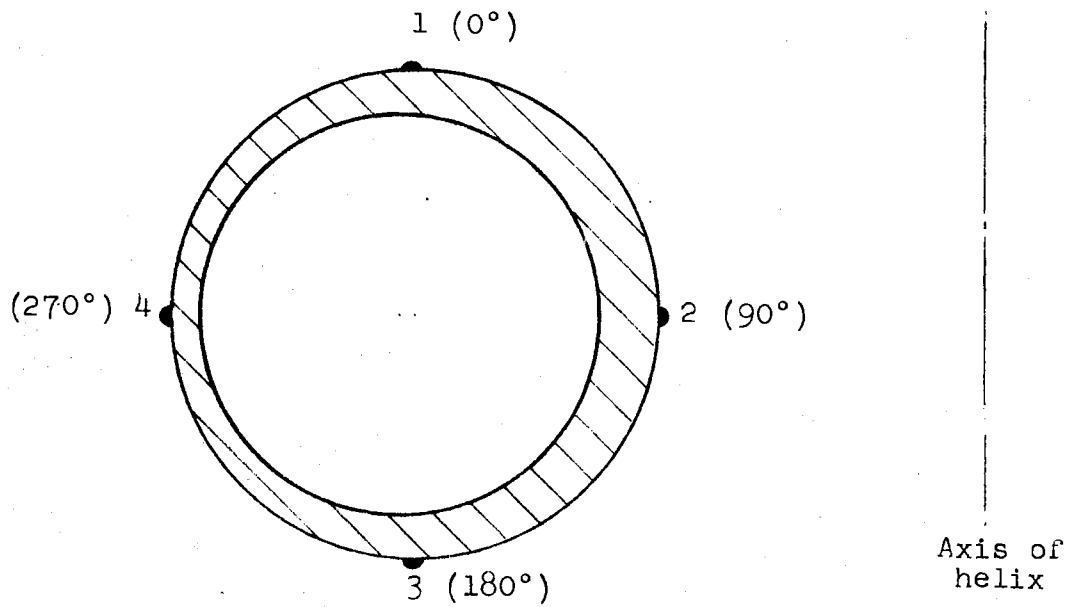


Figure 3. Circumferential Location of Thermocouples at Longitudinal Stations 1, 3, 4, 5, 6, 7, 8, 10

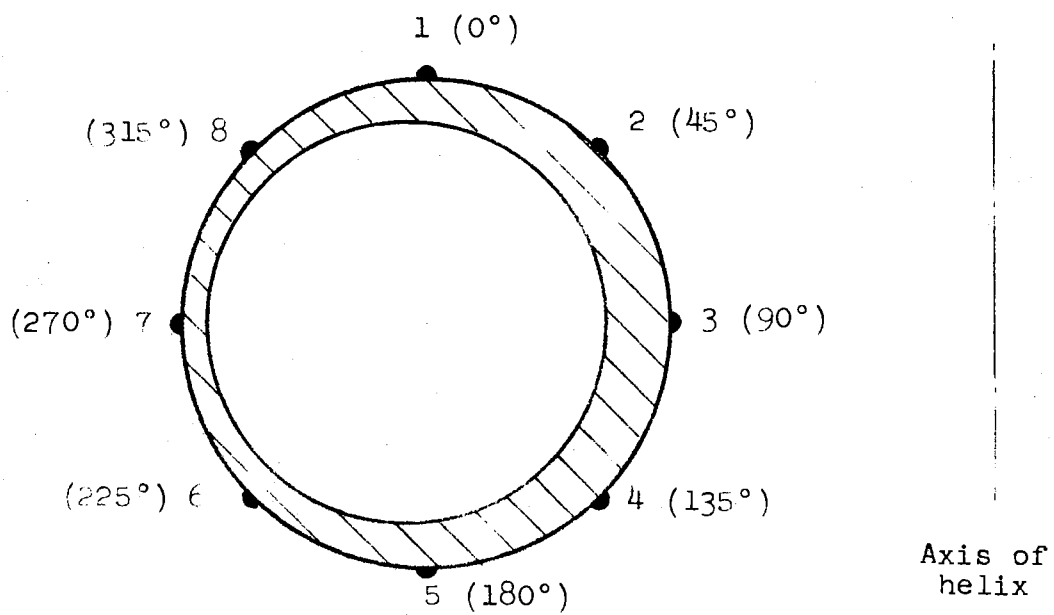


Figure 4. Circumferential Location of Thermocouples at Longitudinal Stations 2 and 9

The outputs of the thermocouples were brought through rotary selector switches to a Leeds and Northrup Model 8687 volt potentiometer. The selector switches were enclosed in a box to insure a uniform temperature at the switches. By use of an auxiliary wiring system, each thermocouple output could be recorded on a Brush Mark 10 single point recorder. Other temperatures in the system, such as those of the test fluid at the coil inlet and outlet, were also read using the same arrangement. An ice bath was used for the reference junction in the above cases.

The pressures at the inlet and outlet of the coil were measured by Bourdon gauges with ranges of 0-30 and 0-10 psig respectively. A strain gauge pressure transducer, Consolidated Electrodynamics Corporation Model 4-316-001, was mounted at the pressure tap at the coil inlet and was used to detect pressure fluctuations. The output from this transducer was periodically recorded on the single point recorder mentioned above. The transducer had a range of 0-50 psig and an output of 0-20 millivolts.

The current in the coil was measured with a Weston Model 931 ammeter having a range of 0-750 amps DC which was placed in parallel with a 50 millivolt shunt. The coil voltage was measured with a Weston Model 931 voltmeter having a range of 0-50 volts DC.

Auxiliary Equipment

Steam was fed into the system from a laboratory supply line. Water was removed from the incoming steam by use of a separator which reversed the steam flow and then filtered the steam through a bed of copper turnings. To insure the complete removal of water, the steam

was passed through a length of copper tubing heated with electrical resistance tape. The use of this heater allowed the steam to be superheated by about 20 °F. The steam flow was passed through a Brooks Model 1110 rotameter which had a maximum capacity of 25.76 SCFM air. This rotameter had a maximum capacity of about 35.0 CFM steam under operating conditions. The rotameter was used only to indicate and control fluctuations in the incoming steam flow. The temperature and pressure of the steam were measured by a thermocouple and Bourdon gage respectively just upstream of the point at which the steam and water flows were mixed.

Distilled water was fed to the system from a constant-temperature bath. Water was circulated through the bath with an Eastern VW-5-A sliding vane pump and the water fed to the system was bled from the circulatory line at a point downstream from the pump. The water flow rate was metered with one of two Fischer and Porter Flowrators, depending upon the magnitude of the flow rate. The temperature of the water was measured with a thermocouple upstream of the point at which the steam and water flows were mixed.

After passing through the coil, the steam and water mixture was separated in a glass cyclone separator which was six inches in diameter at the top. The cyclone was shielded with Lucite to allow visual observation of the separation. The water from the cyclone was cooled in a copper condenser and then flowed to a common collection point. The steam from the cyclone was condensed in a shell and tube exchanger and flowed to the collection point where the total flow was measured by collection of volumetric samples. When a sample was not being

collected, part of the total flow was recirculated to the constant temperature water supply in order to maintain the water level.

CHAPTER IV

EXPERIMENTAL PROCEDURE

Calibration of Thermocouples

The thermocouples in the system were calibrated after they were in place on the coil. Steam was bled through the coil slowly to maintain atmospheric pressure throughout and the thermocouple outputs were measured. A steam bath at atmospheric pressure was used as the reference junction in this calibration. In this way the thermocouple output errors could be read directly. The atmospheric pressure and room temperature were also measured.

To allow the temperature corrections to be adjusted for higher coil temperatures, it was assumed that the error in the thermocouple output was due to conduction through the thermocouple wires to the ambient air. This conduction in turn is proportional to the difference between the coil temperature and the ambient room temperature. Using the calibration data the actual temperature of the thermocouple could be determined. The thermocouple calibration data are shown in Appendix G.

Calibration of Coil Heat Loss

In order to determine the heat loss through the coil insulation during an experimental run a calibration of the heat loss at a known coil temperature had to be performed. Steam was bled slowly through

the coil and the atmospheric pressure and room temperature were measured. The steam flow rate was also measured by collecting the effluent from the coil.

From the calibration data the heat loss rate from the coil at a known temperature differential could be obtained. To calculate the heat loss during an experimental run, the average temperature of each one foot section of the coil was calculated from the corrected thermocouple outputs. The heat loss for each of these sections was then calculated by assuming that this loss is directly proportional to the temperature difference between the coil surface and the ambient room temperature. The total heat loss was obtained by summing the heat losses from each one foot section. The heat loss calibration data is summarized in Appendix G.

Rotameter Calibration

Several attempts were made to obtain a calibration of the rotameter installed on the steam delivery line. However, due to changes in pressure in the rotameter that resulted from the various flow conditions in the coil, no suitable calibration was obtained. Eventually the steam rotameter was used only to indicate fluctuations in the steam flow rate and to provide a visual check of steam conditions, i.e., presence of water in the steam.

Two different water rotameters were used depending on the water flow rate required. The larger rotameter had a maximum flow rate of 3.69 pounds of water per minute. The smaller rotameter had a maximum flow rate of 0.596 pounds of water per minute. The rotameters were calibrated by collecting a known volume of water over a period of time

and measuring the temperature of the water. Since the temperature of the water entering the rotameters was the same for all runs, no temperature correction of the calibration was necessary.

Execution of Single-Phase Runs

Three non-boiling runs with water flowing in the coil were made with the small coil. Two of these runs were under laminar flow conditions at 3.43×10^4 and 6.33×10^4 lb/(hr)(sq. ft.) with Reynolds numbers of approximately 1000 and 2000 respectively. A third run was under turbulent flow conditions with a Reynolds number of approximately 10^4 .

The water flow rate desired through the coil was begun and the heat flux rate was then raised to the desired level. The DC generator required a period of about thirty minutes of running time in order to warm up and maintain a steady output. As soon as the generator output had become steady, the thermocouple emf's were measured on the potentiometer. A period of about ten minutes was required to read all of the thermocouple outputs. Several of the emf's were checked at the end of the measuring period to insure steady conditions. The coil current and potential difference and the room temperature and atmospheric pressure were measured at the beginning and at the end of each run. As soon as the temperature measurements were complete a volume of the coil effluent was collected in order to determine the flow rate in the coil.

Execution of Two-Phase Runs

Experimental runs were performed with the large coil and the small coil in which the test fluid was a mixture of water and steam. Runs

were made encompassing a range of flow rates, heat flux rates, and exit steam qualities. Several runs were performed in which the steam exiting from the coil was superheated.

In order to execute a two-phase run, the steam flow through the coil was first begun and the steam preheater was adjusted to insure that no water was present in the steam. The desired water flow rate was then added to the steam flow and the generator was turned on. After allowing about thirty minutes for the generator to stabilize, the thermocouple emf's were measured on the potentiometer. The coil current and the potential difference and the room temperature and atmospheric pressure were measured at the beginning and end of each run.

After completing the temperature measurements, volume samples of the water and condensed steam streams from the cyclone were taken to determine the total flow rate. The steam rate entering the system was obtained as the difference in the total flow rate and the entering water rate, which was known from the rotameter calibration.

CHAPTER V

EXPERIMENTAL RESULTS

The experiments which were performed deal primarily with heat transfer to high-quality two-phase mixtures of steam and water. However, several single-phase heat transfer runs were executed and pressure drop measurements were taken for all two-phase runs. Stability of the system was also investigated. Results of all of these studies are presented in this chapter.

Single-Phase Heat Transfer

Three single-phase heat transfer runs were made with the small coil. The first two runs were made with water in laminar flow and the third run with water in turbulent flow. The Reynolds number for transition from laminar to turbulent flow in a helical coil may be calculated from the following formula developed by Ito (11):

$$(\text{Re})_{\text{cr}} = 2 \times 10^4 \left(\frac{d}{D}\right)^{0.32} \quad (5-1)$$

The critical Reynolds number for the small coil is 7650. Reynolds numbers for runs 101 and 102 were 1140 and 2100 respectively, both well inside the laminar regime. The Reynolds number for run 103 was 10,800, well into the turbulent regime. Heat transfer coefficients for runs 101 and 102 are shown in Figures 5 and 6. The velocity in run 101 was 0.155 f5/sec. Natural convection effects are evident. The heat

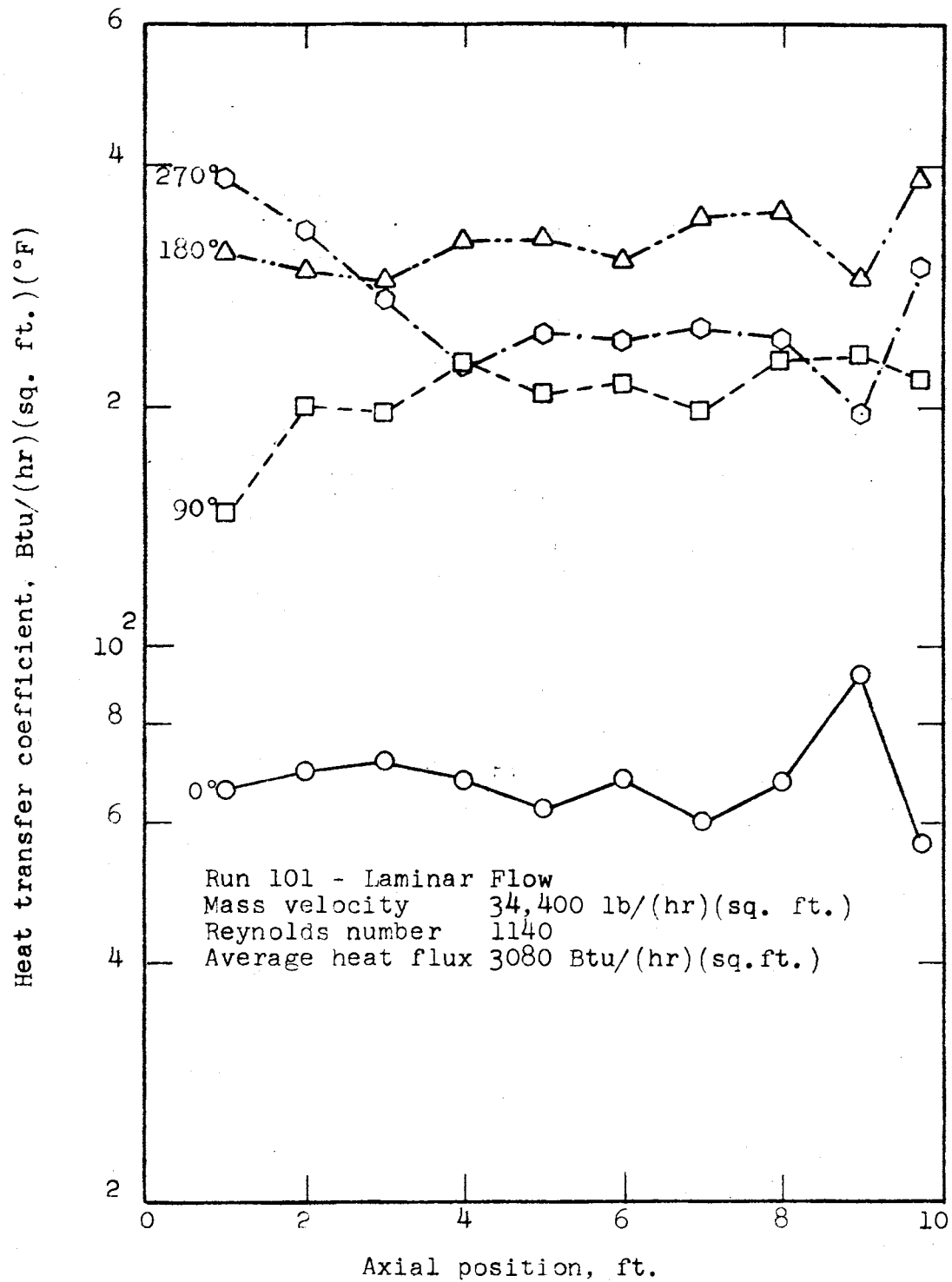


Figure 5. Single-Phase Heat Transfer, Small Coil, Run 101

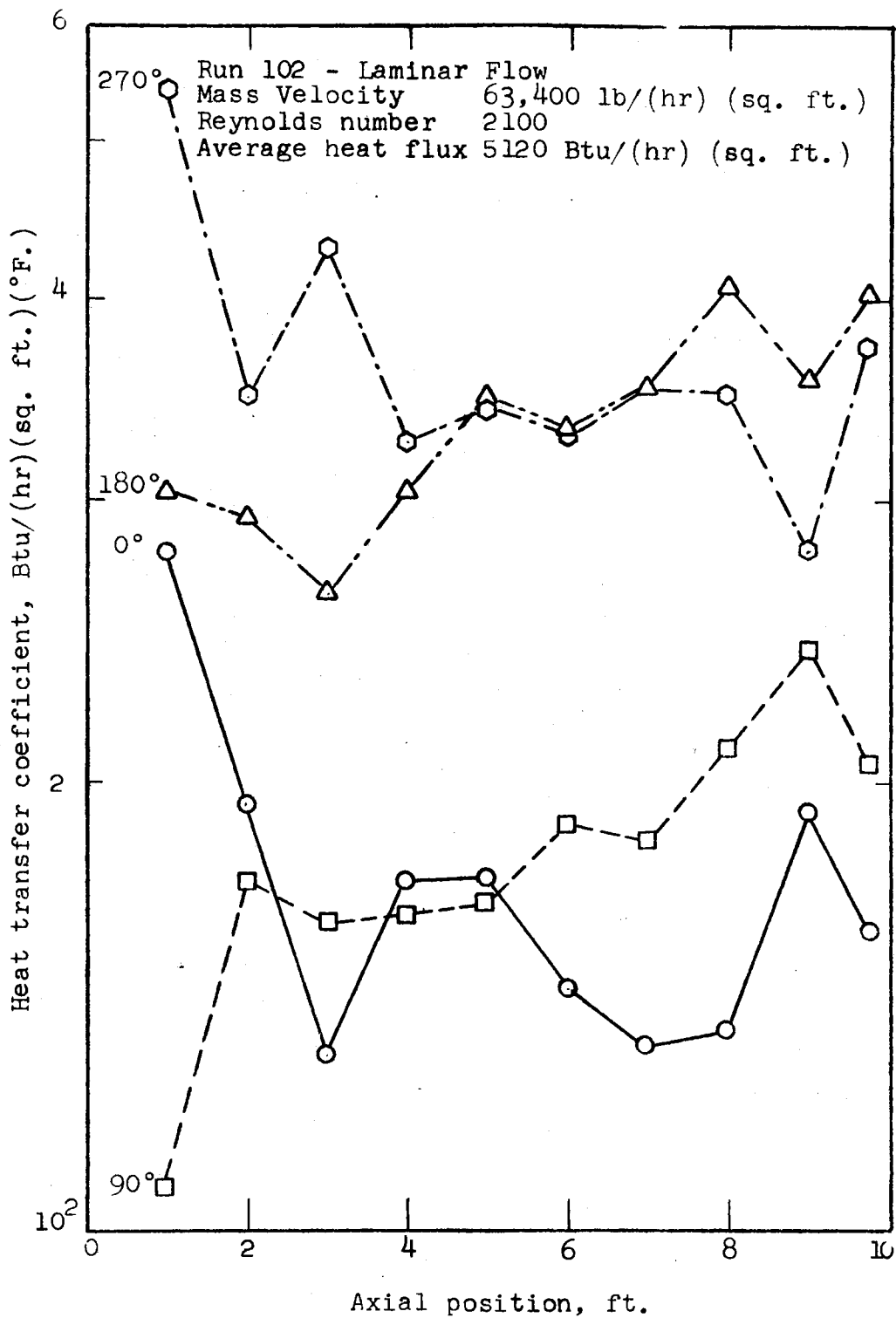


Figure 6. Single-Phase Heat Transfer, Small Coil, Run 102

transfer coefficients at the top of the tube are markedly lower than those at other positions. An entrance effect may be responsible for the relatively high values of the heat transfer coefficients in the outer tube wall near the coil inlet. Wall temperatures are not high enough for subcooled nucleate boiling to occur anywhere in the coil.

The velocity in run 102 was 0.286 ft/sec. Values of the heat transfer coefficients are generally higher than in run 101 due to the higher velocity. Natural convection is again important and its effects are notable.

The average heat transfer coefficients for runs 101 and 102 were compared with heat transfer coefficients calculated from the laminar flow equation of Seban and McLaughlin (29):

$$Nu = 0.13\left(\frac{f}{8}\right)Pr^{1/3}Re^{2/3} \quad (5-2)$$

The friction factor in equation 5-2 is calculated from White's formula (31):

$$\frac{f}{f_s} = \left\{ 1 - \left(1 - \left(\frac{11.6}{Re \left(\frac{d}{D}\right)^{1/2}} \right)^{0.45} \right)^{2.22} \right\}^{-1} \quad (5-3)$$

where

$$f_s = 64/Re \quad (5-4)$$

The average heat transfer coefficients were calculated as the coil average heat flux divided by the average temperature difference between wall and fluid. Measured and calculated values are summarized in Table III. The agreement between values is not good. However, equation 5-2 was developed for Prandtl numbers in the range 100-657 and would not be expected to predict accurate heat transfer coefficients for water.

Heat transfer coefficients for run 103 are shown in Figure 7. As would be expected, the coefficients are markedly higher than those in the laminar flow runs. Heat transfer coefficients at the 90° position are approximately half the coefficients at the other positions on the tube. The average heat transfer coefficient for the coil was compared to a heat transfer coefficient calculated from the Seban-McLaughlin equation (29):

$$\text{Nu} = 0.023 \text{Re}^{0.85} \text{Pr}^{0.4} \left(\frac{d}{D}\right)^{0.1} \quad (5-5)$$

The agreement was excellent, the measured value of the heat transfer coefficient being 759 Btu/(hr)(sq. ft.)(°F) and the calculated value being 739 Btu/(hr)(sq. ft.)(°F).

TABLE III

MEASURED AND CALCULATED HEAT TRANSFER COEFFICIENTS

Run	Reynolds Number	Heat Transfer Coefficient	
		Measured	Calculated
101	1140	185	245
102	2100	234	375

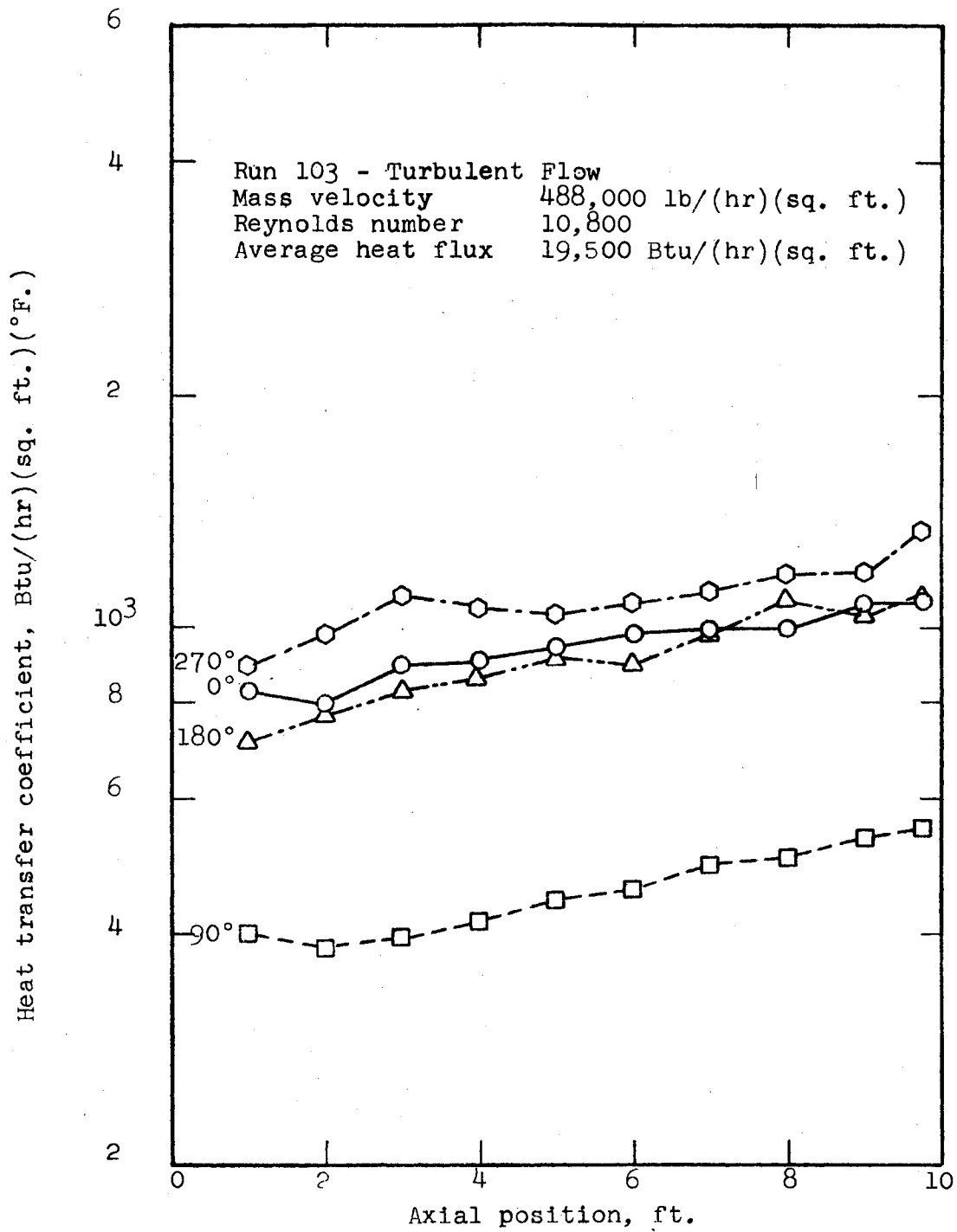


Figure 7. Single-Phase Heat Transfer, Small Coil, Run 103

Two-Phase Heat Transfer

Twenty-two two-phase heat transfer runs were performed. Seventeen of these were performed with the small coil and the remaining five with the large coil. One of the primary aims of this study was to obtain experimental coil heat transfer coefficients in the high quality regime. Inlet qualities were varied from 43.7% to 86.4%. Exit qualities varied from 83.5% to 100% (120 °F. superheated). The range of mass velocities investigated was dictated by equipment limitations. The mass velocity was varied from 33,300 to 91,600 lb/(hr)(sq. ft.). The coil average heat flux was varied from 1900 to 30,500 Btu/(hr)(sq. ft.). A summary of experimental conditions for all two-phase runs is shown in Table IV.

Local heat transfer coefficients for the small coil are shown in Figures 8 through 24. Results for the large coil are shown in Figures 25 through 29. The abscissa in all of the plots is coil axial position, measured from the coil inlet. The heat transfer coefficients were calculated from the following equation:

$$h = \frac{Q/A}{(T_w - T_f)} \quad (5-6)$$

The heat flux, Q/A , and the wall temperature, T_w , were calculated via the numerical solution described in Appendix A. The fluid temperature, T_f , was calculated assuming thermodynamic equilibrium and a linear pressure profile. The assumption of thermodynamic equilibrium is supported by effluent temperature measurements and by the fact that for runs in which the effluent stream was calculated to be slightly superheated, no moisture was observed in the effluent stream. The assumption of a linear pressure profile is justified by the fact that, for the range of

TABLE IV
EXPERIMENTAL CONDITIONS FOR TWO-PHASE RUNS

Run	Mass Velocity	Av. Heat Flux	Quality		Pressure, psia		Temp., °F	
	lb/(hr)(sq.ft.)	Btu/(hr)(sq.ft.)	Inlet	Outlet	Inlet	Outlet	Inlet	Outlet
104	70,000	11,100	69.7	86.5	27.8	20.0	246	228
105	70,900	13,000	69.7	89.4	28.5	20.4	248	229
106	70,900	6,000	80.5	90.0	26.1	18.0	243	222
107	71,300	4,200	80.8	87.6	29.1	20.5	248	229
108	73,500	2,700	81.4	86.1	28.8	20.5	248	229
109	79,200	14,400	65.7	85.1	30.4	21.0	251	230
110 ¹	84,000	27,000	67.6	100.0	34.1	23.3	258	238
111	84,500	26,800	49.5	85.5	36.5	23.4	262	236
113 ¹	80,500	31,800	46.8	83.5	38.6	24.8	265	240
114 ¹	41,700	8,500	67.6	88.3	19.8	16.6	228	213
116	73,700	14,400	63.3	84.2	29.2	19.4	249	226
117 ^{1,2}	76,200	27,000	64.1	100.0	33.9	23.2	257	237
118 ¹	67,800	33,000	59.3	100.0	36.1	24.4	261	359
119 ¹	43,000	15,500	68.2	100.0	21.7	17.3	232	222
120 ¹	33,300	15,000	43.7	87.9	17.6	15.7	221	215
121	72,700	6,100	84.7	94.1	33.1	22.8	256	235
122 ¹	80,700	8,600	86.4	98.1	33.9	23.6	257	237
201 ^{1,3}	67,200	12,900	68.3	88.5	23.5	17.8	237	222
202 ^{1,4}	91,600	31,700	53.5	89.6	32.1	22.4	254	234
203 ^{1,5}	80,700	6,100	86.2	94.6	28.7	21.1	248	231
205 ^{1,6}	78,900	28,000	65.6	100.0	31.0	23.1	252	238
206 ^{1,7}	42,200	15,500	68.5	100.0	21.0	17.5	231	224

¹Mild oscillations.

²Replicate of 110.

³Replicate of 105.

⁴Replicate of 113.

⁵Replicate of 121.

⁶Replicate of 117.

⁷Replicate of 119.

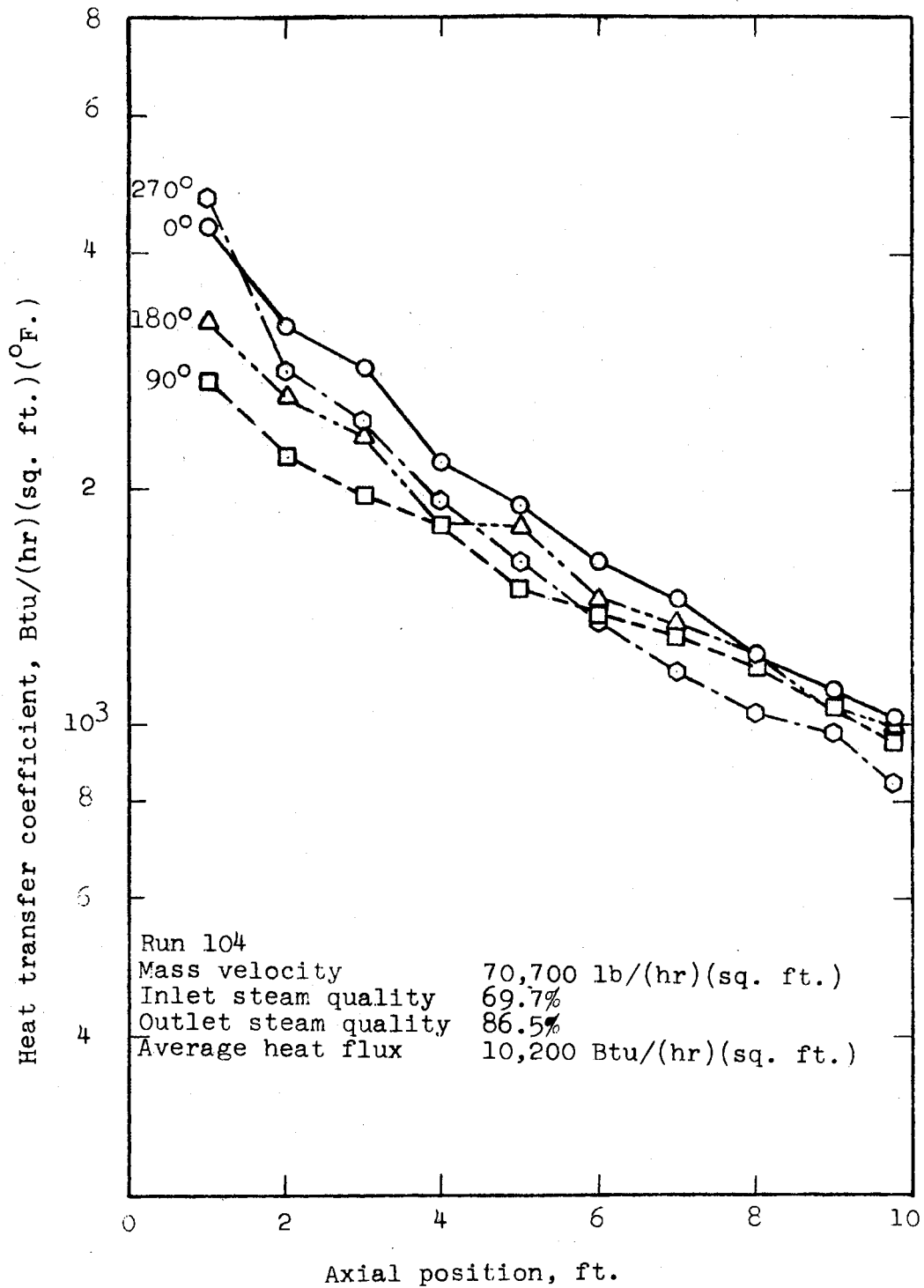


Figure 8. Two-Phase Heat Transfer, Small Coil, Run 104

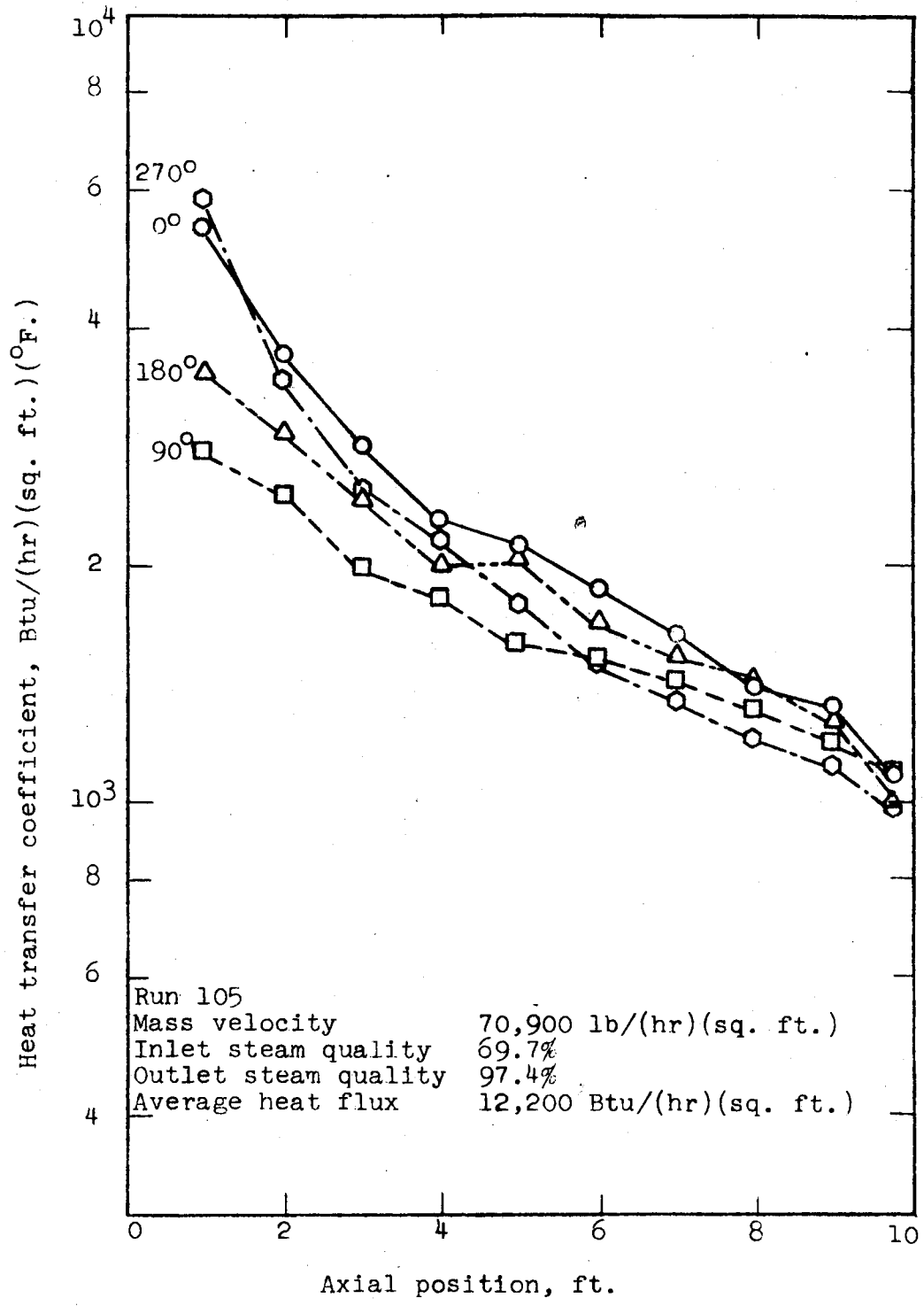


Figure 9. Two-Phase Heat Transfer, Small Coil, Run 105

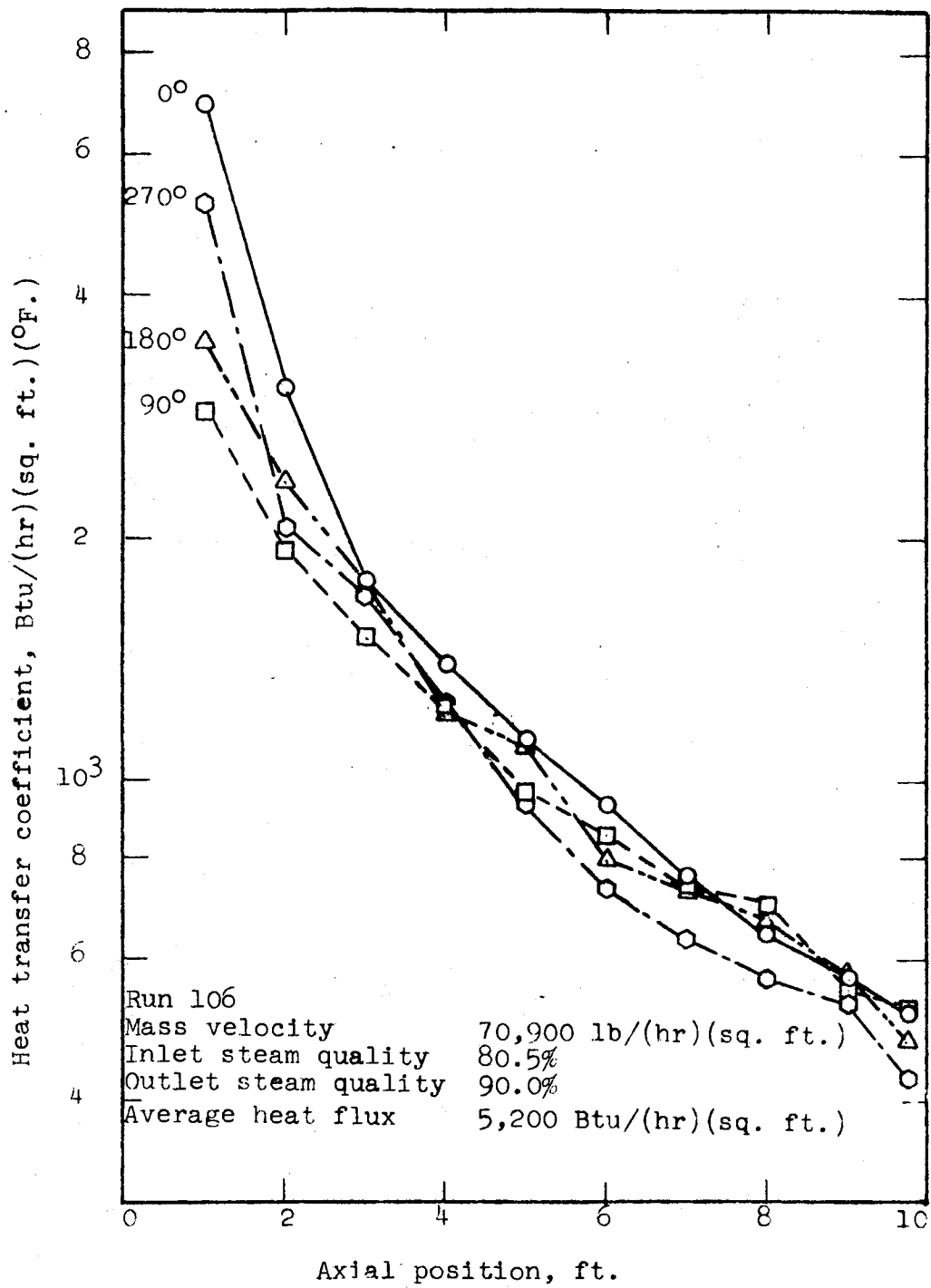


Figure 10. Two-Phase Heat Transfer, Small Coil, Run 106

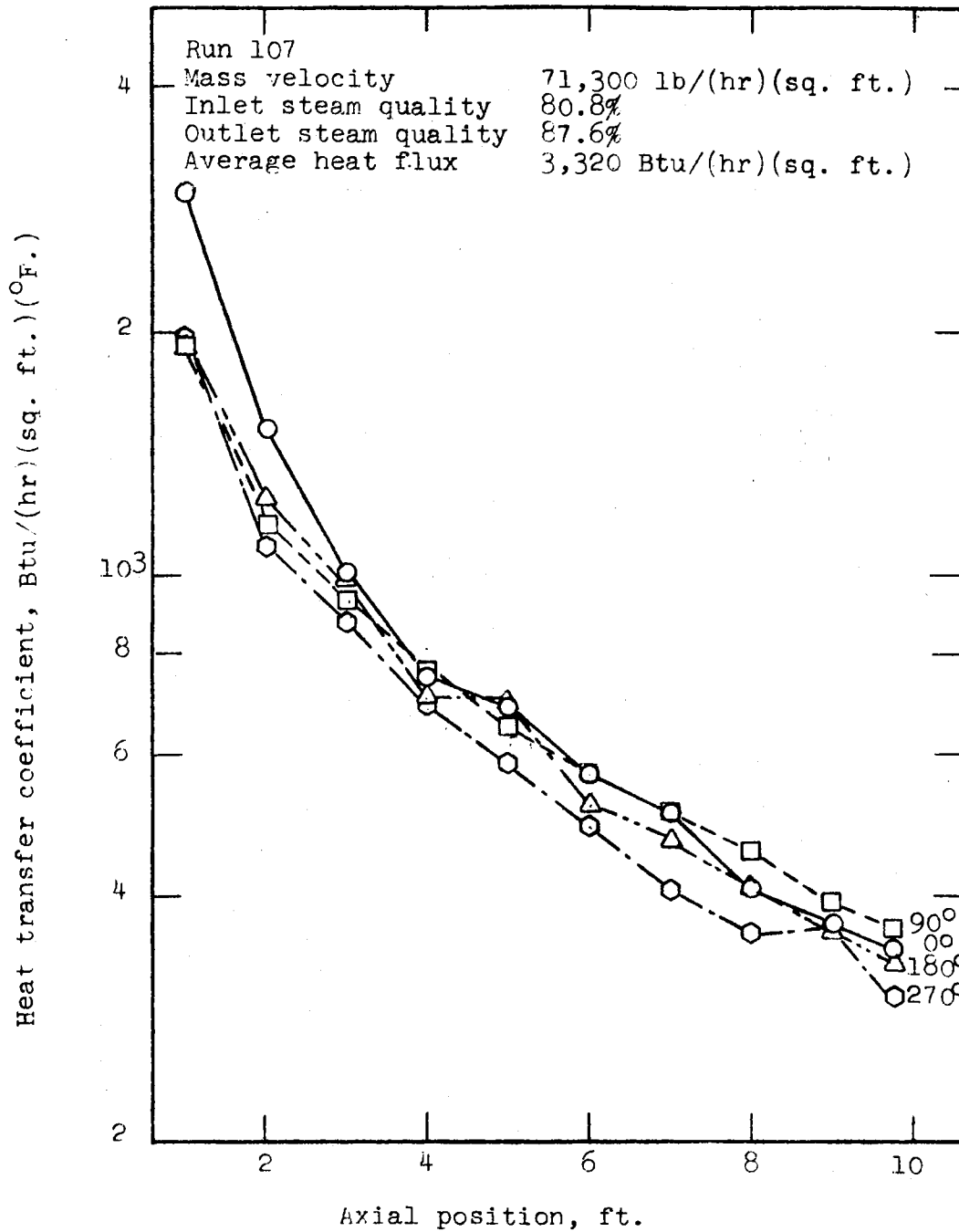


Figure 11. Two-Phase Heat Transfer, Small Coil, Run 107

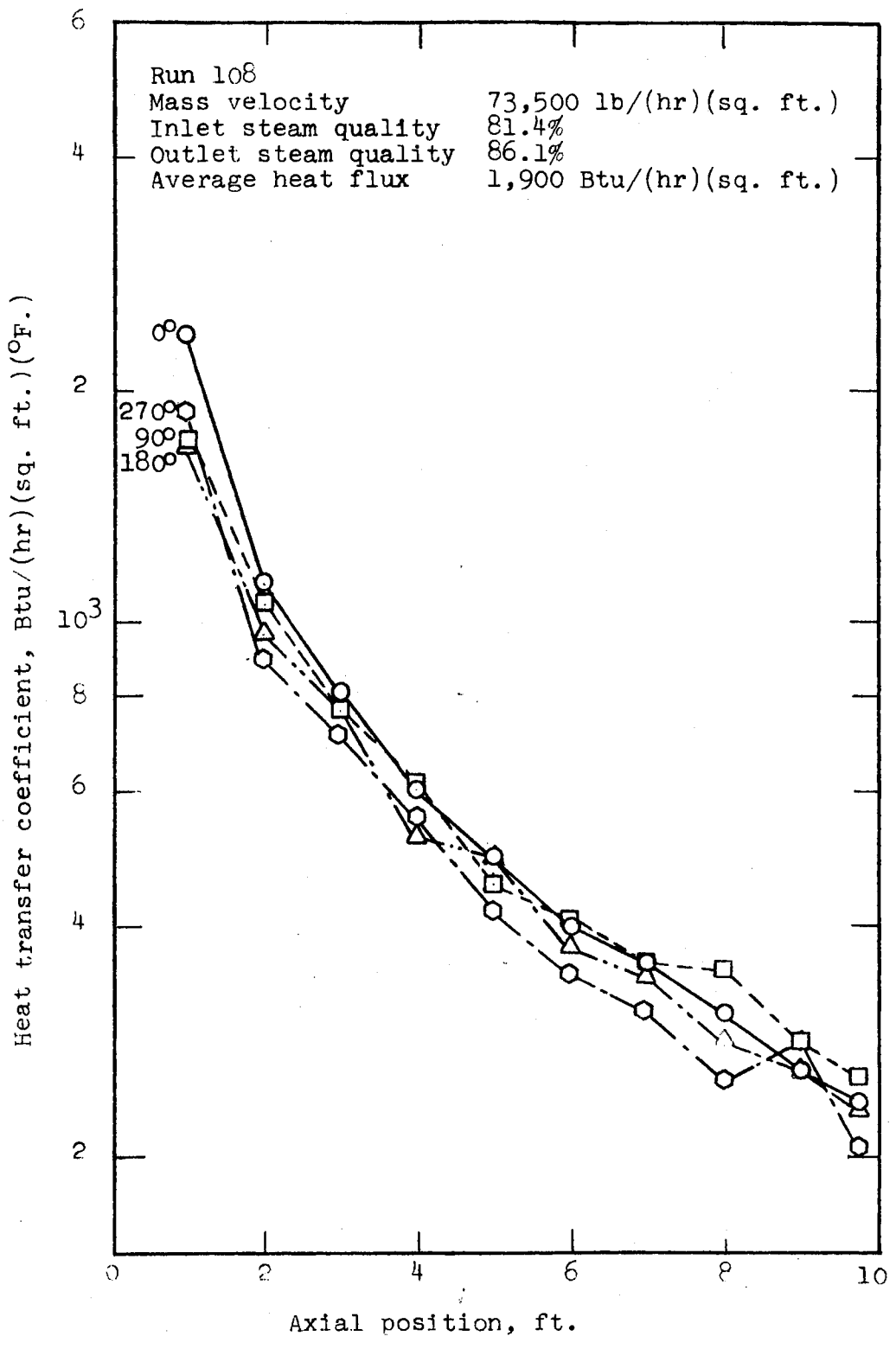


Figure 12. Two-Phase Heat Transfer, Small Coil, Run 108

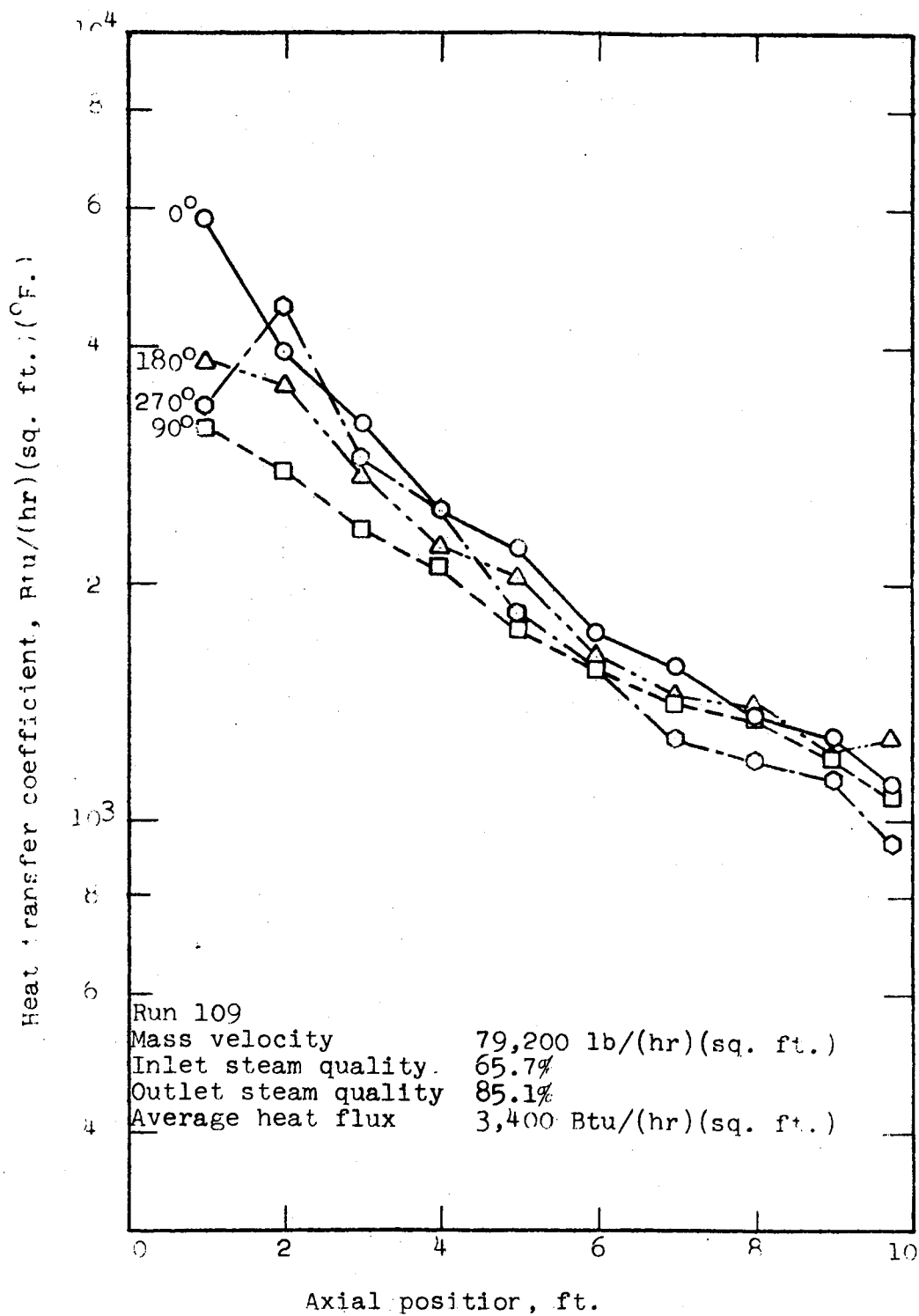


Figure 13. Two-Phase Heat Transfer, Small Coil, Run 109

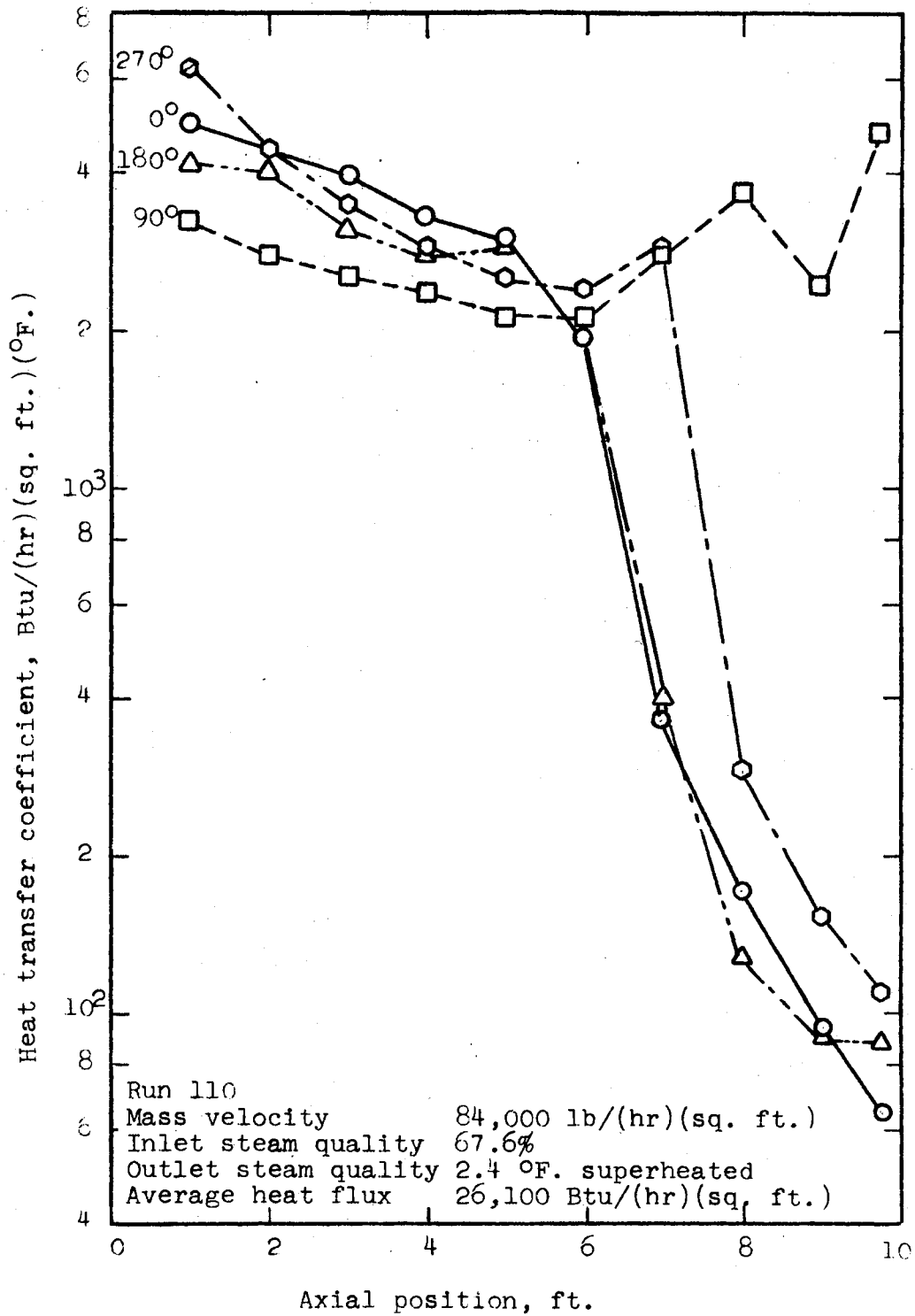


Figure 14. Two-Phase Heat Transfer, Small Coil, Run 110

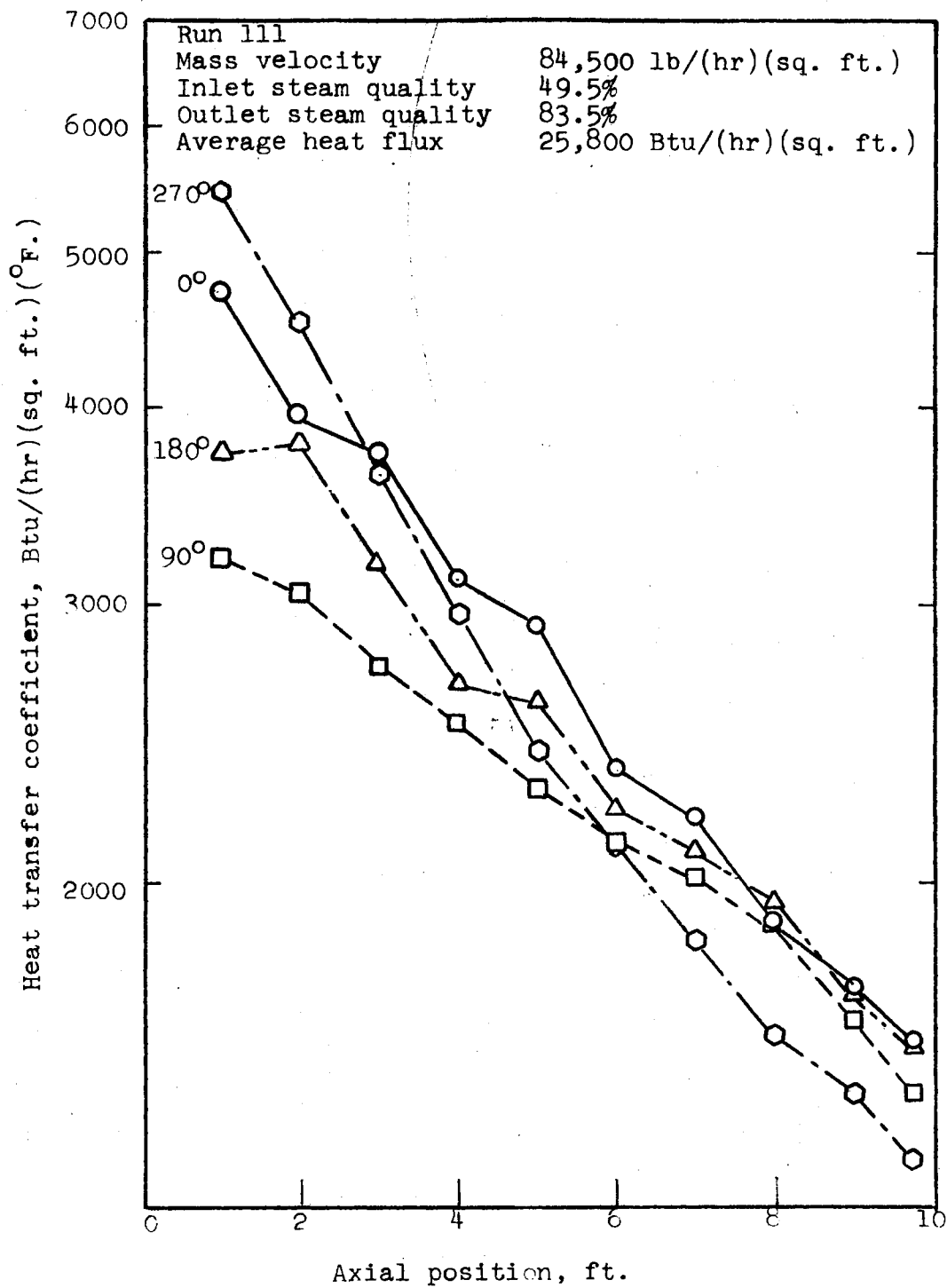


Figure 15. Two-Phase Heat Transfer, Small Coil, Run 111

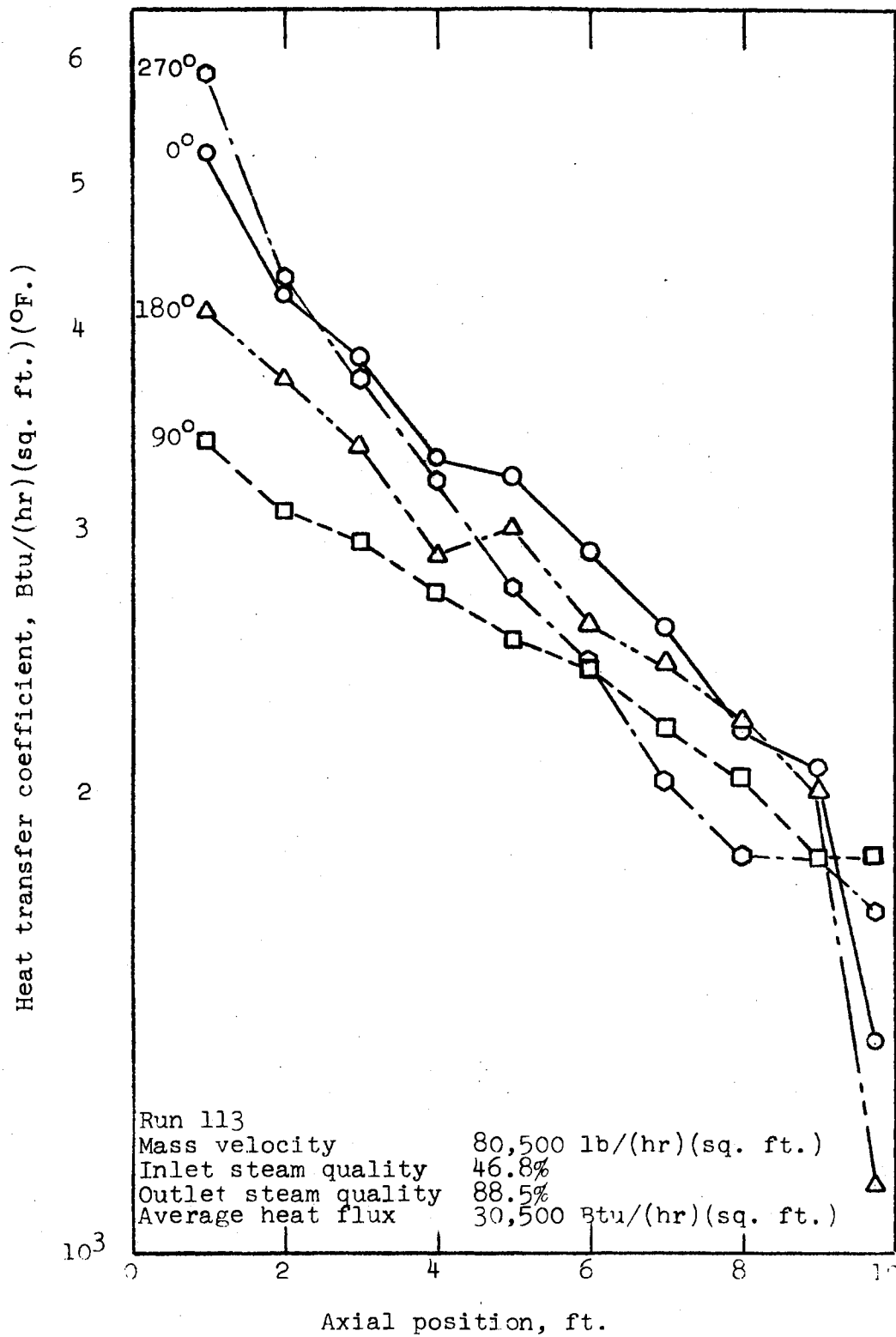


Figure 16. Two-Phase Heat Transfer, Small Coil, Run 113

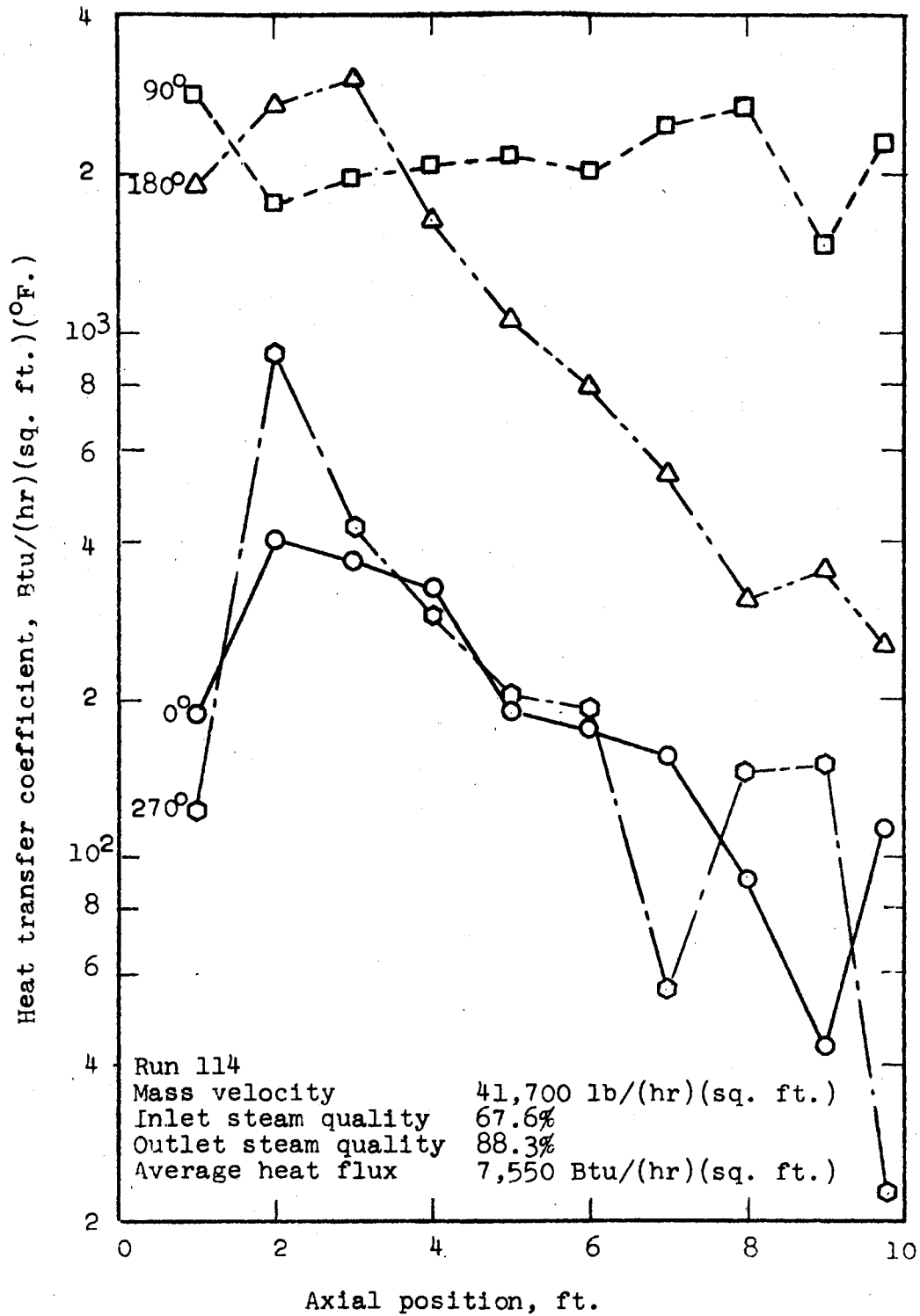


Figure 17. Two-Phase Heat Transfer, Small Coil, Run 114

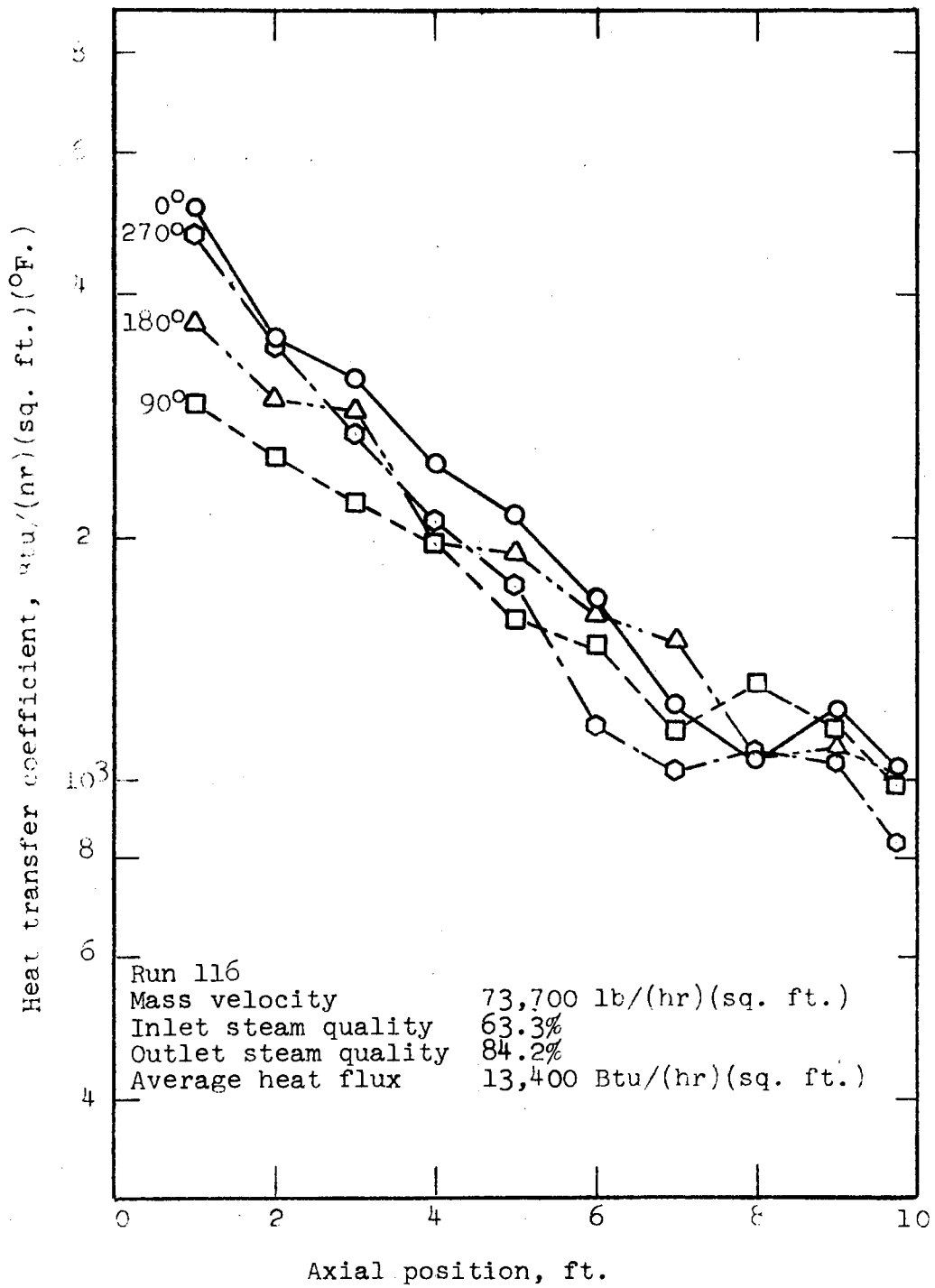


Figure 18. Two-Phase Heat Transfer, Small Coil, Run 116

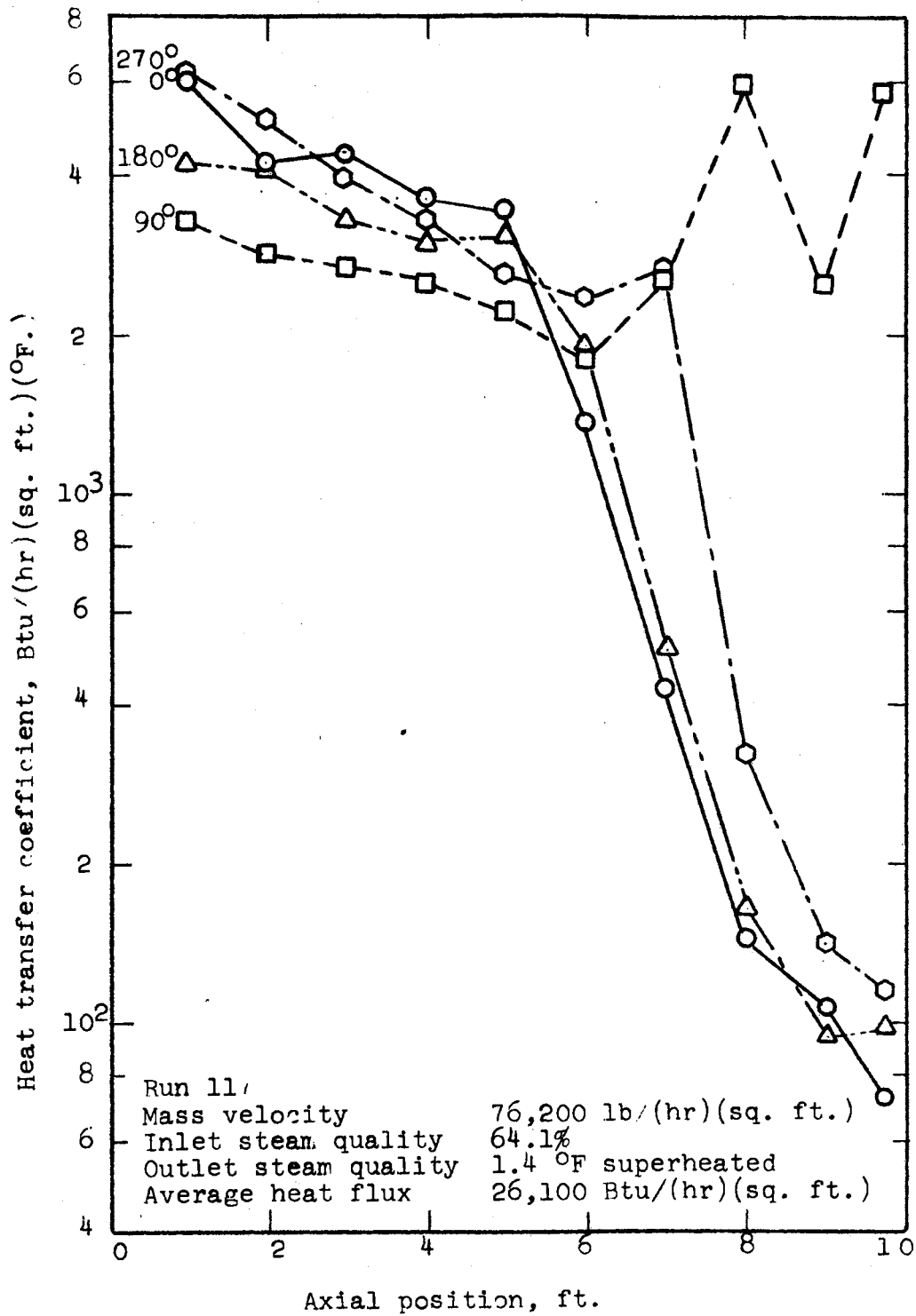


Figure 19. Two-Phase Heat Transfer, Small Coil, Run 117

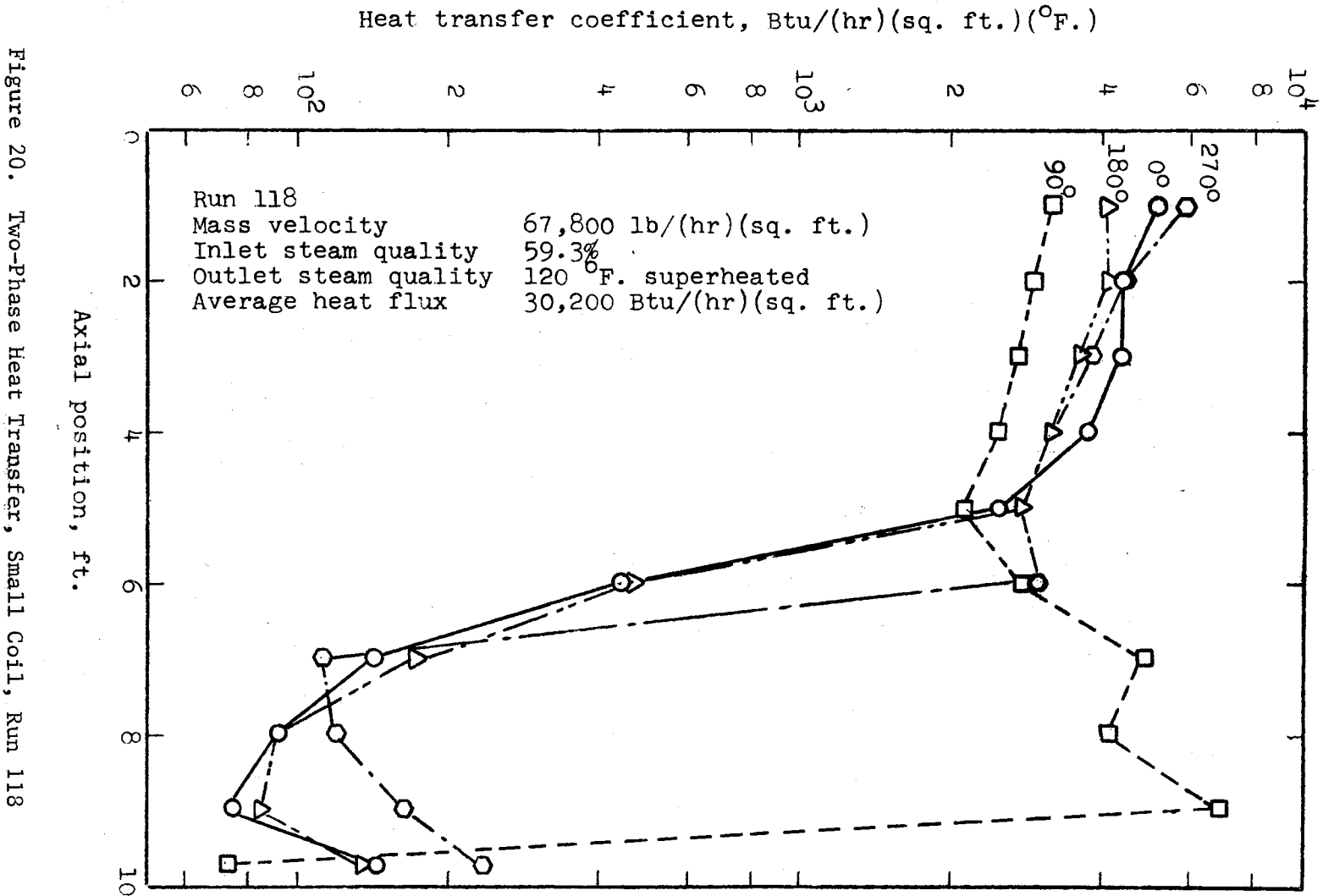


Figure 20. Two-Phase Heat Transfer, Small Coil, Run 118

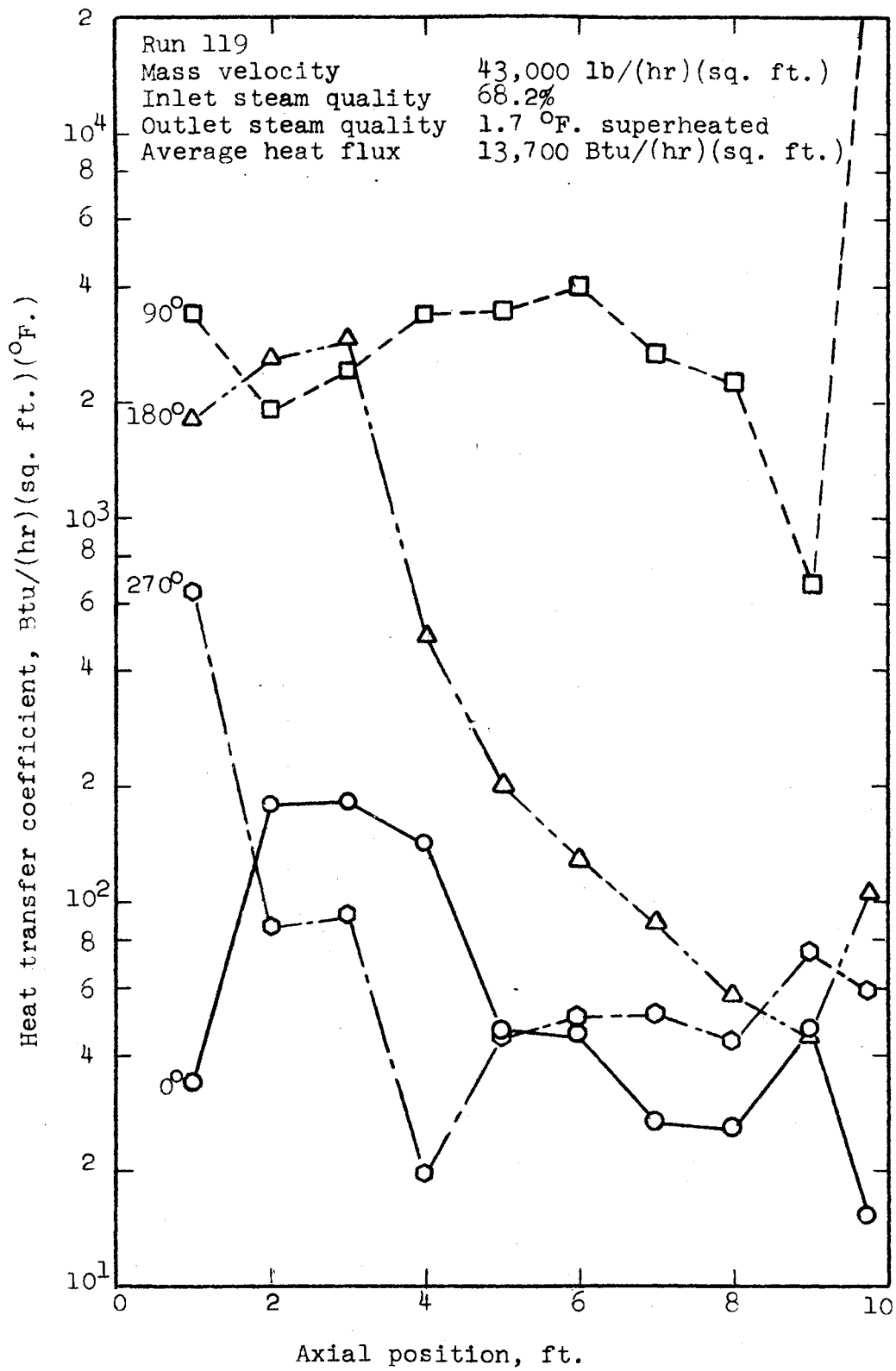


Figure 21. Two-Phase Heat Transfer, Small Coil, Run 119

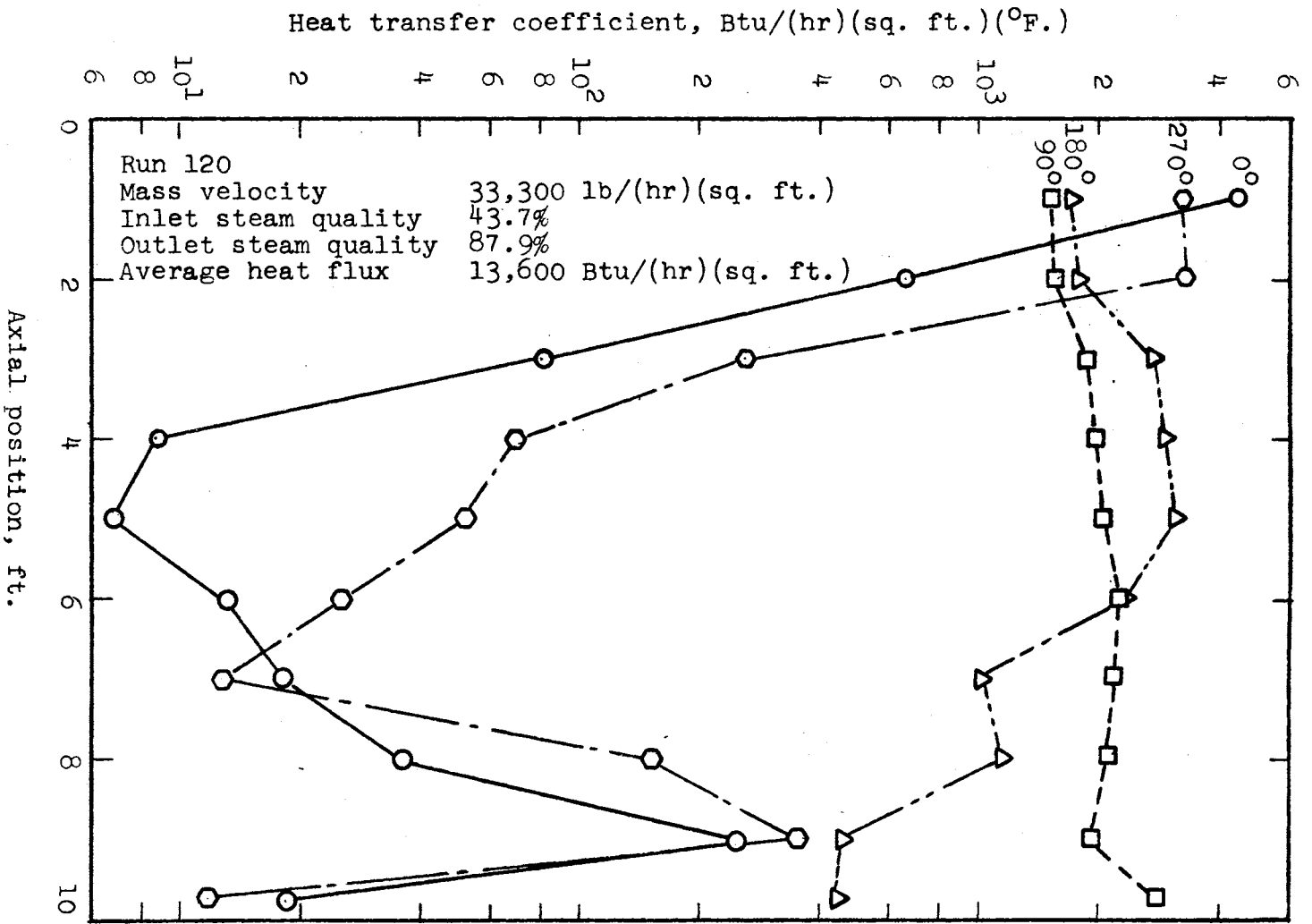


Figure 22. Two-Phase Heat Transfer, Small Coil, Run 120

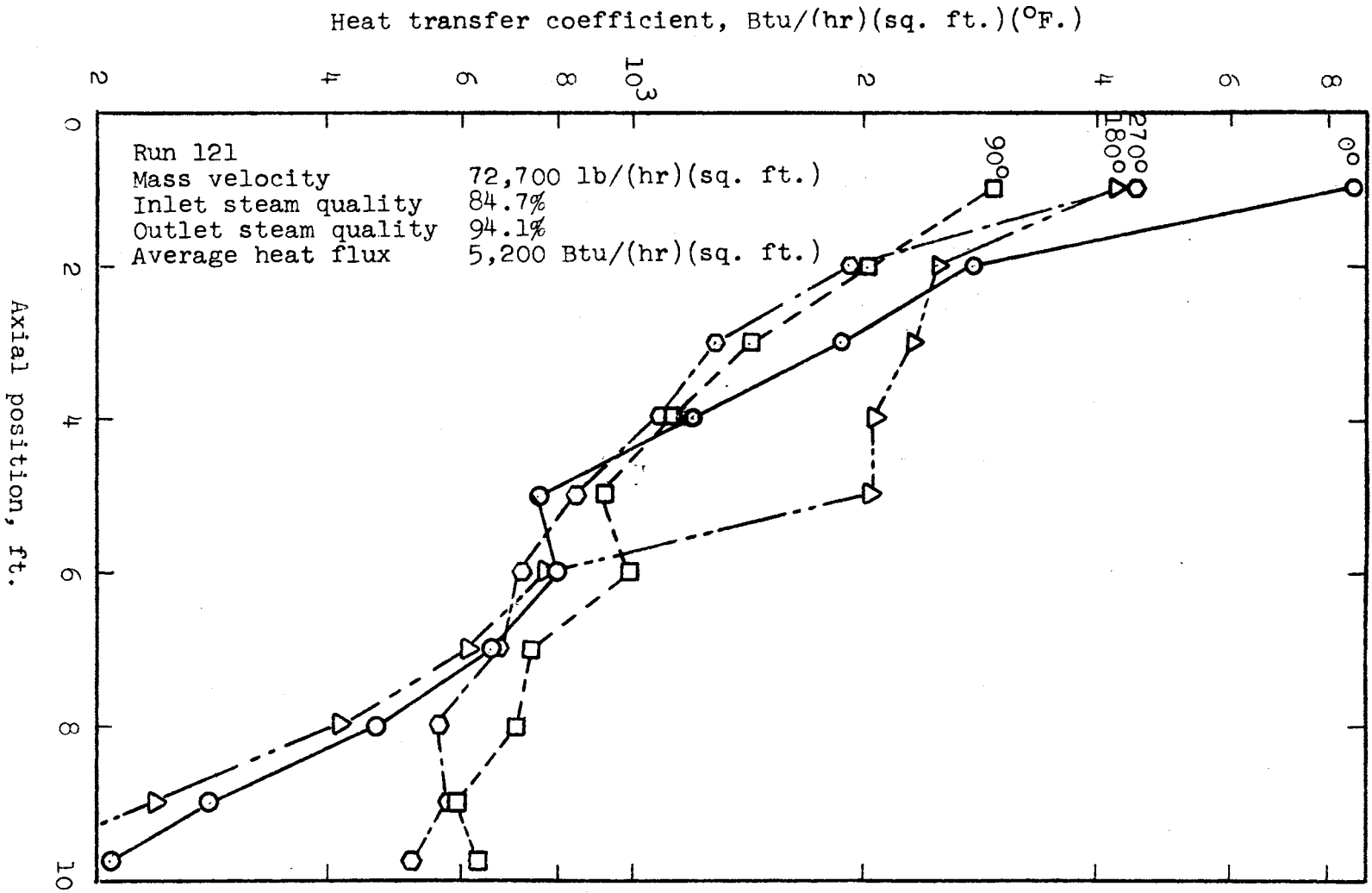


Figure 23. Two-Phase Heat Transfer, Small Coil, Run 121

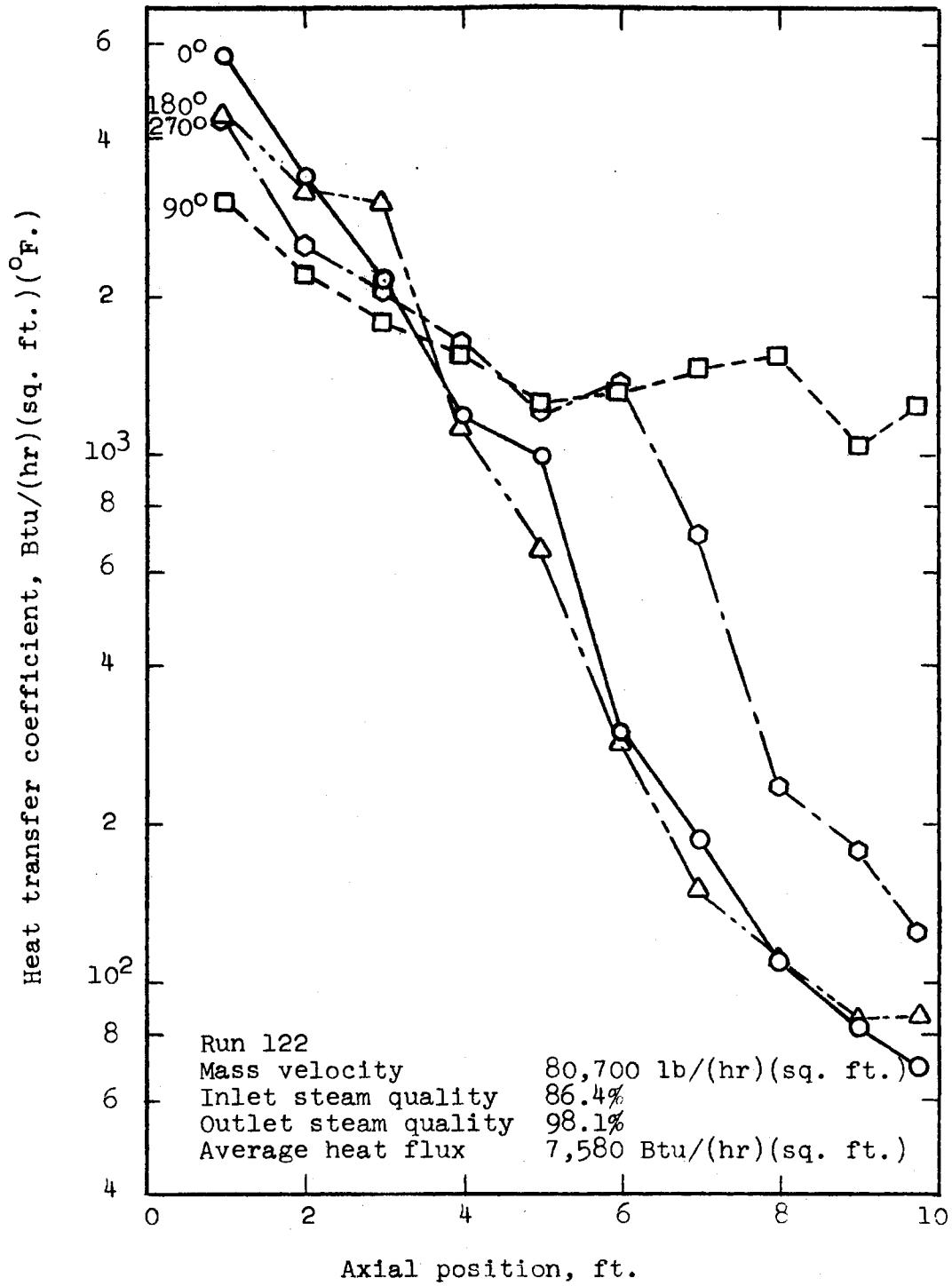


Figure 24. Two-Phase Heat Transfer, Small Coil, Run 122

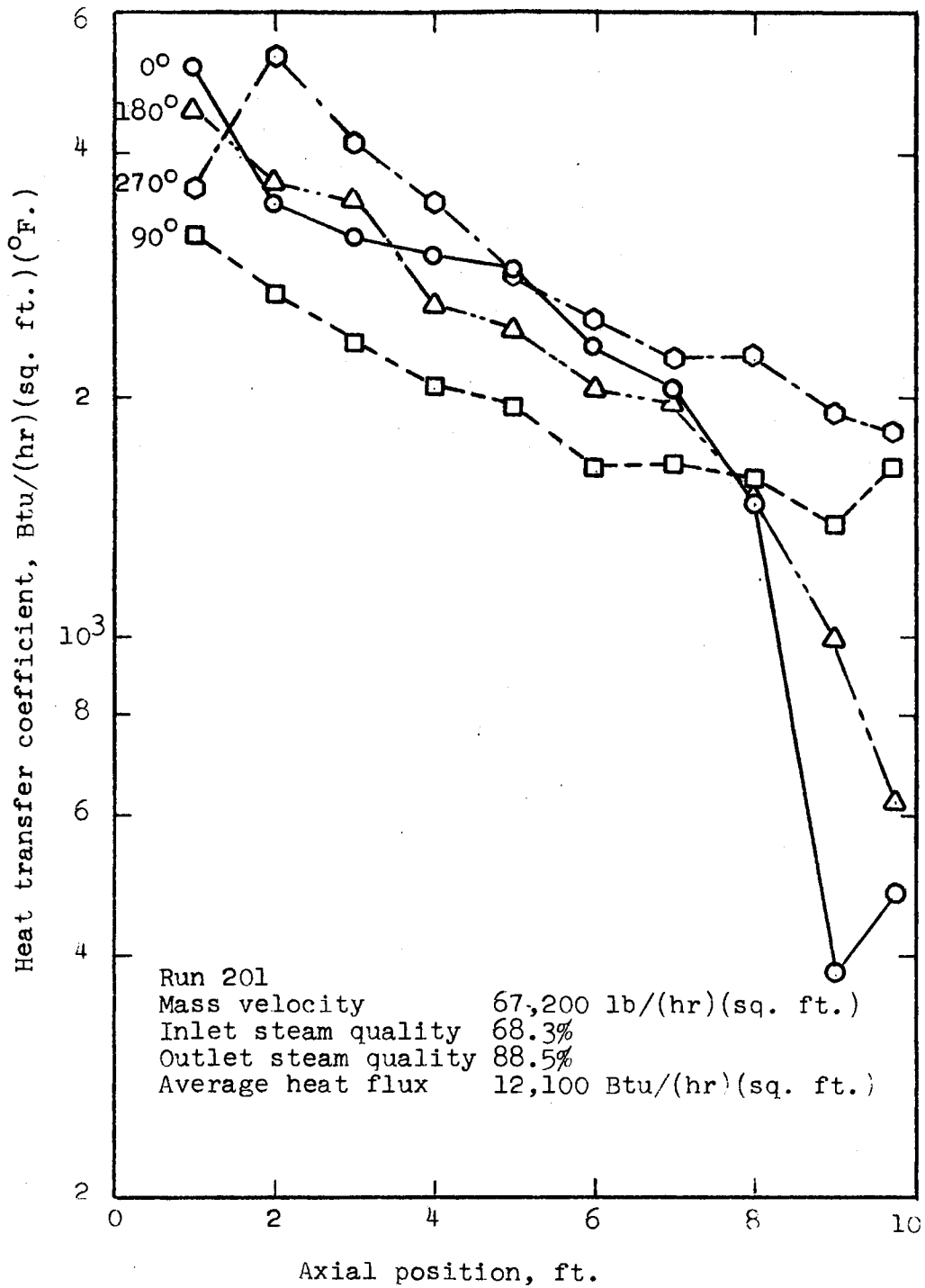


Figure 25. Two-Phase Heat Transfer, Large Coil, Run 201

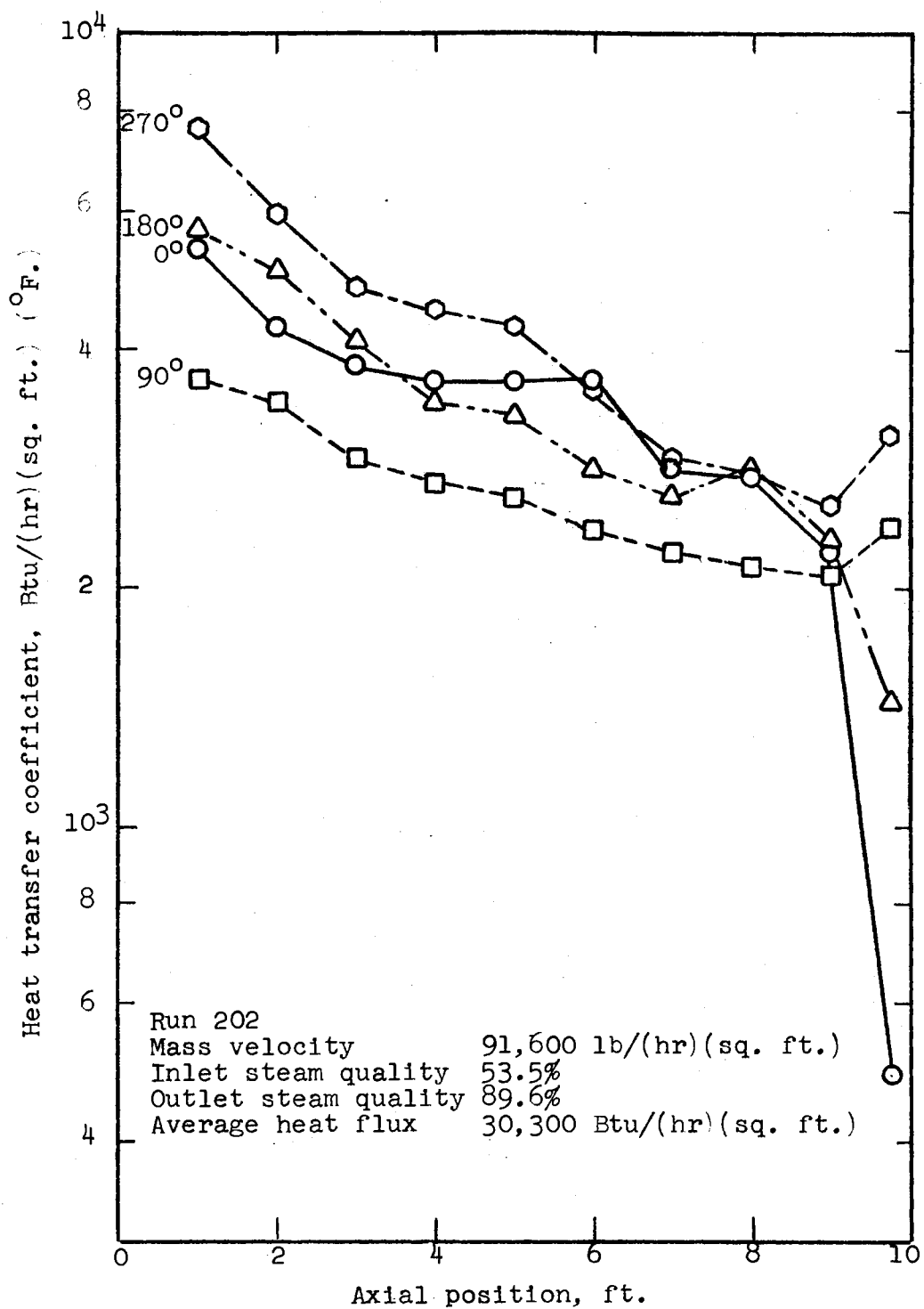


Figure 26. Two-Phase Heat Transfer, Large Coil, Run 202

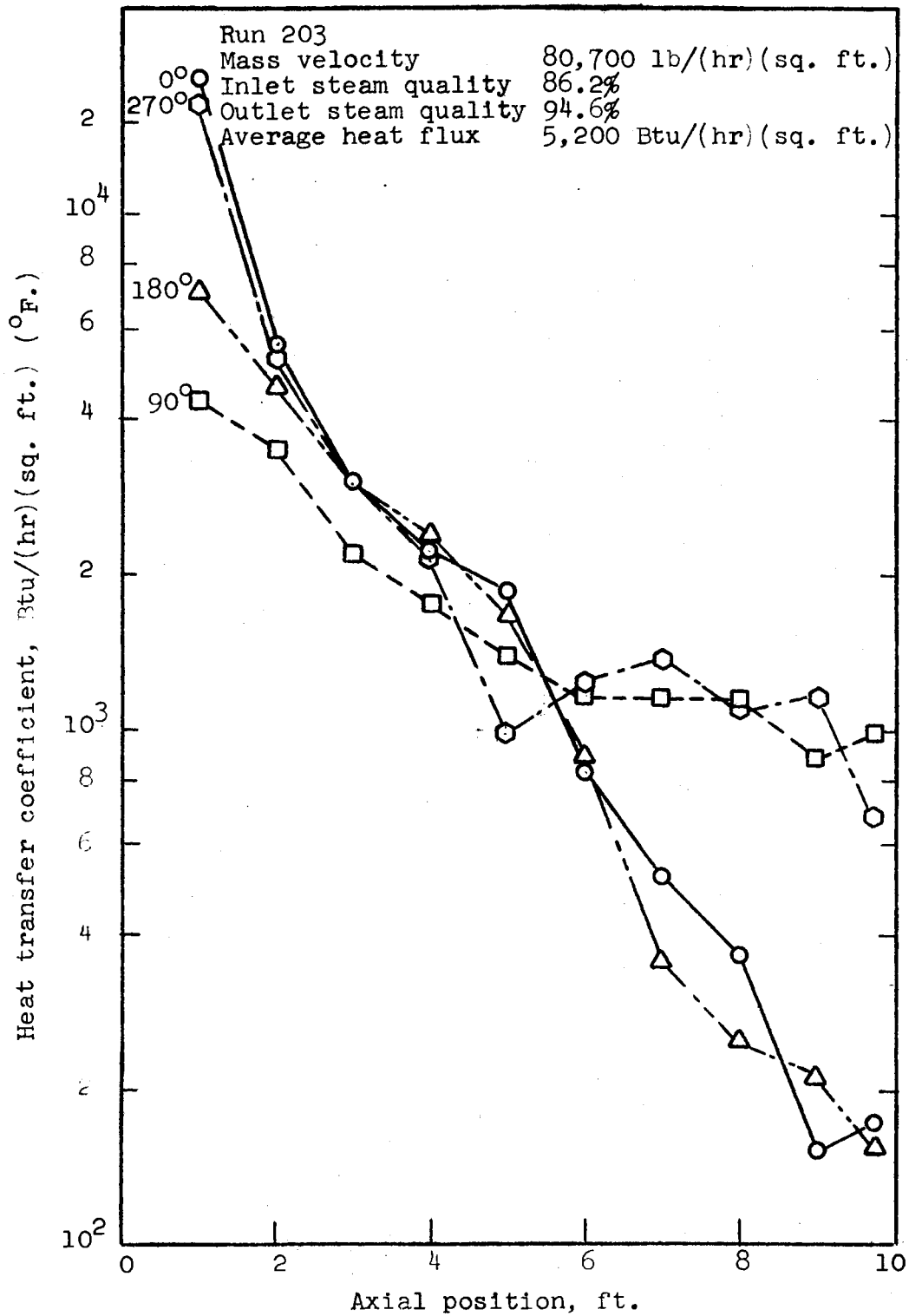
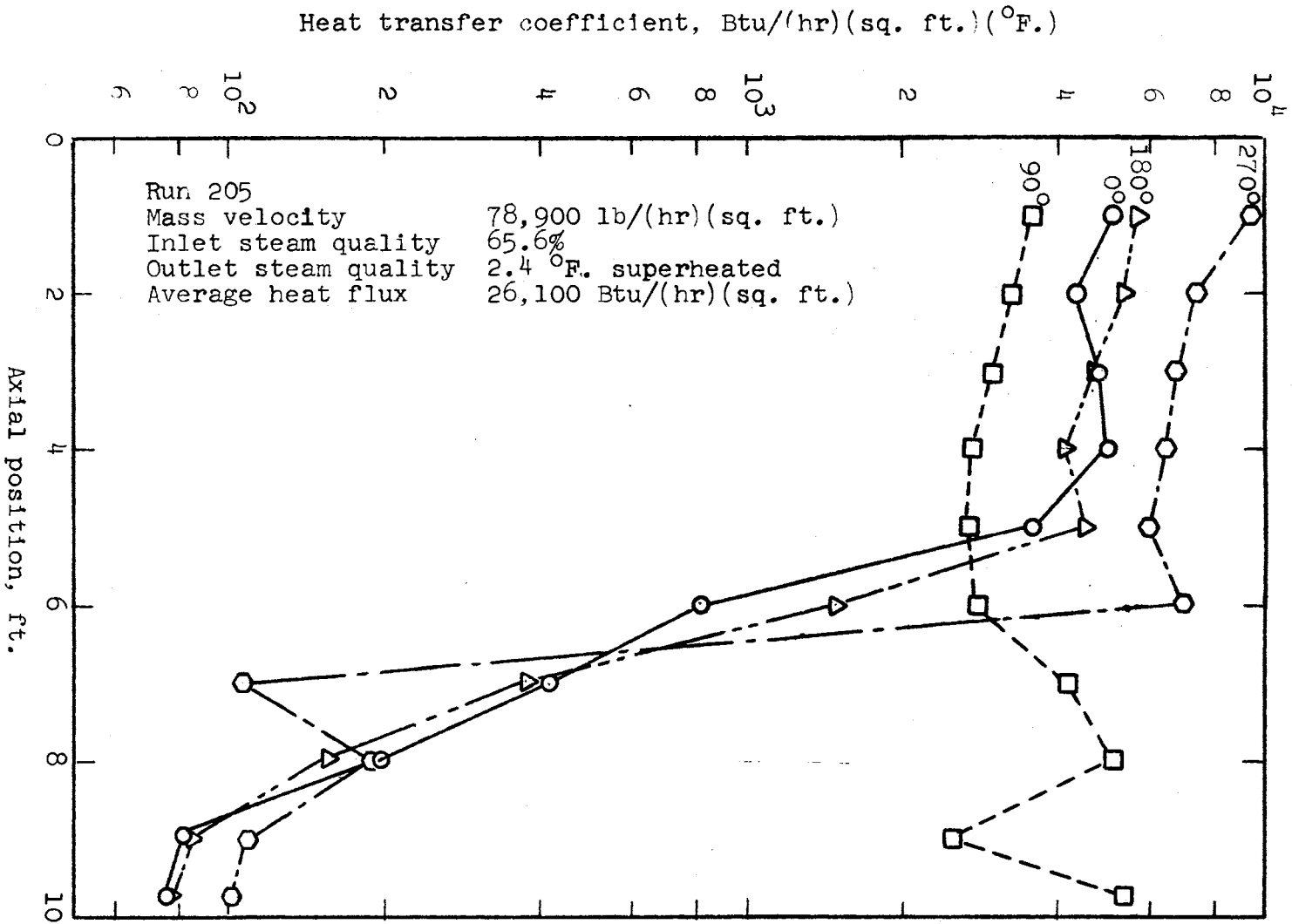


Figure 27. Two-Phase Heat Transfer, Large Coil, Run 203

Figure 28. Two Phase heat Transfer, Large Coil, Run 205



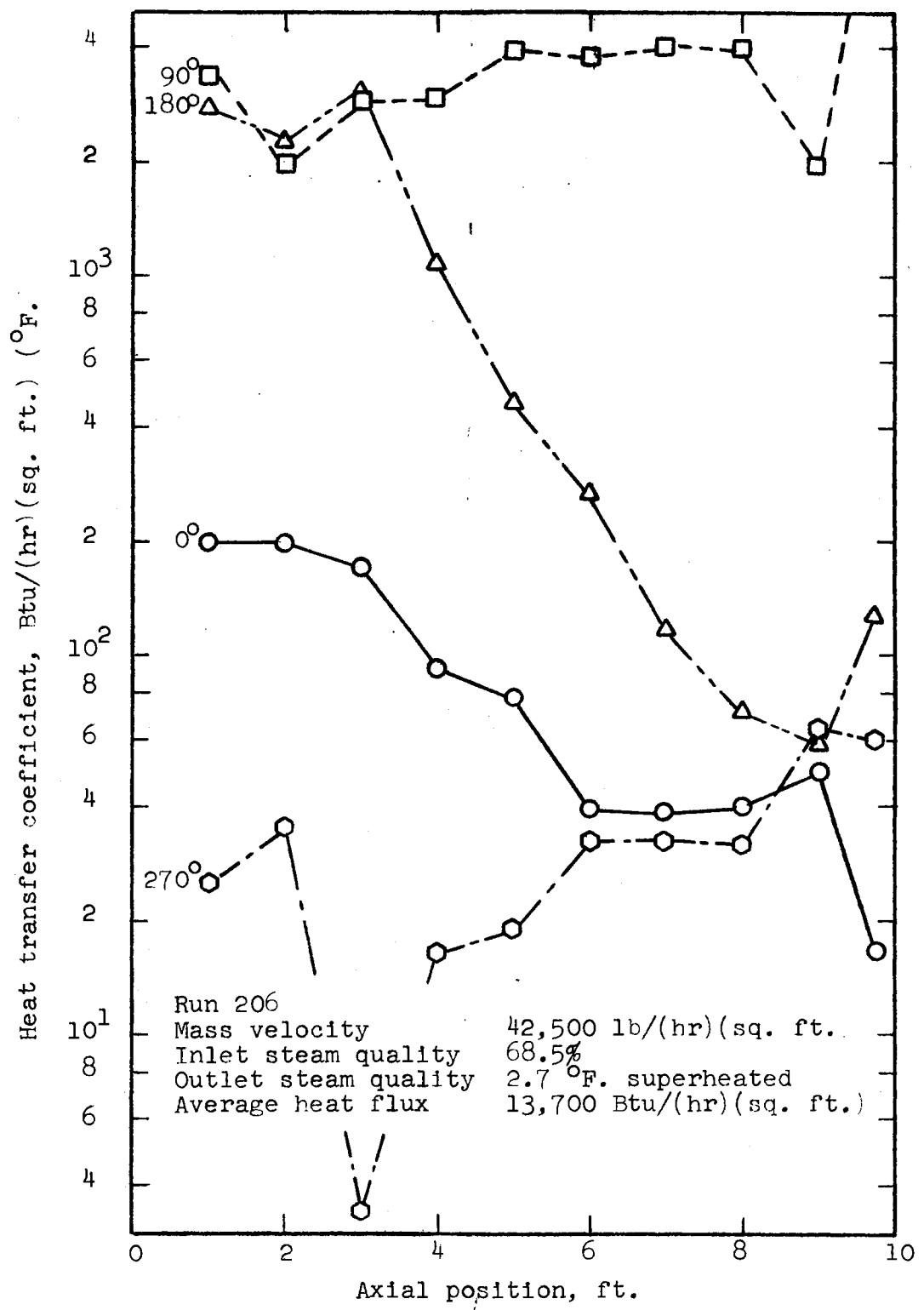


Figure 29. Two-Phase Heat Transfer, Large Coil, Run 206

qualities investigated in this study, void fractions are well in excess of 90% and the change in void fraction along the coil is small.

The first series of runs with the small coil, 104 through 108, was performed by holding the mass velocity approximately constant and varying the inlet quality and heat flux. Results were similar. The local heat transfer coefficients at all positions decrease as the steam quality increases. For the range of qualities encountered in these runs, 70% to 90%, heat transfer coefficients do not vary appreciably in the circumferential direction at a given axial position.

The next series of runs, 109 through 113, was performed by holding the mass velocity approximately constant at a slightly higher value than in the first series and varying the inlet quality and the heat flux. Run 109 produced results similar to those in the first series. In run 110, however, the quality in the coil exceeded 90%, and the heat transfer coefficients show a marked decrease. The local heat transfer coefficients at the 0° and 180° positions decrease first, at an axial position between six and seven feet from the coil inlet. The calculated equilibrium quality at this point is between 88 and 91%. At the same axial position the coefficients at the 90° and 270° positions increase slightly. Between seven and eight feet from the coil inlet the local heat transfer coefficient at the 270° position also decreases. The quality at this point is between 91 and 95%. The heat transfer coefficient at the 90° position continues to increase all the way to the last axial position, at which point the steam is calculated to be slightly superheated. Coefficients at the other positions continue to decrease all the way to the end of the coil. Several observations can be made from the behavior exhibited in this run. The first is the fact that

the secondary circulation pattern provides excellent distribution of the liquid present in the two-phase flow. Good cooling is maintained up to a quality in the neighborhood of 90%. Beyond a quality of 90%, liquid is present at the 90° and 180° positions and finally, only at the 90° position. The presence of liquid at the 90° position was detected up to a calculated quality of 100%. The mechanism by which liquid is distributed by the secondary flow is discussed in detail in Appendix B.

Run 111 had an inlet quality of 49.5%. The heat transfer coefficients are higher than those in previously described runs but decreases in the same manner as quality increases. Conditions in run 113 were similar. However, the heat flux was slightly higher, and as the steam quality approaches 90%, the coefficients at the 0° and 180° positions decrease as was seen in run 110.

Run 114 was one in which the mass velocity was fairly low. The behavior of the local heat transfer coefficients is somewhat erratic, probably because the velocity was low enough that a strong secondary circulation pattern was not established. Near the coil inlet, the heat transfer coefficients at the 90° and 180° positions are markedly higher than those at the 0° and 270° positions. The local heat transfer coefficients decrease as quality increases at all positions except the 90° position. Coefficients at these points remain essentially constant along the length of the coil.

Results of run 116 are similar in all respects to those of runs 104 through 108. In runs 117 and 118 the coil effluent was superheated steam. The effluent in run 117 was calculated to be 1.4°F . superheated. The local heat transfer coefficients at the 0° and 180° positions

begin to decrease at a point between five and six feet from the coil inlet where the steam quality was between 83 and 86%. Between six and seven feet from the coil inlet the quality was between 86 and 90% and the coefficients at the 0° and 180° positions decrease markedly. The heat transfer coefficient at the 270° position decreases at a point between seven and eight feet from the coil inlet where the quality is between 90 and 94%. The local heat transfer coefficients at the 90° position remain high all the way to the end of the coil. The effluent in run 118 is calculated to be 120°F . superheated. The coefficients at the 0° and 180° positions decrease at a quality between 83 and 87% and the coefficient at the 270° position decreases at a quality between 87 and 92%. Notable in this run is a decrease in the heat transfer coefficient at the 90° position in the last one foot section of the coil with an accompanying outside wall temperature of almost 760°F .

Runs 119 and 120 are similar to run 114 in that the mass flow rate was fairly low and the behavior of local heat transfer coefficients is erratic. The effluent in runs 121 and 122 was saturated in both cases. However, the inlet quality was high and sufficiently high qualities were reached to cause the decrease in local heat transfer coefficient noted in other runs.

As noted in Table IV, the runs with the large coil were replicates of small coil runs. No notable differences between small and large coil results were found. The difference in coil diameters was probably not great enough to produce a noticeable effect.

The most striking result of the two-phase runs is the decrease in local heat transfer coefficients at the 0° and 180° positions and at the 270° position while the coefficient at the 90° position remains high.

The local conditions corresponding to this behavior are summarized in Table V.

TABLE V
LOCAL CONDITIONS FOR SECONDARY FLOW EFFECT

Run	Mass Velocity lb/(hr)(sq. ft.)	Av. Heat Flux Btu/(hr)(sq. ft.)	Local Quality	
			Decrease in 0° and 180°	Decrease in 270°
110	84,000	26,100	84-88	91-95
113	80,500	30,500	84-87	-
117	76,200	26,100	83-86	90-94
118	67,800	30,200	83-87	87-92
121	72,700	5,200	90-91	-
122	80,700	7,580	90-91	93-95
201	67,700	12,100	82-84	-
202	91,600	30,300	86-89	-
203	80,700	5,200	90-91	93-94
205	78,800	26,100	83-87	87-90

Two-Phase Pressure Drop

Static pressures were measured at the coil inlet and outlet during all two-phase runs. From these readings the total coil pressure drop was obtained. The pressure drop measurements are summarized in Table VI.

TABLE VI
TWO-PHASE PRESSURE DROP

Run	Pressure Drop, psi		
	Total	Acceleration	Friction
104	7.8	0.26	7.5
105	8.1	0.28	7.8
106	8.1	0.27	7.8
107	8.6	0.21	8.4
108	8.3	0.21	8.1
109	9.4	0.34	9.1
110	10.8	0.50	10.3
111	13.1	0.47	12.6
113	13.8	0.45	13.3
114	3.2	0.095	3.1
116	9.8	0.34	9.5
117	10.7	0.43	10.3
118	11.7	0.45	11.3
119	4.4	0.17	4.2
120	1.9	0.099	1.8
131	10.3	0.24	10.1
122	10.3	0.30	10.0
201	5.7	0.26	5.4
202	9.7	0.57	9.1
203	7.6	0.27	7.3
205	7.9	0.43	7.5
206	3.5	0.16	3.3

Frictional pressure drops were calculated by assuming that the static pressure drop was negligible and by calculating the accelerational pressure drop from the following equation:

$$\Delta P_{\text{acc}} = \frac{G^2}{2g_c} \left(\frac{1}{\rho_{\text{out}}} - \frac{1}{\rho_{\text{in}}} \right) \quad (5-7)$$

The frictional pressure drop is then calculated as:

$$\Delta P_f = \Delta P_t - \Delta P_{\text{acc}} \quad (5-8)$$

Stability

The first few two-phase heat transfer runs were carried out at fairly low heat flux conditions. In the first run at moderately high heat flux conditions, run 110, oscillations in some of the outside wall temperatures were noted. The oscillations in run 110 were not periodic, but random in nature. Later runs at other flow and heat flux conditions produced oscillations which were periodic. Examples of the two types of oscillations are shown in Figure 30. For identical flow conditions a heat flux of 9,770 Btu/(hr)(sq. ft.) produced the periodic oscillations shown in Figure 30a while a heat flux of 8,670 Btu/(hr)(sq. ft.) produced the random oscillations shown in Figure 30b. Runs in which oscillations were observed are indicated by a superscript 1 in Table IV. It was noted in general that as the heat flux was increased at a given flow rate random oscillations appeared at the stations near the coil exit. As the heat flux was further increased the random oscillations moved toward the coil inlet. At higher heat fluxes the oscillations near the coil exit became periodic in nature and at even higher heat fluxes the periodic oscillations moved toward the coil

Figure 30. Oscillations

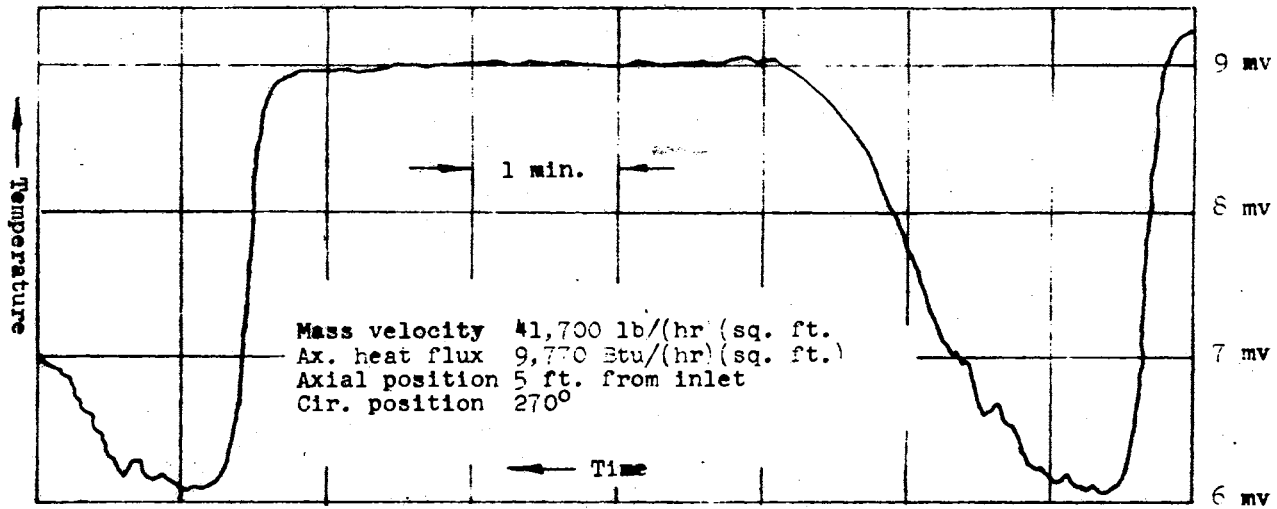


Figure 30a. Periodic Oscillations

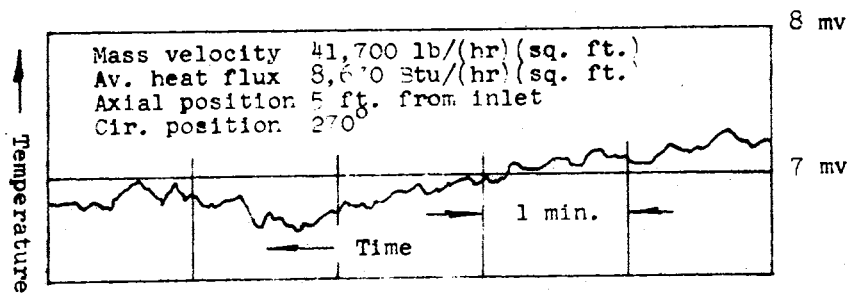


Figure 30b. Random Oscillations

inlet while the oscillations near the coil exit disappeared. In most cases the periodic decreases in temperature were accompanied by in-phase increases in the liquid content of the two-phase mixture leaving the coil. The physical evidence noted during oscillating behavior is typical of the density wave oscillations accompanied by temperature oscillations described by Bergles et al. (4). Slow-moving density waves pass through the system in which the liquid content of the two-phase mixture increases. The change in liquid content causes changes in the flow rate and pressure drop and also changes in wall temperatures due to changing heat transfer conditions.

Local conditions corresponding to the axial point of onset of oscillations are summarized in Table VII. It can be noted from the table that an increase in mass velocity stabilizes the system, as would be expected. The traces shown in Figure 30 indicate that an increase in heat flux makes the system more unstable, also as would be expected.

Two special runs were made to investigate stability of the coils. One run was made with each of the coils. Results are shown in Figure 31. Conditions of mass velocity and heat flux were identical for each coil. The large coil was more stable than the small coil, exhibiting only small oscillations. The small coil exhibited the periodic oscillations described earlier. Thermocouples at all four circumferential locations at a point five feet from the coil inlet were recorded simultaneously. The temperature at the 270° position on the small coil fluctuated from about 350 °F. to 235 °F. This fluctuation probably reflects the alternate presence of vapor and liquid at this position. Similar, but less severe, fluctuations are noted at the 0° and 180° positions.

TABLE VII
 LOCAL CONDITIONS FOR OSCILLATORY BEHAVIOR

Run	Mass Velocity lb/(hr)(sq.ft.)	Average Heat Flux Btu/(hr)(sq.ft.)	Axial Position		Quality	
			Appear	Disappear	Appear	Disappear
110	84,000	27,000	6	9.75	87.7%	100.0%
113	80,500	31,800	10	-	87.4%	--
114	41,700	8,500	1	-	69.7%	--
117	76,200	27,000	6	9	86.2%	97.6%
118	67,800	33,000	5	9	82.6%	100.0%
119	43,000	15,500	1	9	71.6%	100.0%
120	33,300	15,000	2	-	52.2%	--
122	80,700	8,600	6	9	93.3%	96.8%
201	67,200	12,900	9	-	86.4%	--
202	91,600	31,700	9	-	85.9%	--
203	80,700	6,100	9	-	93.7%	--
205	78,900	28,000	5	-	83.2%	--
206	42,200	15,500	1	-	72.0%	--

Figure 31. Comparison of Stability of Small and Large Coils

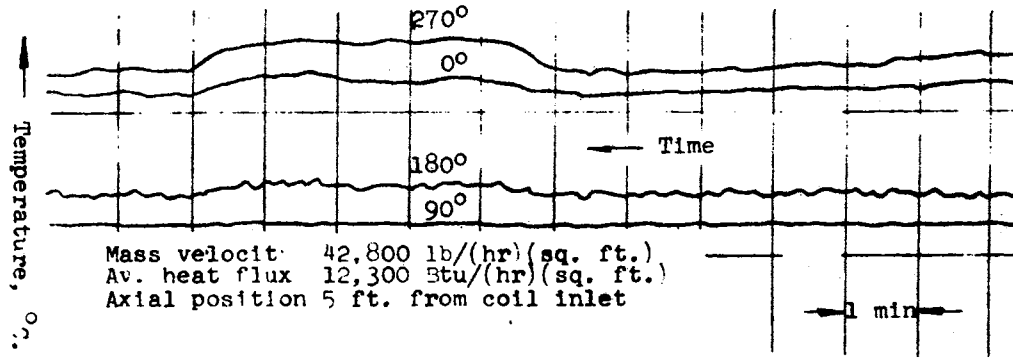


Figure 31a. Large Coil

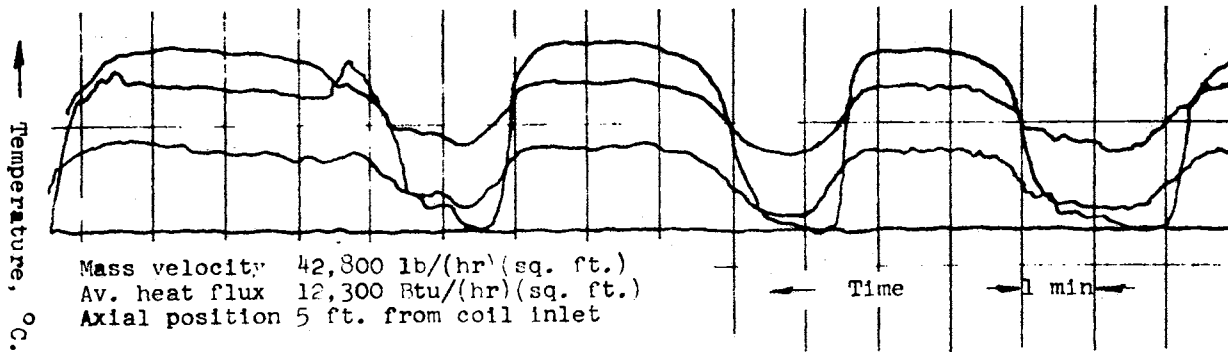


Figure 31b. Small Coil

CHAPTER VI

CORRELATION AND DISCUSSION OF RESULTS

Many of the correlations for two-phase heat transfer in straight tubes and coils utilize the Lockhart-Martinelli parameter as the correlating parameter. Correlations by Dengler and Addoms (8), Bennett, et al (3), Schrock and Grossman (28), Chen (6), Owhadi et al. (2, 23, 24), and de La Harpe et al. (7) all utilize the Lockhart-Martinelli parameter in one form or another. The Lockhart-Martinelli parameter arose from an analysis and empirical correlation of isolated thermal two-phase, two-component pressure drop data in straight horizontal tubes (15). It was later utilized in correlation of boiling two-phase pressure drop data by Martinelli and Nelson (16). The parameter is defined as:

$$X = \frac{(dp/dl)_l}{(dp/dl)_g} \quad (6-1)$$

For two-phase conditions in which both the liquid and vapor phases are turbulent (as determined by the superficial one-phase Reynolds number) this parameter can be expressed as:

$$X_{tt} = \left(\frac{1-x}{x}\right)^{0.9} \left(\frac{\rho_g}{\rho_l}\right)^{0.5} \left(\frac{\mu_l}{\mu_g}\right)^{0.1} \quad (6-2)$$

There are other expressions for the Lockhart-Martinelli parameter for each of the other three combinations of laminar and turbulent gas and

liquid phases. The parameter X_{tt} was chosen as the correlating variable for this study even though a few of the data points were taken at very high qualities where the Reynolds number for the liquid phase was in the laminar regime. It should be noted that the variation in X_{tt} is due primarily to the variation of steam quality since only slight changes of the steam and water properties occur due to the pressure and temperature variations of the two-phase mixture encountered in this study.

Previous authors have correlated the ratio of the heat transfer coefficient for two-phase flow to a heat transfer coefficient calculated as if only the liquid were flowing in the tube. For the steam quality range covered in this study the ratio of the heat transfer coefficient for two-phase flow to a heat transfer coefficient calculated as if only the vapor were flowing in the tube was deemed to be more appropriate. The Seban-McLaughlin equation (29) was used to calculate the vapor heat transfer coefficient, h_{gc} . The equation is:

$$Nu = 0.023 Re^{0.85} Pr^{0.4} \left(\frac{d}{D}\right)^{0.1} \quad (6-3)$$

The data are presented both in the form of circumferential average heat transfer coefficients and in the form of local heat transfer coefficients. The circumferential average heat transfer coefficient, \bar{h} , was calculated for each longitudinal location along the coil. The circumferential average heat transfer coefficient was defined as the ratio of the average heat flux to the average temperature difference between the inner tube surface and the two-phase mixture. The average heat flux and the average temperature difference are arithmetic circumferential averages. The correlation of \bar{h}/h_{gc} for the small coil is shown in

Figure 32 and the correlations for the local heat transfer coefficients are shown in Figures 33 through 36. As evidenced by the scatter in the correlation, the Lockhart-Martinelli parameter does not correlate data in the high-quality regime as well as data at lower qualities. In addition, the presence of slip between vapor and liquid phases and of thermal nonequilibrium between the phases cause correlational difficulties. The general trend is evident, however. As would be expected, \bar{h}/h_{gc} asymptotically approaches unity as $1/X_{tt}$ becomes very large. By referring to the symbols and conditions for each experimental run summarized in Table IV, several things can be noted. The mass velocities in runs 114, 119, and 120 were lower than the mass velocities for other experimental runs. At the lower mass velocities the local heat transfer coefficients at the 0° and 270° positions behave irregularly and in general are much lower than the local heat transfer coefficients for runs with higher mass velocities. The local heat transfer coefficients at the 90° position for these runs are generally higher than those for other runs while the coefficients at the 180° position are about the same. The net effect of the variation of local coefficients is to make the circumferential average coefficients fall on the low side of coefficients for other runs. This behavior is probably due to flow patterns similar to those observed in the visual flow studies (Appendix B) where liquid was present at the 90° position in the form of a wavy stream but was not distributed to other portions of the tube wall.

There also appears to be an effect of heat flux on the heat transfer coefficients. Heat flux is included in the correlations of Schrock and Grossman (28) and Bennett, et al (3). The heat flux in runs 107 and 108 was lower than the heat flux for other experimental runs. The

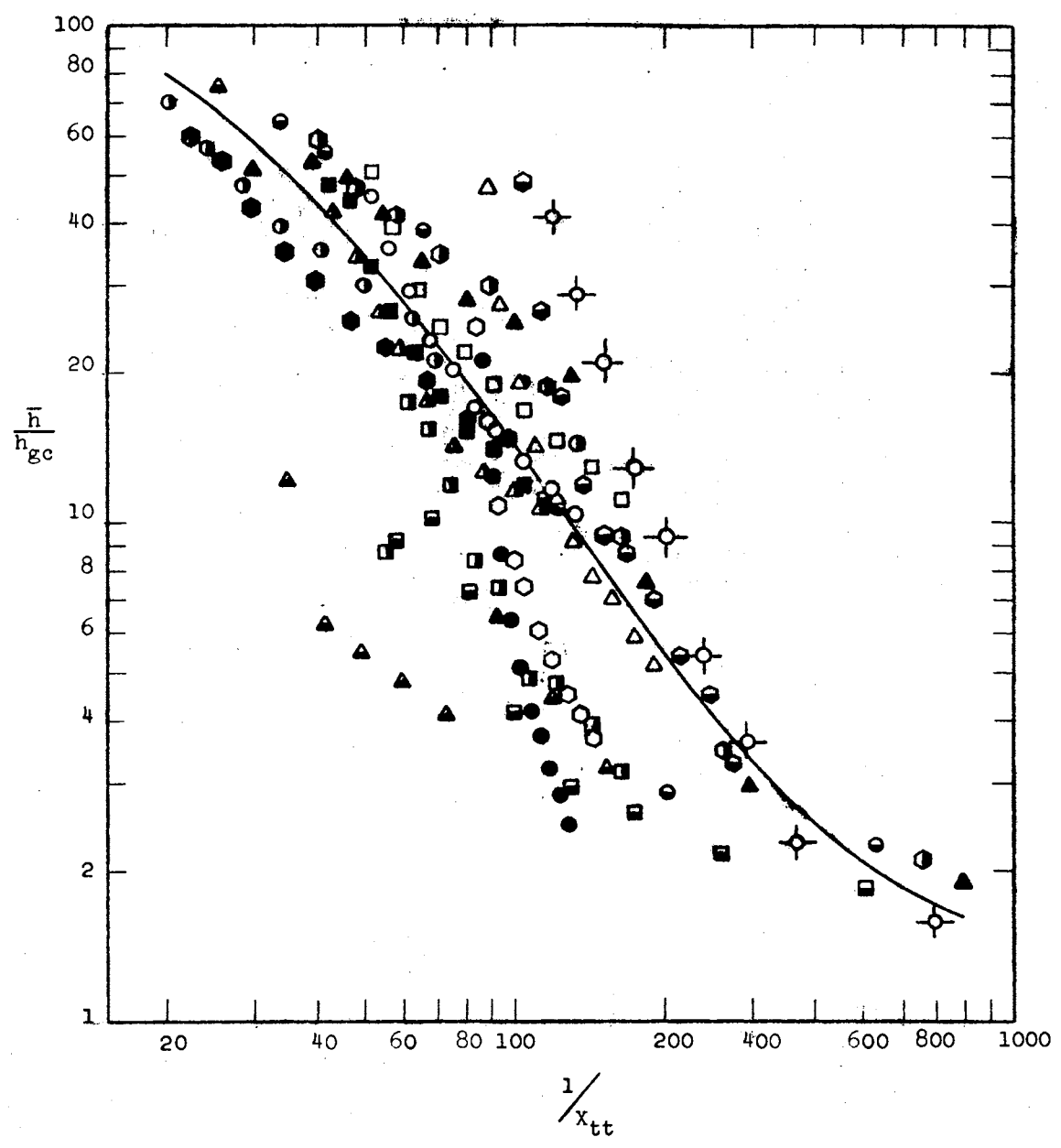


Figure 32. Correlation of Circumferential Average Heat Transfer Coefficients, Small Coil

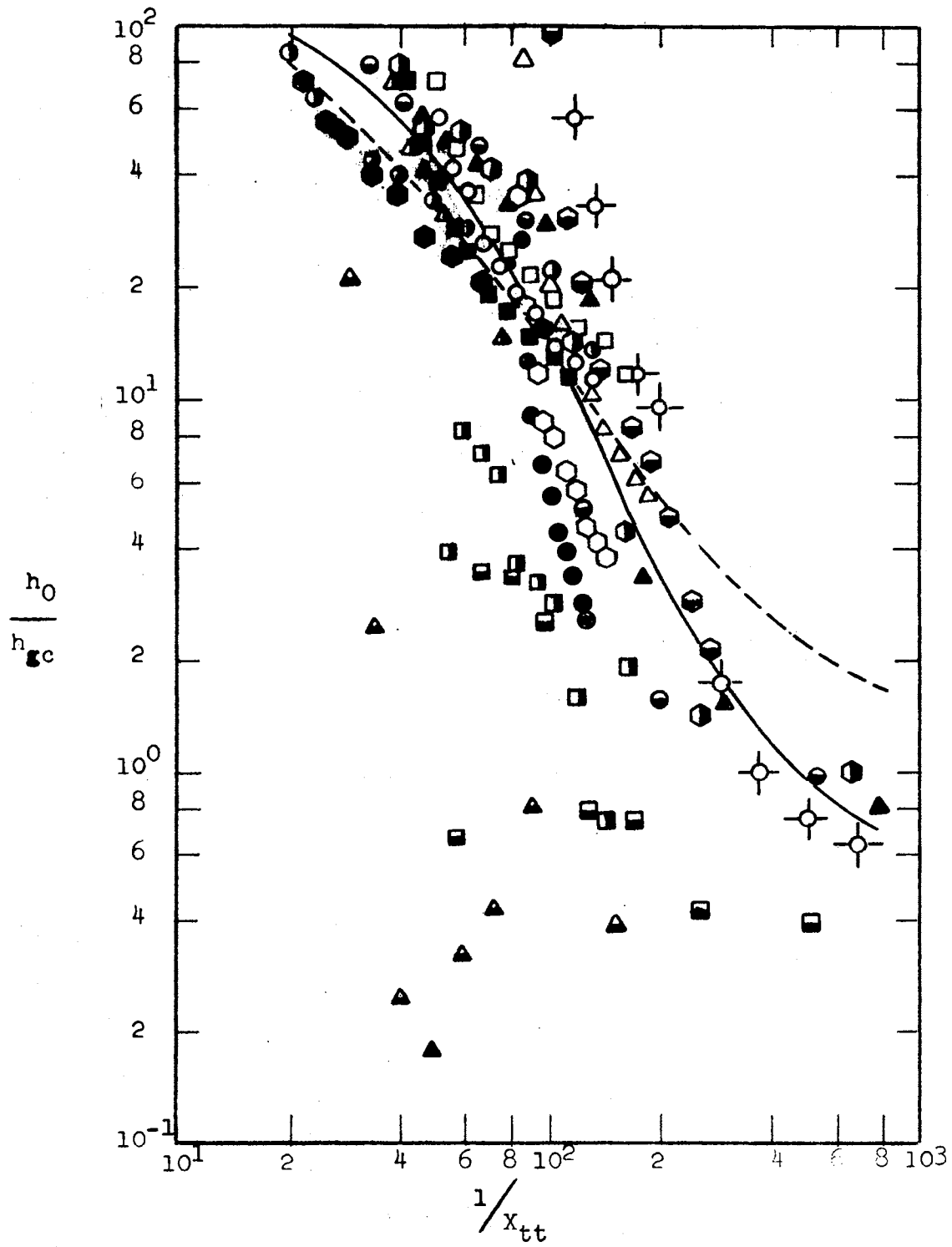


Figure 33. Correlation of Local Heat Transfer Coefficients, 0° Position, Small Coil

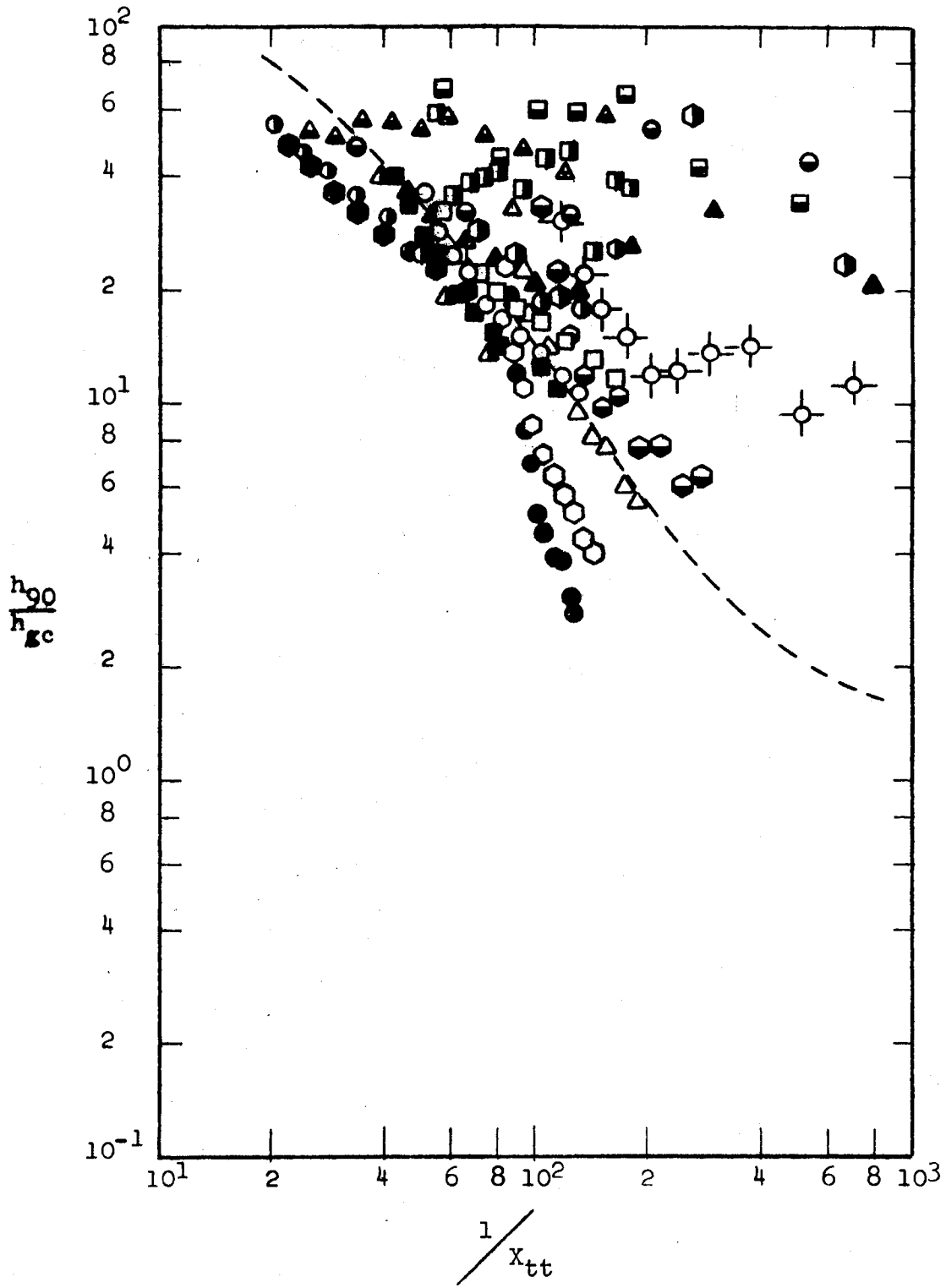


Figure 34. Correlation of Local Heat Transfer Coefficients, 90° Position, Small Coil

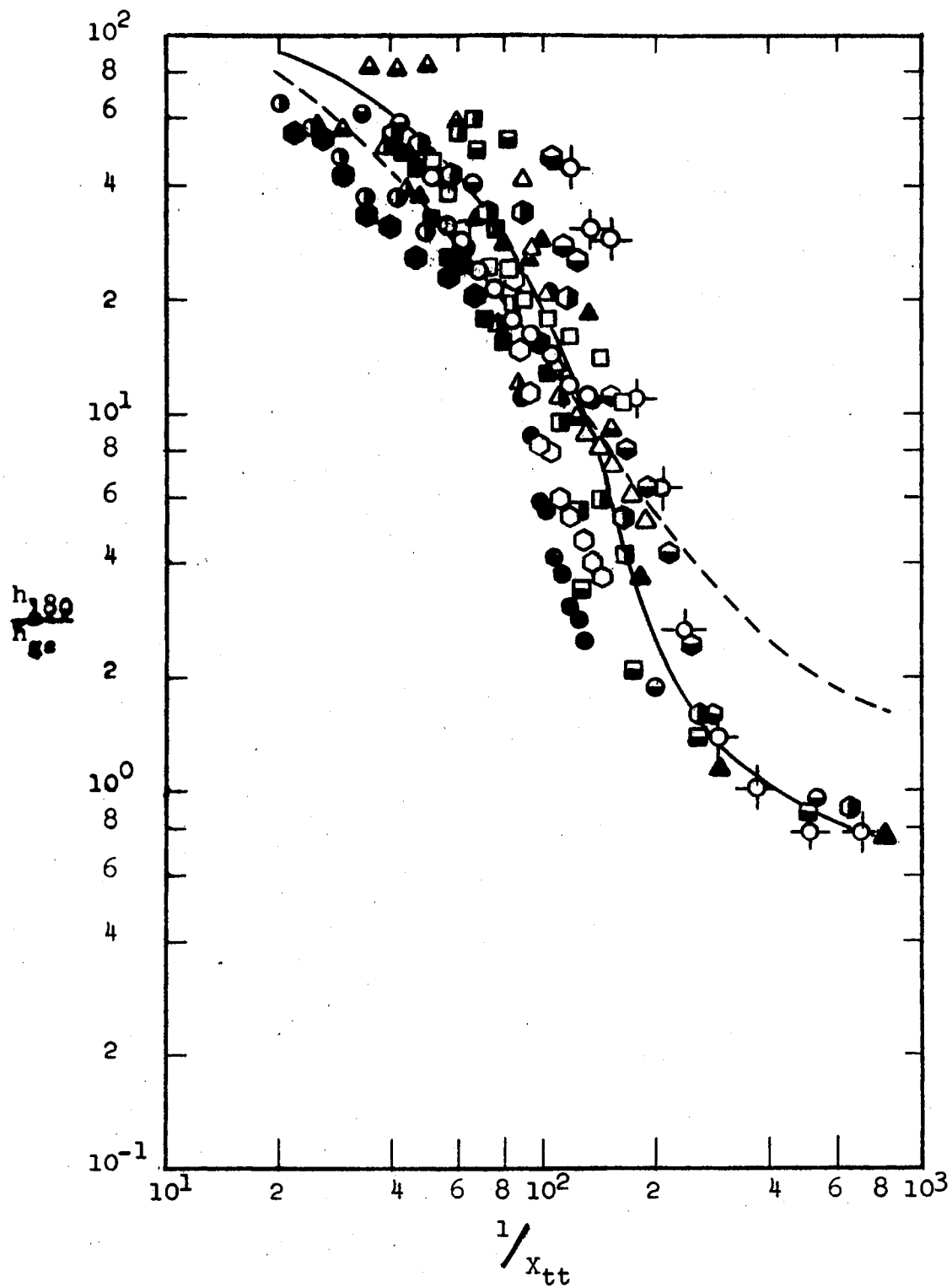


Figure 35. Correlation of Local Heat Transfer Coefficients, 180° Position, Small Coil

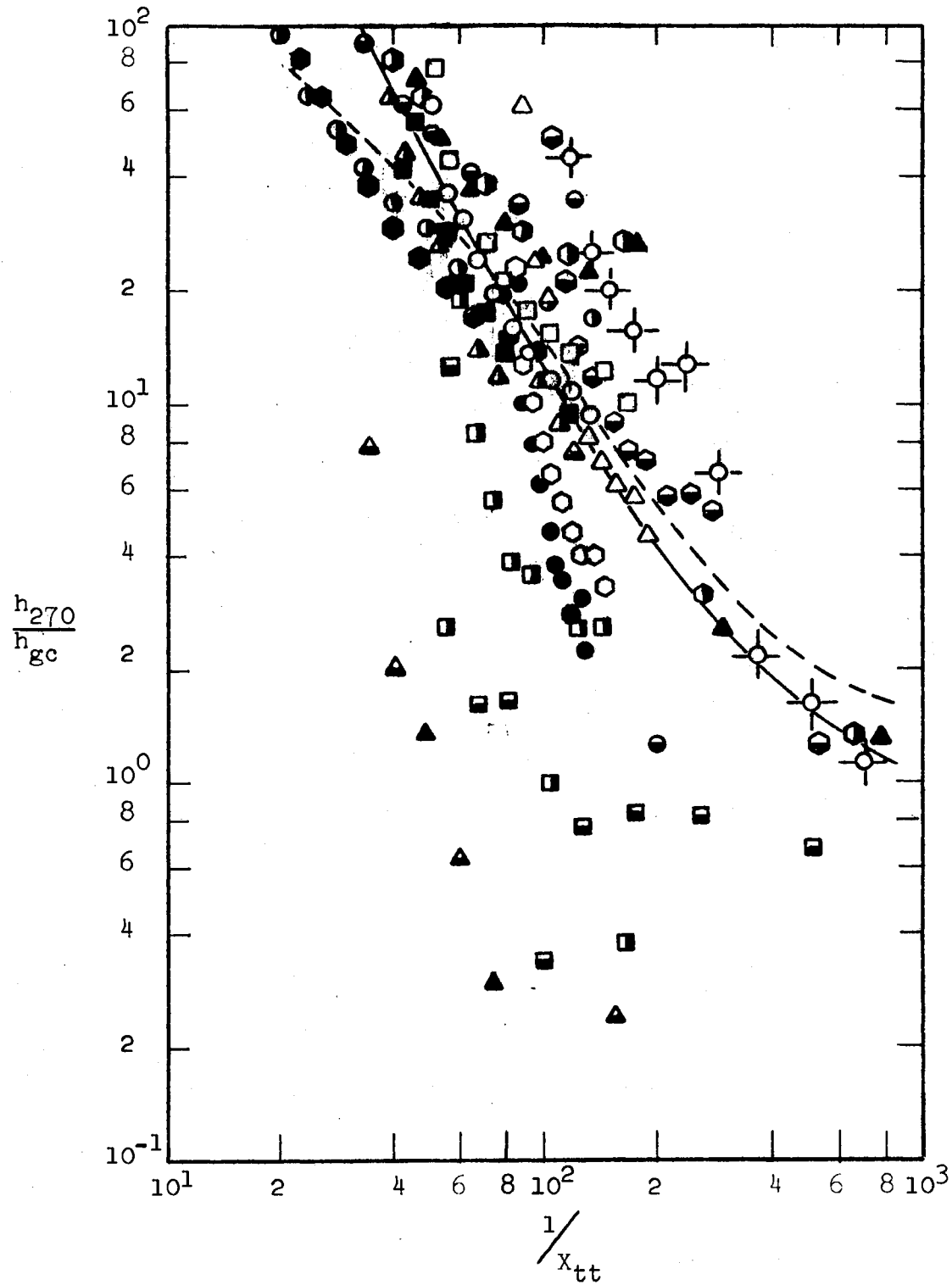


Figure 36. Correlation of Local Heat Transfer Coefficients, 270° Position, Small Coil

local and circumferential average heat transfer coefficients for these runs are lower than those for other runs. For purposes of comparing local heat transfer coefficients to the circumferential average heat transfer coefficients, the correlating line for the circumferential average heat transfer coefficients is shown as a dashed line in Figures 33 through 36. The local coefficients at the 0° , 180° , and 270° positions are lower than the circumferential average coefficients at higher qualities while the coefficients at the 90° position are much higher. This behavior is the result of the secondary circulation pattern, which evidently provides liquid at the 90° position even at very high qualities.

Correlations for the large coil are shown in Figures 37 through 41. They are similar to the small coil results in all respects. In comparing the heat transfer coefficients for the large and small coils it can be noted that the \bar{h}/h_{gc} values for the large coil are slightly higher than those for the small coil. This is probably due to the fact that values of h_{gc} for the large coil, as calculated from the Seban-McLaughlin equation, are about 7% lower than values of h_{gc} for the small coil.

The present correlation is compared to the correlations of Owhadi (22) and de La Harpe et al. (7) in Figure 42. In order to compare the correlations, results of the present study were presented as the ratio of the two-phase heat transfer coefficient to the heat transfer coefficient calculated as if the liquid were flowing alone in the coil, \bar{h}/h_{lc} . The results show a decrease in heat transfer efficiency starting at a value of $1/X_{tt}$ of about 50. This decrease was not noted by Owhadi. The correlation of de La Harpe et al. for liquid helium-I

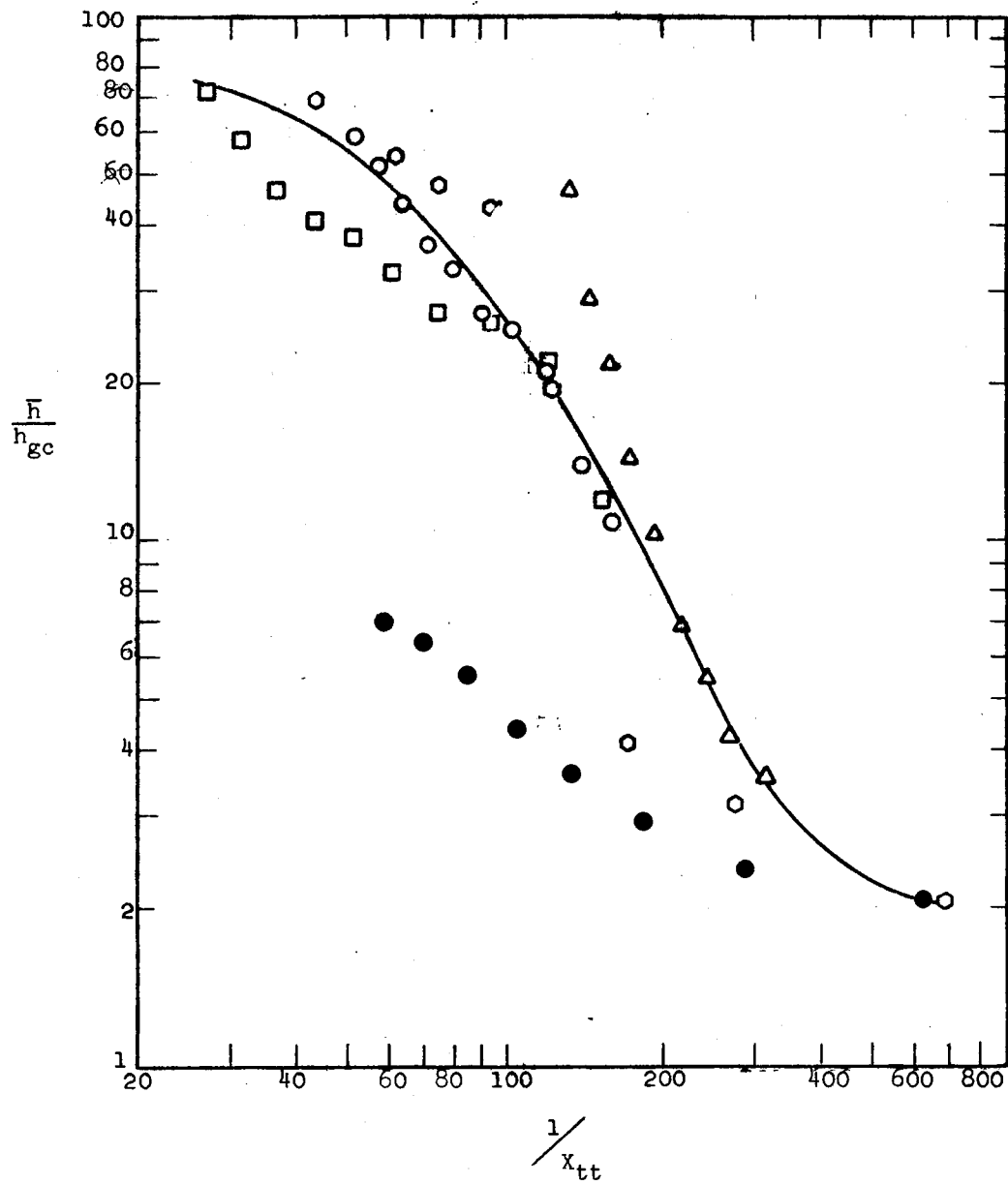


Figure 37. Correlation of Circumferential Average Heat Transfer Coefficients, Large Coil

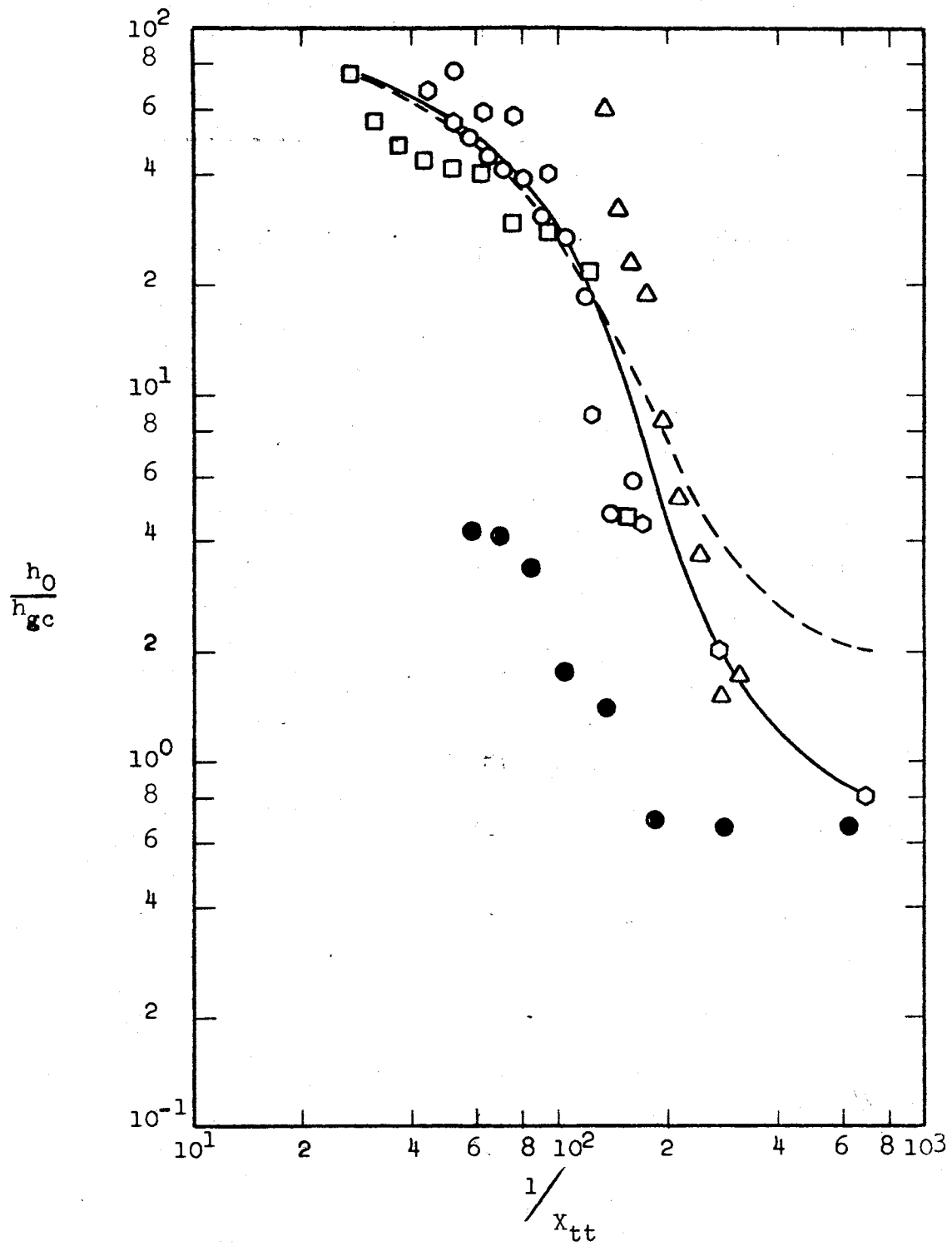


Figure 38. Correlation of Local Heat Transfer Coefficients, 0° Position, Large Coil

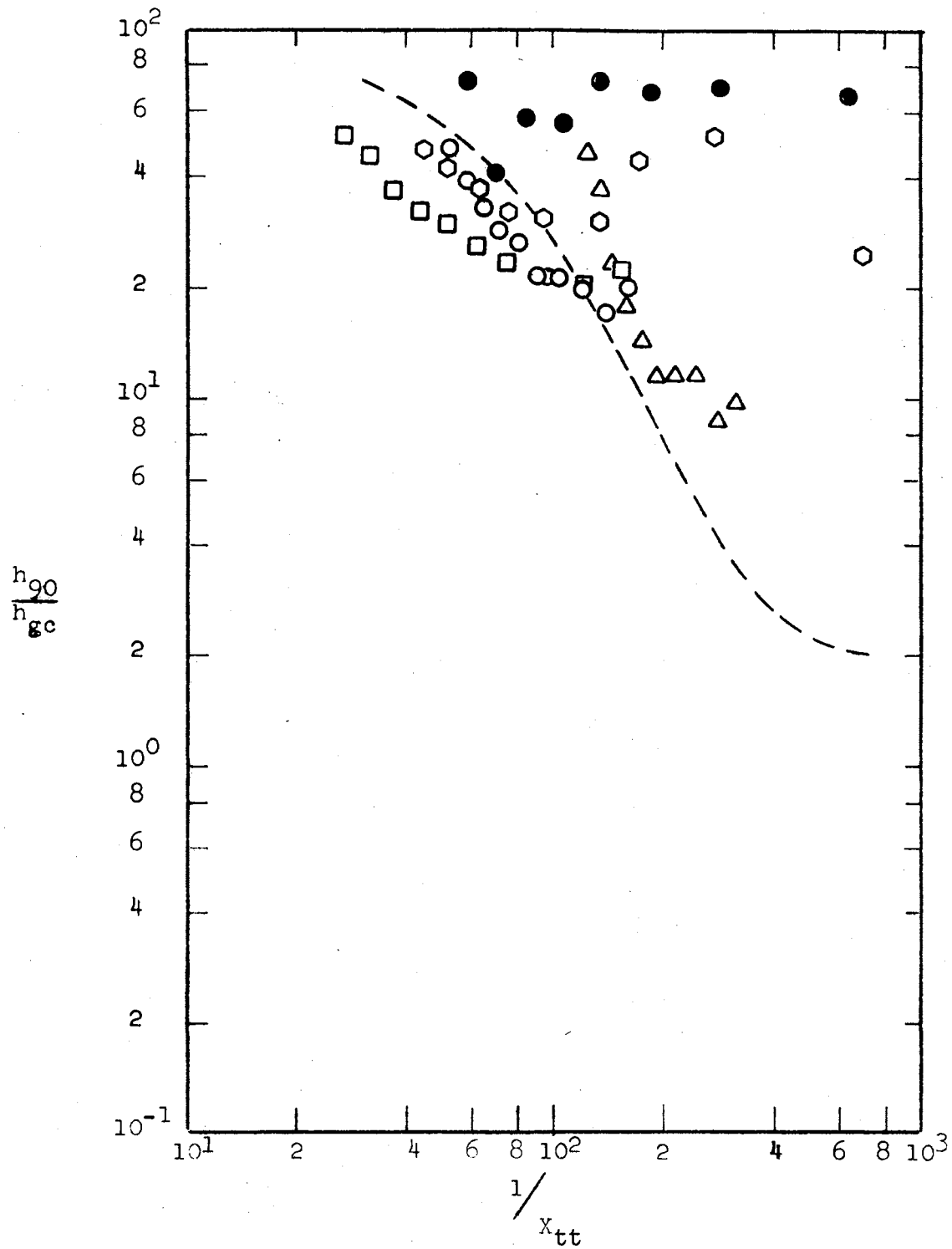


Figure 39. Correlation of Local Heat Transfer Coefficients, 90° Position, Large Coil

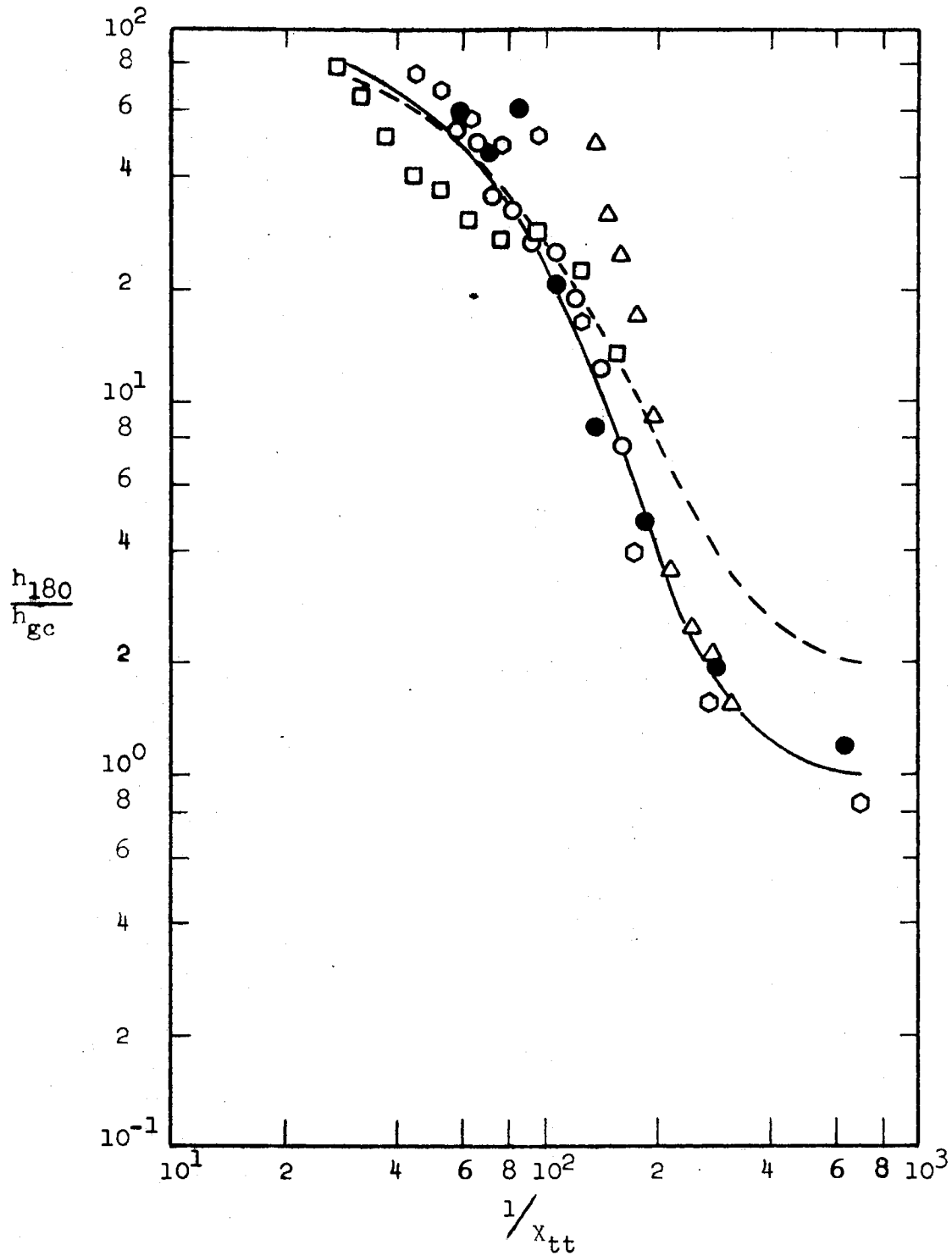


Figure 40. Correlation of Local Heat Transfer Coefficients, 180° Position, Large Coil

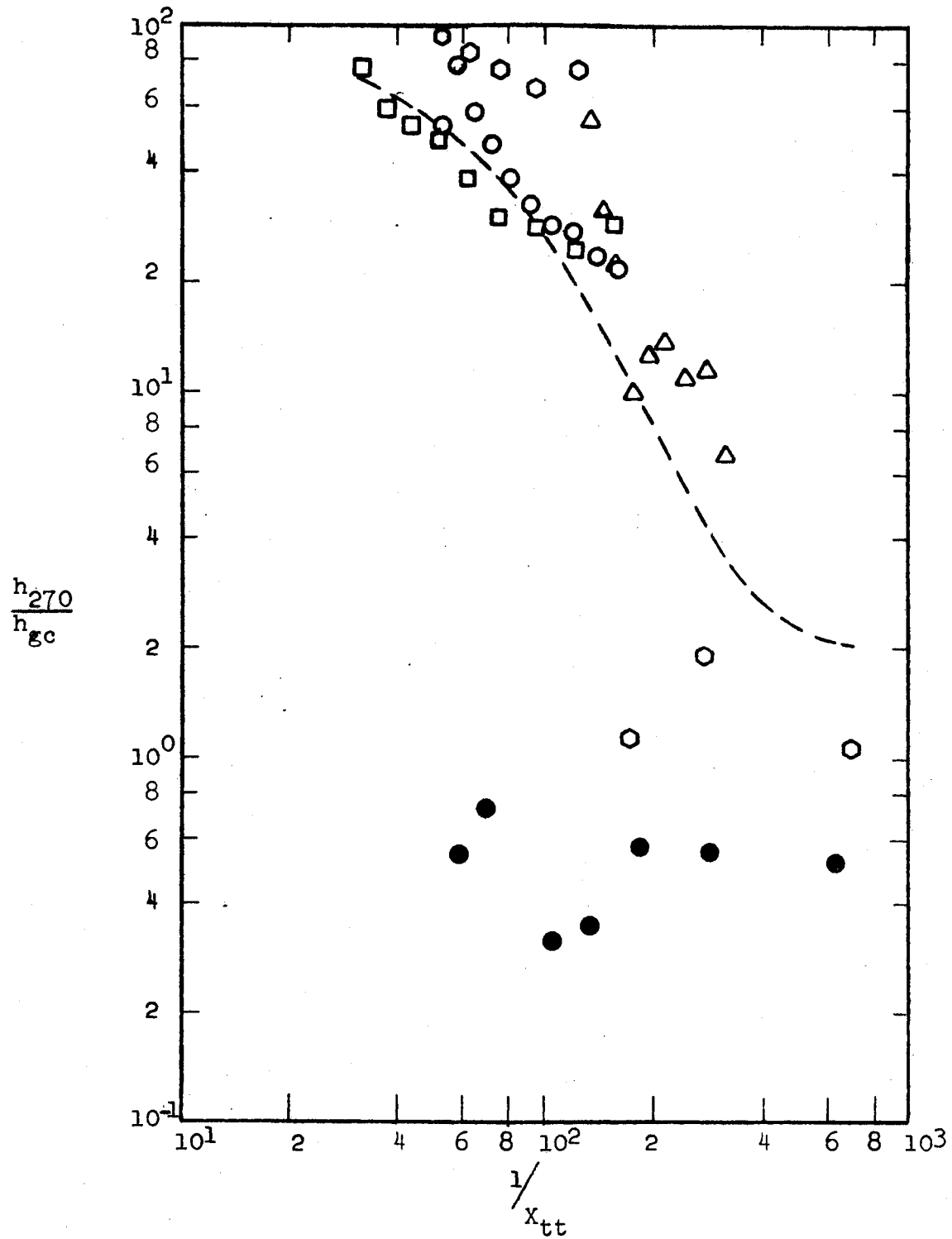


Figure 41. Correlation of Local Heat Transfer Coefficients, 270° Position, Large Coil

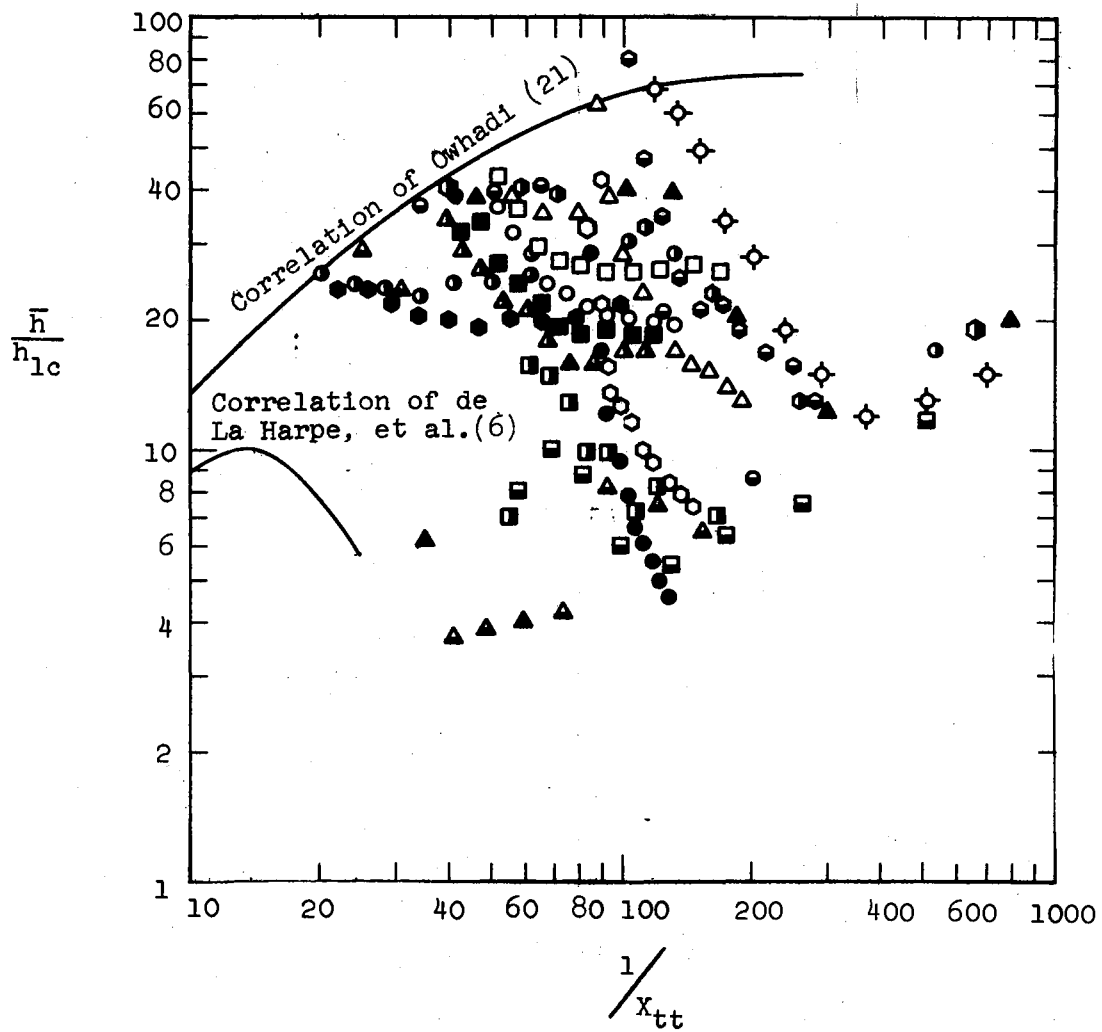


Figure 42. Comparison of Results with Results of Owhadi and de La Harpe, et al.

begins to decrease at a value of $1/X_{tt}$ of about 13. Figure 42 indicates that h_{1c} is not a satisfactory reducing variable for data in the high quality regime.

CHAPTER VII

CONCLUSIONS AND RECOMMENDATIONS

Forced convection heat transfer to high-quality two-phase mixtures of water and steam was studied in two helical coils with diameters of 9.99 and 20.64 inches. The coils were constructed of 0.495 inch ID stainless steel tubing in which heat was generated electrically. Local and circumferential heat transfer coefficients were correlated as a function of the Lockhart-Martinelli parameter. Studies were made of single-phase heat transfer and of system stability. A visual flow study was made with air-water mixtures in a transparent coil.

The secondary circulation is quite efficient in distributing liquid to the surface of the tube. Heat transfer coefficients at all circumferential positions remain high up to qualities of approximately 90%. At 90% vapor quality the heat transfer coefficients at the 0° and 180° positions decrease sharply and at a quality slightly greater than 90% the heat transfer coefficient at the 270° position decreases. The heat transfer coefficient at the 90° position remains substantial at qualities up to essentially 100%.

Visual observations confirm the presence of a secondary flow pattern and the presence of a slow-moving liquid stream at the 90° position. The study of system stability confirmed that an increase in mass velocity increases the system stability while an increase in heat flux

decreases the system stability. The large coil was more stable than the small coil.

Heat transfer results were correlated with the Lockhart-Martinelli parameter in the high-quality regime.

Further studies are needed to better define the effect of mass velocity on heat transfer. Equipment should be designed to allow a much larger variation of mass velocity while measuring more detailed circumferential temperature profiles. A fairly long coil with a short, highly-instrumented heated section would provide more detailed information on flow patterns.

SELECTED BIBLIOGRAPHY

- (1) Banerjee, S., E. Rhodes, and D. S. Scott, "Pressure Drops, Flow Patterns, and Holdup in Helically Coiled Tubes," Preprint 24C presented at the Second Joint AIChE-IIQPR Meeting, Tampa, Fla. (1968).
- (2) Bell, K. J., and A. Owhadi, "Local Heat Transfer Measurements During Forced Convection Boiling in a Helically Coiled Tube," Symp. on Measurements in Two-Phase Flow, University of Leeds, United Kingdom (1969).
- (3) Bennett, J. A. R., J. G. Collier, H. R. C. Pratt, and J. D. Thornton, "Heat Transfer to Two-Phase Gas-Liquid Systems," AERE Report AERE-R3159 (1956).
- (4) Bergles, A. E., L. S. Tong, and J. A. Boure, "Review of Two-Phase Flow Instability," Preprint 71-HT-42 presented at the ASME-AIChE Heat Transfer Conference, Tulsa, Okla. (1971).
- (5) Carver, J. R., C. R. Kakarala, and J. S. Slotnik, "Heat Transfer in Coiled Tubes with Two-Phase Flow," AED Document TID 20983 (1964).
- (6) Chen, J. C., "A Correlation for Boiling Heat Transfer to Saturated Fluids in Convective Flow," ASME Paper 63-HT-34 (1963).
- (7) de La Harpe, A., S. Lehongre, J. Mollard, and C. Johannes, "Boiling Heat Transfer and Pressure Drop of Liquid Helium-I Under Forced Circulation in a Helically Coiled Tube," Advances in Cryogenic Engineering, 14, 170 (1968).
- (8) Dengler, C. E., and J. N. Addoms, "Heat Transfer Mechanism for Vaporization of Water in a Vertical Tube," CEP Symposium Series, 52, No. 18, 95 (1956).
- (9) Dravid, A. N., K. A. Smith, E. W. Merrill, and P. L. T. Brian, "Effect of Secondary Fluid Motion on Laminar Flow Heat Transfer in Helically Coiled Tubes," AIChE Journal, 17, No. 5, 1114 (1971).
- (10) Hendricks, R. C., and F. F. Simon, "Heat Transfer to Hydrogen Flowing in a Curved Tube," Multi-Phase Flow Symposium-ASME, New York, 90 (1963).

- (11) Ito, H., "Friction Factors for Turbulent Flow in Curved Pipes," ASME Journal of Basic Engineering, D, 81, 123 (1959).
- (12) Keenan, J. H., and F. G. Keyes, Thermodynamic Properties of Steam, 1st edition, 26th printing, John Wiley, New York (1954).
- (13) Kreith, F., and D. Margolis, "Heat Transfer and Friction in Swirling Turbulent Flow," Proc. Heat Transfer and Fluid Mech. Inst. (1958).
- (14) Kubair, V., and N. R. Kuloor, "Heat Transfer to Newtonian Fluids in Coiled Pipes in Laminar Flow," Int. J. Heat Mass Transfer, 9 (1966).
- (15) Lockhart, R. W., and R. C. Martinelli, "Proposed Correlation of Data for Isothermal Two-Phase, Two-Component Flow in Pipes," Chem. Eng. Prog., 45, 39 (1949).
- (16) Martinelli, R. C., and D. B. Nelson, "Prediction of Pressure During Forced Circulation Boiling of Water," Trans. ASME, 70, 695 (1948).
- (17) Miropolskiy, Z. L., K. Annadudiyev, and A. Kakabaev, "Heat Transfer and Pressure Drop in the Heating and Cooling of Liquids in Curvilinear Channels," Int. Chem. Eng., 9, No. 3, 410 (1969).
- (18) Miropolskiy, Z. L., and V. Y. Pikus, "Critical Boiling Heat Fluxes in Curved Channels," Heat Transfer-Soviet Research, 1, No. 1, 74 (1969).
- (19) Miropolskiy, Z. L., V. J. Pikus, and M. E. Shitsman, "Regimes of Deteriorated Heat Transfer at Forced Flow of Fluids in Curvilinear Channels," Proc. Third Int. Heat Transfer Conf., II, 95 (1966).
- (20) Mori, Y., and W. Nakayama, "Study on Forced Convection Heat Transfer in Curved Pipes (1st Report--Laminar Region)," Int. J. Heat Mass Transfer, 8, 67 (1965).
- (21) Mori, Y., and W. Nakayama, "Study on Forced Convection Heat Transfer in Curved Pipes (2nd Report--Turbulent Region)," Int. J. Heat Mass Transfer, 10, 37 (1967).
- (22) Owhadi, A., "Boiling in Self-Induced Radial Acceleration Fields," Ph. D. Thesis, Oklahoma State Univ., Stillwater (1966).
- (23) Owhadi, A., and K. J. Bell, "Forced Convection Boiling Inside Helically Coiled Tubes," Int. J. Heat Mass Transfer, 10, 397 (1967).
- (24) Owhadi, A., K. J. Bell, and B. Crain, Jr., "Forced Convection Boiling Inside Helically Coiled Tubes," Int. J. Heat Mass Transfer, 11, 1779 (1968).

- (25) Perry, J. H., ec., Chemical Engineers' Handbook, 3rd edition, McGraw-Hill, New York (1950).
- (26) Rippel, G. R., C. M. Eidt, Jr., and H. B. Jordan, Jr., "Two-Phase Flow in a Coiled Tube," I and EC Proc. Design and Development, 5, No. 1, 32 (1966).
- (27) Rogers, G. F. C., and Y. R. Mayhew, "Heat Transfer and Pressure Loss in Helically Coiled Tubes with Turbulent Flow," Int. J. Heat Mass Transfer, 7, 1207 (1964).
- (28) Schrock, V. E., and L. M. Grossman, "Forced Convection Boiling in Tubes," Nucl. Sci. and Eng., 12, 474 (1962).
- (29) Seban, R. A. and E. F. McLaughlin, "Heat Transfer in Tube Coils with Laminar and Turbulent Flow," Int. J. Heat Mass Transfer, 6, 387 (1963).
- (30) Wattendorf, F. L., "A Study of the Effect of Curvature of Fully Developed Turbulent Flow," Proc. Royal Soc. London, A, 148, 565 (1934).
- (31) White, C. M., "Streamline Flow Through Curved Pipes," Proc. Royal Soc. London, A, 123, 645 (1929).
- (32) Yudovich, A., "Forced Convection Boiling in a Coil," M. S. Thesis, Oklahoma State Univ., Stillwater, Okla. (1966).

APPENDIX A -

NUMERICAL SOLUTION OF WALL TEMPERATURE
GRADIENT FOR A COILED TUBE WITH INTERNAL HEAT
GENERATION IN THE WALL

NUMERICAL SOLUTION OF WALL TEMPERATURE GRADIENT
FOR A COILED TUBE WITH INTERNAL HEAT
GENERATION IN THE WALL

The process used to bend a straight tube into a coil produces changes in the dimensions of the wall. This process involves filling of the tube with a relatively incompressible substance, bending of the tube around a mandrel of appropriate diameter, and dissolving of the incompressible filler. Using this method the elliptical deformation of the tube wall is minimized. The elliptical deformation of the two coils used in this study was measured and the results are shown in Table VIII.

The principal effect of bending is the thickening of the tube wall on the side nearest the axis of the helix and the thinning of the tube wall on the side farthest from the axis of the helix. The effects of variable wall thickness on heat conduction with electrical heat generation are twofold:

- 1) The distance for radial heat conduction varies around the circumference of the tube.
- 2) The cross-sectional area for axial electrical conduction varies around the circumference of the tube.

In addition, the axial length of the electrical conduction path varies around the circumference of the tube. The following discussion describes the geometrical considerations taken in the numerical solution of the wall temperature gradient.

Heat Balance on Incremental Element

Consider a small element in the wall of a straight tube as shown in Figure 43a. When the straight tube is bent into a helix, the cylindrical element becomes deformed, an exaggerated view of which is shown in Figure 43b. A steady state heat balance may be written around the element. The following assumptions are utilized in the derivation:

TABLE VIII
VARIATION IN OUTSIDE DIAMETER OF THE COILS

Station	Axial Dist., ft.	Small Coil		Large Coil	
		Major Dia., in.	Minor Dia., in.	Major Dia., in.	Minor Dia., in.
1	1	0.637	0.614	0.630	0.626
2	2	0.637	0.613	0.631	0.625
3	3	0.637	0.614	0.630	0.626
4	4	0.635	0.616	0.631	0.625
5	5	0.634	0.617	0.630	0.625
6	6	0.636	0.618	0.631	0.625
7	7	0.635	0.618	0.630	0.625
8	8	0.635	0.618	0.631	0.626
9	9	0.635	0.618	0.631	0.625
10	9.75	0.635	0.618	0.630	0.625

Average major diameter, small coil = 0.636 in.
 Average minor diameter, small coil = 0.616 in.
 Average major diameter, large coil = 0.631 in.
 Average minor diameter, large coil = 0.625 in.

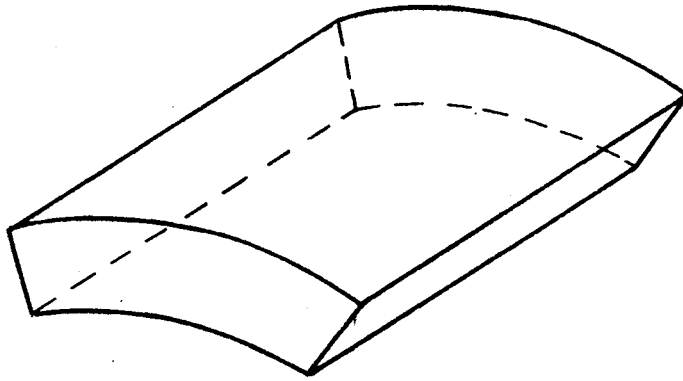


Figure 43a. Cylindrical Element

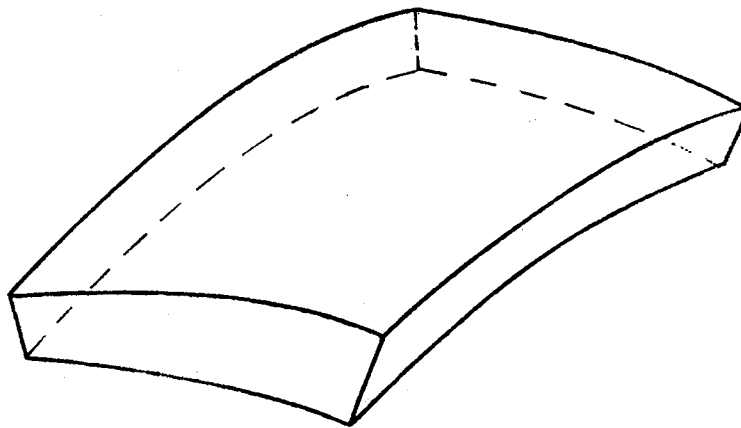


Figure 43b. Skewed Element

Figure 43. Effect of Bending on Tube Wall

- 1) The ellipticity of the tube is neglected.
- 2) Axial conduction of heat is neglected.
- 3) Electrical current flows parallel to the axis.
- 4) The pitch of the helix is neglected, i.e., the tube axis is planar.

Figure 44a shows a cross section of the tube with element (i,j) and its surrounding elements. Figure 44b is an enlargement of element (i,j) showing geometrical features of interest. A steady state heat balance around element (i,j) following the convention that heat in is positive yields the following result:

$$\begin{aligned}
 & \textcircled{2} \quad \bar{k}(i,j)(i,j-1) [T(i,j-1) - T(i,j)] \frac{a\phi(i,j)}{d\phi(i,j)} \quad \frac{D_{14}}{hr-ft^2-F} \quad \frac{ft^2}{ft} \\
 & \textcircled{3} \quad + \bar{k}(i,j)(i,j+1) [T(i,j+1) - T(i,j)] \frac{a\phi(i,j+1)}{d\phi(i,j+1)} \\
 & + \bar{k}(i,j)(i-1,j) [T(i-1,j) - T(i,j)] \frac{a_r(i,j)}{d_r(i,j)} \quad \textcircled{1} \\
 & + \bar{k}(i,j)(i+1,j) [T(i+1,j) - T(i,j)] \frac{a_r(i+1,j)}{d_r(i+1,j)} \\
 & - 3,413 \rho_e(i,j) \frac{d_z(i,j)}{a_z(i,j)} I(i,j)^2 = 0 \quad (A-1)
 \end{aligned}$$

where \bar{k} is the average thermal conductivity between two adjacent elements, a is the area for conduction between two adjacent elements, d is the distance for conduction between the centroids of two adjacent elements, ρ_e is the electrical resistivity of the element, and I is the electrical current flowing in the element. Solving equation (A-1) for $T(i+1,j)$ yields:

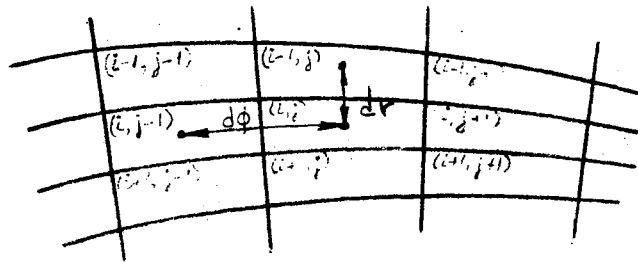


Figure 44a. Cross-Section of Tube Wall

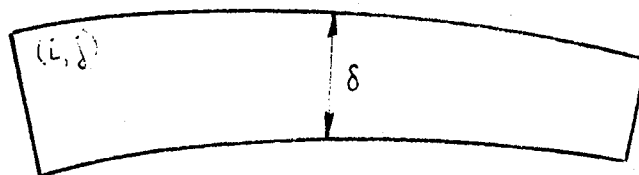


Figure 44b. Cross-Section of Element
(i, j)

Figure 44. Tube Cross-Sections

$$\begin{aligned}
T(i+1,j) = & \frac{a\phi(i,j)}{d\phi(i,j)} \frac{d_r(i+1,j)}{a_r(i+1,j)} \frac{\bar{k}(i,j)(i,j-1)}{\bar{k}(i,j)(i+1,j)} [T(i,j) - T(i,j-1)] \\
& + \frac{a\phi(i,j+1)}{d\phi(i,j+1)} \frac{d_r(i+1,j)}{a_r(i+1,j)} \frac{\bar{k}(i,j)(i,j-1)}{\bar{k}(i,j)(i+1,j)} [T(i,j) - T(i,j+1)] \\
& + \frac{a_r(i,j)}{d_r(i,j)} \frac{d_r(i+1,j)}{a_r(i+1,j)} \frac{\bar{k}(i,j)(i-1,j)}{\bar{k}(i,j)(i+1,j)} [T(i,j) - T(i-1,j)] \leftarrow \\
& - 3,413 \frac{d_r(i+1,j)}{a_r(i+1,j)} \frac{1}{\bar{k}(i,j)(i+1,j)} \frac{d_z(i,j)}{a_z(i,j)} \rho_e(i,j) I(i,j)^2 \\
& + T(i,j) \tag{A-2}
\end{aligned}$$

Equation (A-2) is the basic equation for the numerical solution of the wall temperature gradient. Given the point-wise temperature distribution on the outer surface of the tube (measured by thermocouples), a stepping solution gives the temperatures of the elements in the second ring from the surface. In this manner the temperature distribution on the inner surface may be determined. The solution also yields the heat flux distribution on the inner surface. An iterative solution is necessary to take into account the temperature dependence of the thermal conductivity and electrical resistivity. An initial temperature distribution is assumed and properties are evaluated at the assumed temperature. At the end of the first iteration the properties are re-evaluated at the calculated temperature. This process is repeated until the calculated temperature distribution ceases to change. Special heat balance equations are required for the elements at the outer surface of the tube. In these special equations the term describing radial conduction in the outward direction is replaced with a term

describing heat loss through the outer insulation (obtained via calibration).

The solution of the wall temperature gradient requires the evaluation of the distances and areas for conduction between adjacent elements and the distance and area for electrical conduction through the elements. The skewed nature of the elements makes the equations describing the geometrical features fairly complex. It is possible to make all of the equations rigorous. In some cases, however, it was possible to use a numerical approximation without adversely affecting the accuracy of the solution.

Heat Conduction Distances and Areas for Adjacent Elements

The distance for radial heat conduction between two adjacent elements (shown in Figure 44a) can be expressed as:

$$d_r = \frac{\delta}{n} \quad (\text{A-3})$$

where δ is the wall thickness at the center of the element in question and n is the number of slices into which the tube wall has been divided. The wall thickness is a function of the angular position of the center of the element, ϕ , as shown in Figure 45 and has been expressed by Owhadi (22) as:

$$\delta = \delta_m \left(\frac{R}{R - r_m \sin \phi} \right) \quad (\text{A-4})$$

where δ_m and r_m are the wall thickness and mean radius of the tube before bending and R is the radius of the helix. Substituting equation (A-4) into equation (A-3) yields the expression for the distance for

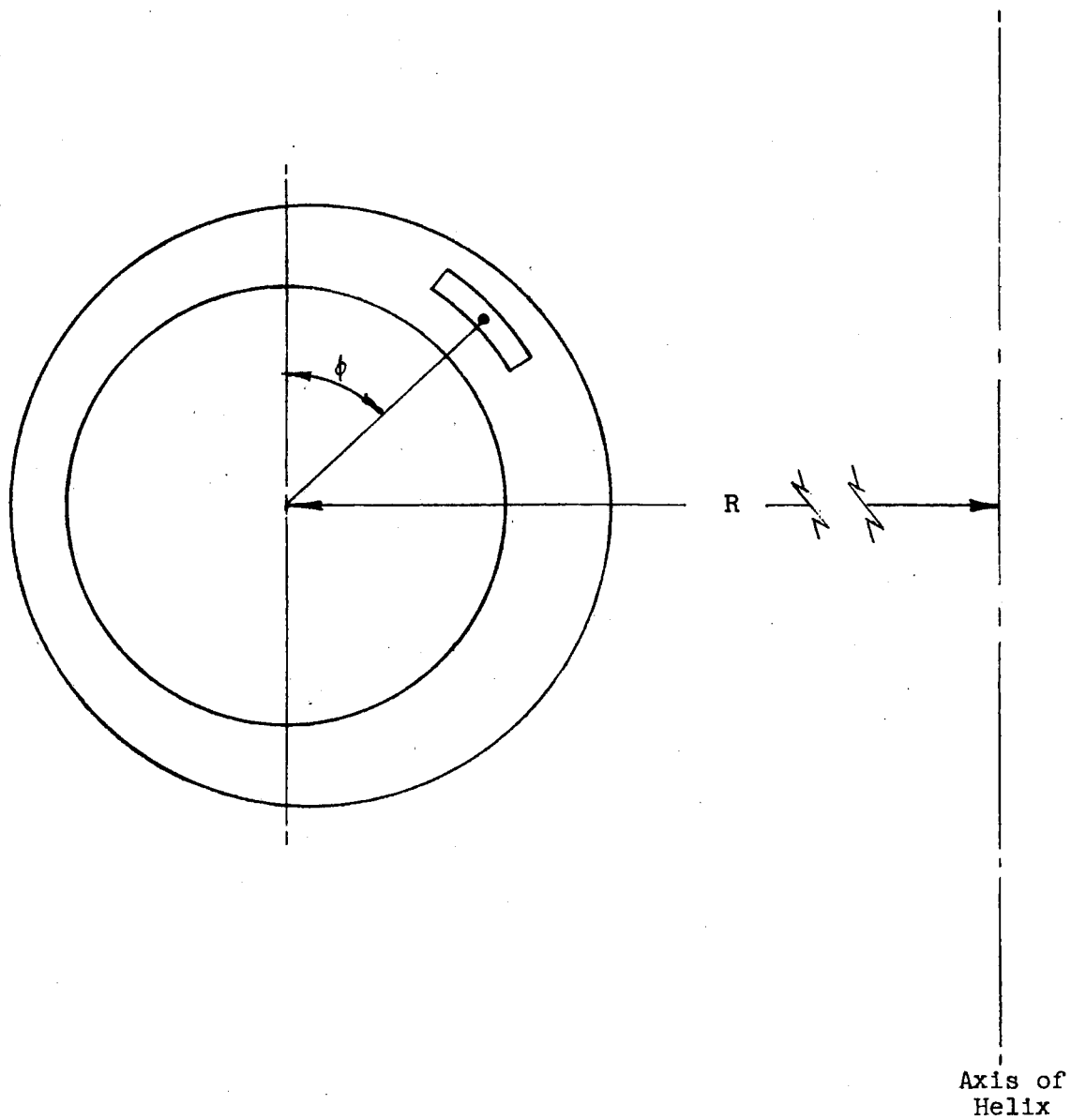


Figure 45. Angular Position of Incremental Element

radial conduction between two adjacent elements as a function of the angular position of the element:

$$d_r = \frac{\delta_m}{n} \left(\frac{R}{R - r_m \sin \phi} \right) \quad (\text{A-5})$$

The angular distance for heat conduction between two adjacent elements, d_ϕ , is a function of both angular and radial position in the tube wall. This distance is taken as the distance along a curved line between the centers of two adjacent elements where the line lies midway between the radial boundaries of the elements. The length of this line can be approximated as the arc of a circle subtended by the angular increment $\Delta\phi$, where the circle has a radius equal to the mean of the two radii from the center of the tube to the centers of the two adjacent elements, or:

$$d_\phi = \bar{r}_\phi \Delta\phi \quad (\text{A-6})$$

The mean radius is a function of the angular position of the element and for element (i,j) can be written as:

$$\bar{r}_\phi = r_m + \frac{\delta_m}{2} \left(\frac{n-2i+1}{n} \right) \left(\frac{R}{R - r_m \sin \phi} \right) \quad (\text{A-7})$$

Substituting equation (A-7) into (A-6), the angular distance for heat conduction between two adjacent elements becomes:

$$d_\phi = \left[r_m + \frac{\delta_m}{2} \left(\frac{n-2i+1}{n} \right) \left(\frac{R}{R - r_m \sin \phi} \right) \right] \Delta\phi \quad (\text{A-8})$$

Derivations similar to the ones above yield the following equations for the areas for radial and angular heat conduction, respectively:

$$a_r = \left[R - r_m \sin \phi - \frac{\delta_m}{2} \left(\frac{n-2i+2}{n} \right) \left(\frac{R \sin \phi}{R - r_m \sin \phi} \right) \right] \left[r_m + \frac{\delta_m}{2} \left(\frac{n-2i+2}{n} \right) \left(\frac{R}{R - r_m \sin \phi} \right) \right] \theta \Delta \phi \quad (A-9)$$

$$a_\phi = \frac{\delta_m}{2} \left(\frac{R}{R - r_m \sin \phi} \right) \left[R - r_m \sin \phi - \frac{\delta_m}{2} \left(\frac{n-2i+1}{2} \right) \left(\frac{R \sin \phi}{R - r_m \sin \phi} \right) \right] \theta \quad (A-10)$$

where θ is the angle that subtends a one-foot length of coil as measured along the axis of the tube.

Distance and Area for Electrical Conduction

The length for electrical conduction along an increment is a function of the radial and angular position and can be expressed as:

$$d_z = \left[R - r_m \sin \phi - \frac{\delta_m}{2} \left(\frac{n-2i+1}{n} \right) \left(\frac{R \sin \phi}{R - r_m \sin \phi} \right) \right] \theta \quad (A-11)$$

The area for electrical conduction can be obtained by integration of the cross-sectional area of an increment:

$$a_z = \int_{\phi_1}^{\phi_2} \int_{r_1}^{r_2} r \, dr \, d\phi \quad (A-12)$$

Performing the inner integration and substituting:

$$a_z = \frac{r_m \delta_m R}{n} \int_{\phi_1}^{\phi_2} \frac{d\phi}{R - r_m \sin \phi} + \left(\frac{n-2i+1}{2} \right) \left(\frac{\delta_m R}{n} \right)^2 \int_{\phi_1}^{\phi_2} \frac{d\phi}{(R - r_m \sin \phi)^2} \quad (A-13)$$

The area for each element is calculated via numerical integration of equation (A-13).

Results of Solution

Typical results of the numerical solution are shown in Figures 46 through 48. Plotted in these figures are the inside and outside temperature distribution and the heat flux distribution for the inner wall. Also shown on the figures is a comparison of the experimentally measured coil power generation and the power generation calculated via the numerical solution. Agreement is excellent in all cases.

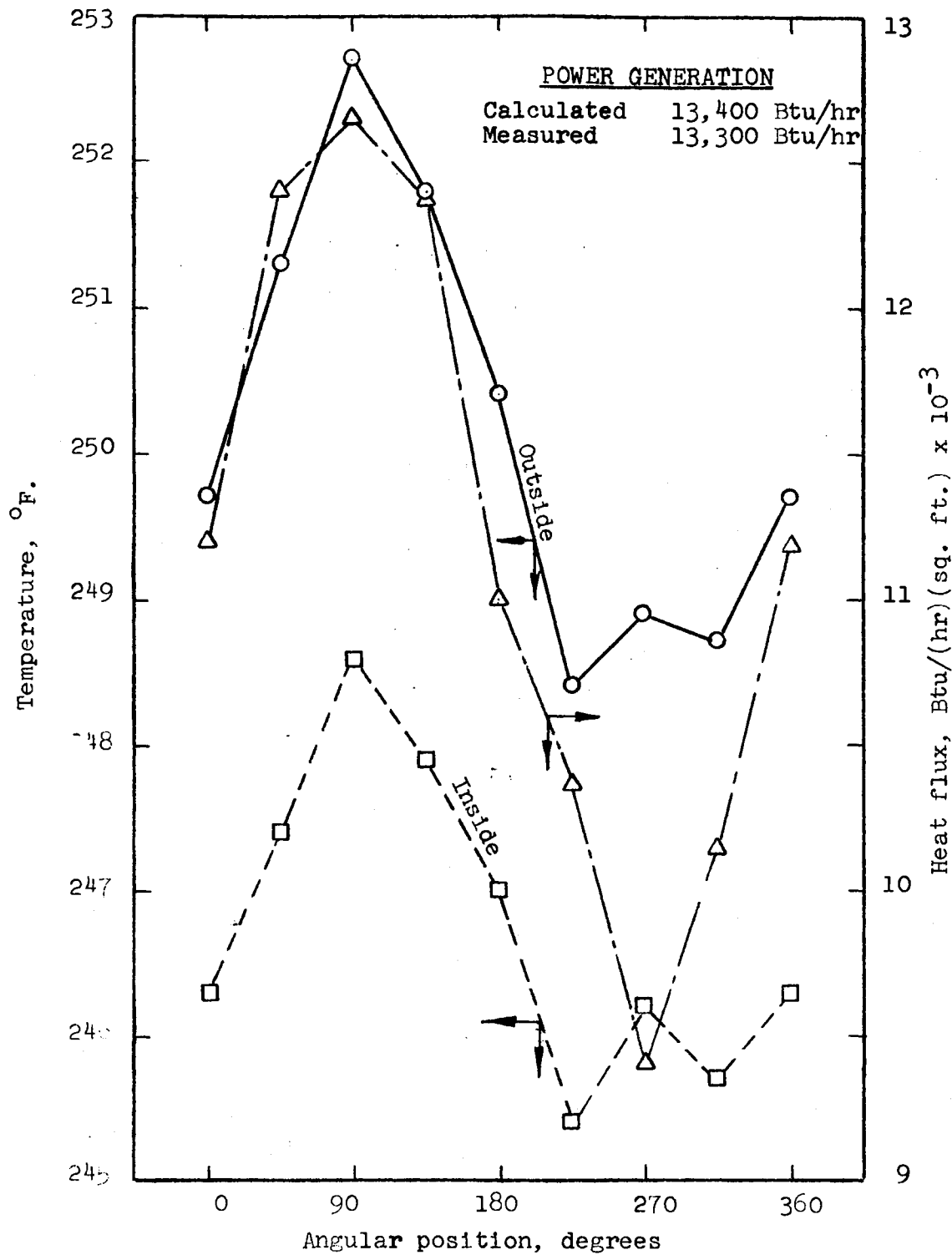


Figure 46. Temperature Profiles for Run 104, Station 2

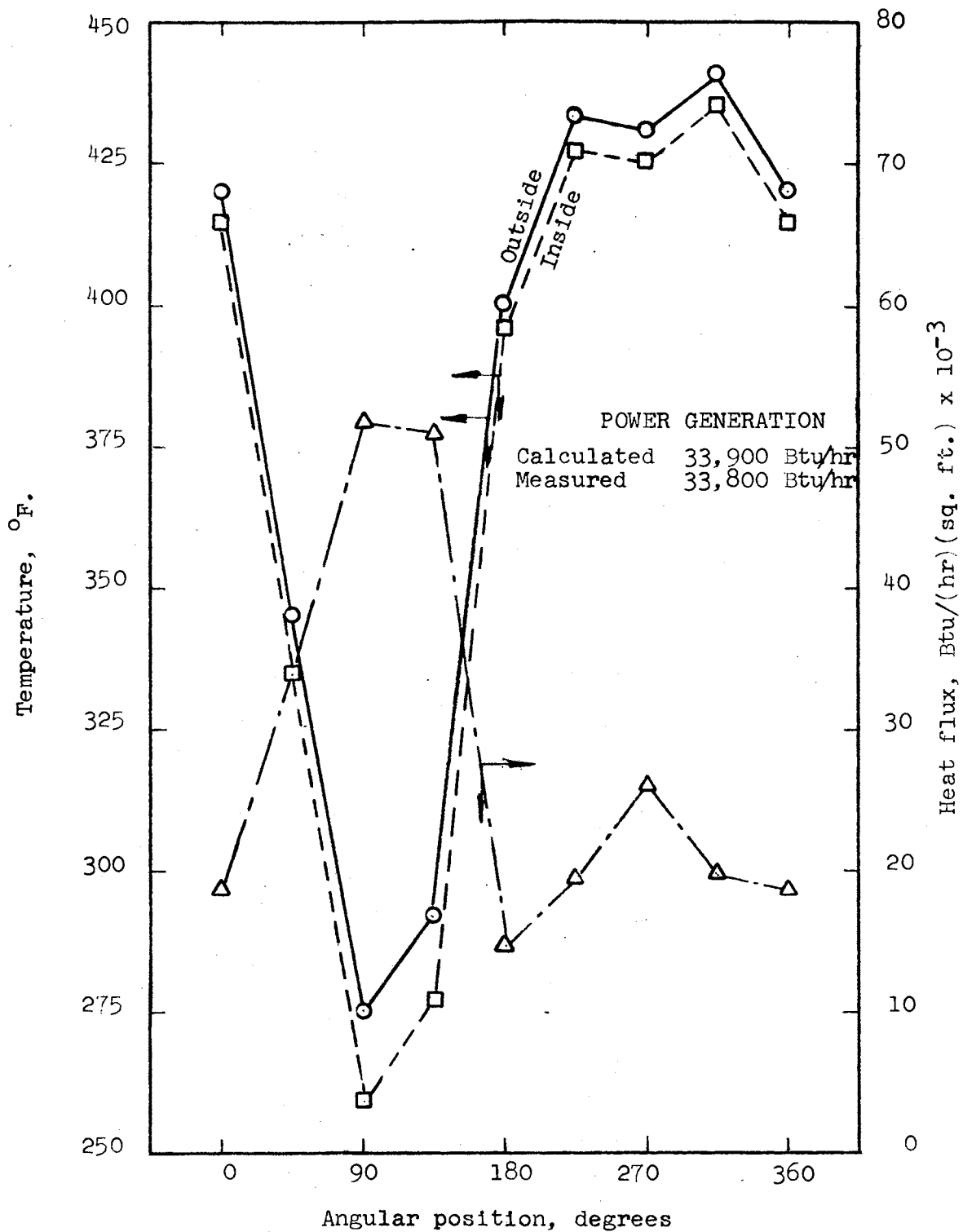


Figure 47. Temperature Profiles for Run 117, Station 9

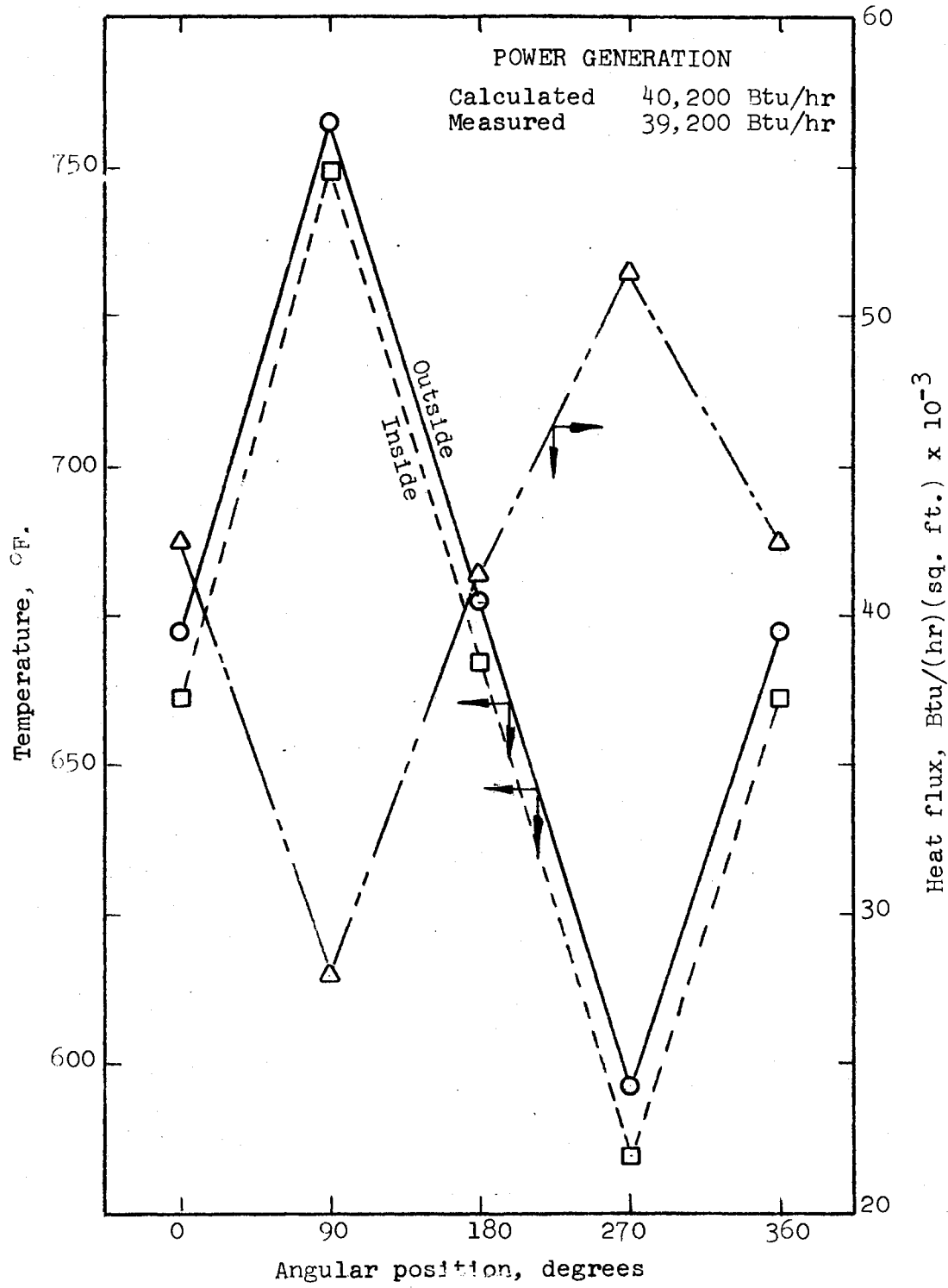


Figure 48. Temperature Profiles for Run 118, Station 10

APPENDIX B

VISUAL FLOW OBSERVATIONS

Several previous investigations of two-phase flow in helical coils, both with and without heat transfer, have indicated the presence of secondary flow patterns. Rippel et al. (26) proposed that the fact that liquid holdup in a helical coil is less than that in a straight horizontal pipe was due to the presence of a secondary flow pattern. Banerjee et al. (1), visually observed liquid films on the tube wall of a coil nearest the coil axis at certain combinations of gas and liquid flow rate. They termed this behavior "film inversion." Owhadi (22) suggested the presence of a secondary flow pattern which caused large circumferential variations of the tube wall temperature during two-phase heat transfer in a helical coil.

In order to investigate the flow patterns which occur during high-quality two-phase flow in a helical coil, a visual flow study was conducted. A transparent coil was constructed by wrapping 5/8-inch OD x 1/2-inch ID Tygon tubing around a cylindrical mandrel. The resulting coil had approximately the same dimensions as the small stainless steel coil used in the heat transfer study. A mixture of air and water was passed through the coil and visual observations and photographs were made. A photograph of the apparatus is shown in Figure 49.

Figure 50 shows a slow-moving stream of liquid on the inner wall of the tube. A short section of one of the turns of the coil is visible. Flow is from left to right and the water was colored to enhance

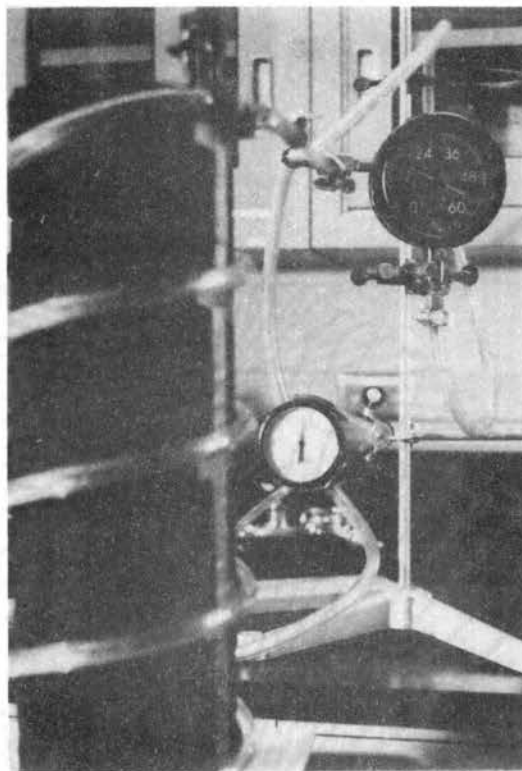


Figure 49. Visual Flow Apparatus

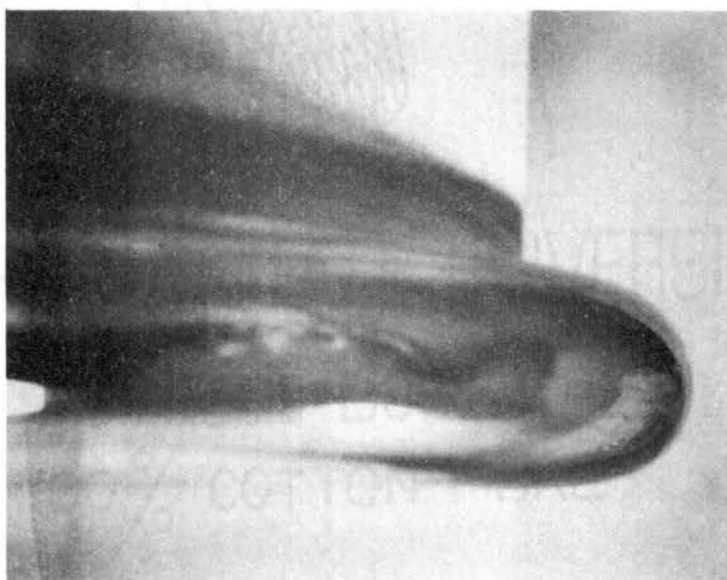


Figure 50. Flow Pattern on Inside Tube Wall

the photography. For the combination of liquid rate and air velocity shown in this photograph no liquid was entrained by the air stream. Figure 51 shows the flow pattern at a higher air velocity and a higher liquid rate. Under these conditions water is entrained by the air and flung onto the outer wall of the tube. From this point it spirals back to the inner wall as it moves through the coil and is redeposited in the liquid stream. The secondary circulation pattern can be seen on the outer surface of the tube in this photograph.

Figure 52 shows a close-up photograph focused on the outer wall of the tube. Flow is from left to right. The effect of the secondary circulation pattern on liquid drops on the outer tube wall can be clearly seen. The droplets spiral back toward the inner wall of the tube as they move along the coil.

The evidence gathered from the visual flow observations confirms the presence of a secondary flow pattern and indicates that a helical coil is very efficient in distributing liquid onto the tube surface. The presence of a liquid stream on the inner wall of the tube provides an explanation for the low wall temperatures measured at this position in the heat transfer experiments.

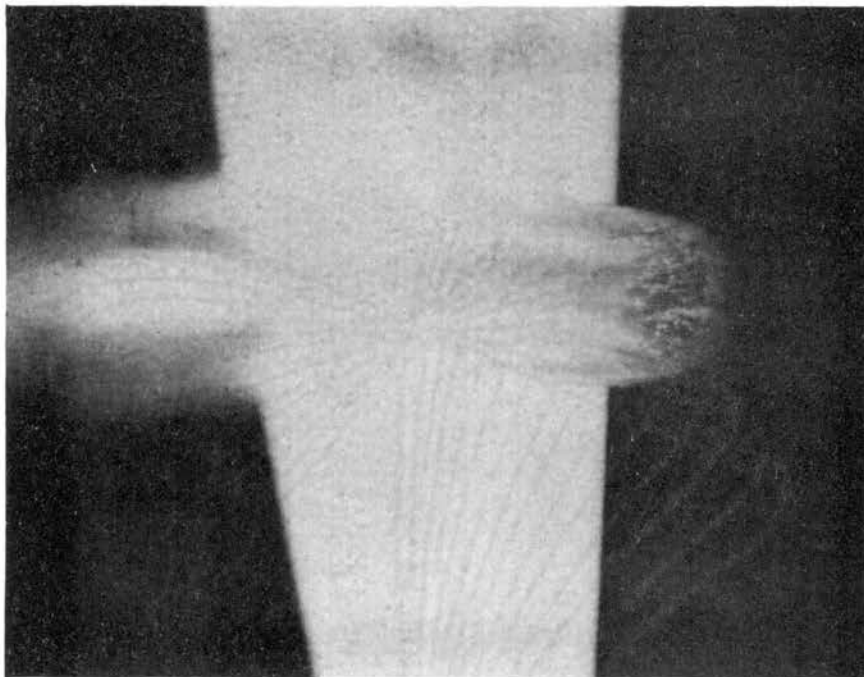


Figure 51. Flow Pattern at Higher Air Velocity
and Liquid Rate

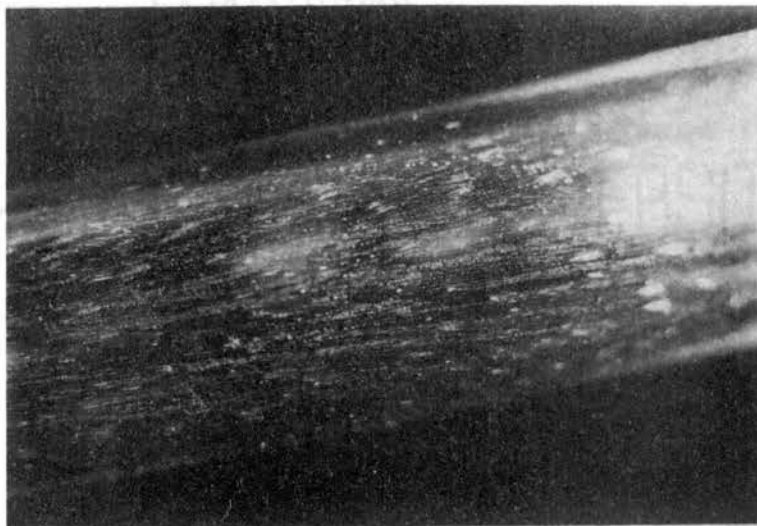


Figure 52. Close-Up of Outer Tube Wall

APPENDIX C

SAMPLE CALCULATIONS

SAMPLE CALCULATIONS

All data were reduced on a digital computer. The sample calculations in this appendix are provided as an example of how the calculations were made. The sample calculations will be performed for the 0° position at station 7 for run 109. Raw data for this run are shown in Table IX.

TABLE IX

RAW DATA FOR RUN 109

Coil current = 400 amps
Coil voltage = 12.7 volts
Coil inlet pressure = 18.35 psig
Coil outlet pressure = 6.10 psig
Volume condensed effluent steam collected = 1000 cc
Temperature condensed effluent steam = 88 °F.
Volume effluent water collected = 67 cc
Temperature effluent water = 84 °F.
Collection time = 1.33 min.
Atmospheric pressure = 14.4 psia
Room temperature = 84 °F.
Coil inlet temperature = 253.7 °F.
Coil outlet temperature = 229.3 °F.
Thermocouple 71 reading = 6.430 mv

The total flow rate for run 109 was calculated from the volumetric samples collected. The density of water at the collection temperatures

was calculated from the following polynomial fit of data from Perry's Handbook((25):

$$\rho_{\text{H}_2\text{O}} = 1.0016 + 2.771 \times 10^{-5} T - 1.133 \times 10^{-6} T^2$$

At 84 °F. the density of water is:

$$\rho_{\text{H}_2\text{O}} = 0.9959 \text{ gm/cc}$$

At 88 °F. the density of water is:

$$\rho_{\text{H}_2\text{O}} = 0.9953 \text{ gm/cc}$$

The flow rate of coil effluent steam is:

$$\begin{aligned} W_{\text{steam}} &= \frac{1000 \text{ cc}}{1.33 \text{ min}} \times 0.9953 \text{ gm/cc} \times 0.002205 \text{ lb/gm} \\ &= 1.65 \text{ lb/min} \end{aligned}$$

The flow rate of coil effluent water is:

$$\begin{aligned} W_{\text{H}_2\text{O}} &= \frac{67 \text{ cc}}{1.33 \text{ min}} \times 0.9959 \text{ gm/cc} \times 0.002205 \text{ lb/gm} \\ &= 0.111 \text{ lb/min} \end{aligned}$$

The total mass flow rate is:

$$W_{\text{total}} = 1.65 + 0.111 = 1.76 \text{ lb/min}$$

The mass velocity is:

$$\begin{aligned} G &= \frac{1.76 \text{ lb/min}}{1.336 \times 10^{-3} \text{ sq. ft.}} \times 60 \text{ min/hr} \\ &= 79,040 \text{ lb/(hr)(sq. ft.)} \end{aligned}$$

For all cases in which the coil inlet and outlet streams were saturated, it was felt that the temperatures of the inlet and outlet streams were

a much more accurate indication of fluid conditions than the inlet and outlet pressures which were measured on gauges. The coil inlet and outlet pressures were thus calculated from temperature measurements. The coil inlet pressure at point of temperature measurement is calculated from the following equation which is derived from the steam tables of Keenan and Keyes (12):

$$p = e \left[15.91 - \frac{880}{(T + 460)} \right]$$

The inlet pressure is:

$$P_{in} = 32.1 \text{ psia}$$

The point of inlet temperature measurement was 18 inches from the coil inlet. The coil inlet pressure was corrected to this point by linear interpolation using the inlet and outlet pressures. The corrected coil inlet pressure is:

$$P_{in} = 32.1 - \frac{18}{134} (32.1 - 20.5) = 30.5 \text{ psia}$$

The coil outlet pressure is:

$$P_{out} = 20.6 \text{ psia}$$

The point of outlet temperature measurement was 6 inches from the coil outlet. The coil outlet pressure was corrected to this point by linear interpolation using the inlet and outlet pressures. The corrected coil outlet pressure is:

$$P_{out} = 20.6 + \frac{6}{126} (30.5 - 20.6) = 21.1 \text{ psia}$$

The temperatures at the coil inlet and outlet were calculated from the following polynomial fit of saturation temperature versus pressure derived from the steam tables of Keenan and Keyes (12):

$$T_{\text{sat}} = 151.3 + 5.195 p - 0.07944 p^2 + 0.5498 \times 10^{-3} p^3$$

The coil inlet temperature calculated from the corrected coil inlet pressure is:

$$T_{\text{in}} = 251.4 \text{ } ^\circ\text{F.}$$

The coil outlet temperature calculated from the corrected coil outlet pressure is:

$$T_{\text{out}} = 230.7 \text{ } ^\circ\text{F.}$$

The coil inlet quality is calculated from a heat balance at the coil inlet. Given the enthalpy and flow rates of the makeup steam and water streams before mixing and the pressure and temperature conditions of the stream after mixing, a simple heat balance yields the coil inlet quality:

$$x_{\text{in}} = 65.7\%$$

The outside wall temperature for thermocouple 71 is calculated via a trial and error solution. Thermocouples were calibrated by bleeding steam through the coil at atmospheric pressure. Each thermocouple was referenced to a thermocouple in a steam bath. The millivolt reading obtained under these conditions is the thermocouple correction factor which was assumed to be due to the conduction of heat through the thermocouple wires. The correction factor is therefore proportional to the difference between the thermocouple junction temperature and room

temperature. The thermocouple correction factor for thermocouple 71 was 0.012 mv and the coil and room temperatures at which the correction factor was measured were 210.63 °F. and 75 °F. respectively. The thermocouple junction temperature is estimated from the following polynomial fit of the thermocouple tables:

$$T = 32.44 + 35.33 \text{ EMF} - 0.2903 \text{ EMF}^2 + 0.01163 \text{ EMF}^3 - 1.607 \times 10^{-4} \text{ EMF}^4$$

The measured emf for thermocouple 71 was 6.430 mv. The estimated temperature is therefore:

$$T_{\text{est}} = 250.4 \text{ } ^\circ\text{F.}$$

The correction factor for this temperature is calculated as:

$$\text{TCF} = 0.012 \left(\frac{250.4 - 84}{210.6 - 75} \right) = 0.0147$$

The actual emf is:

$$\text{EMF} = 6.430 + 0.0147 = 6.445 \text{ mv}$$

The new estimated temperature is:

$$T_{\text{est}} = 250.9 \text{ } ^\circ\text{F.}$$

The correction factor for this temperature is:

$$\text{TCF} = 0.012 \left(\frac{250.9 - 84}{210.6 - 75} \right) = 0.0148$$

The actual emf is thus the same as the emf calculated in the previous trial:

$$\text{EMF} = 6.430 + 0.0148 = 6.445 \text{ mv}$$

The new estimated temperature is also the same:

$$T_{\text{est}} = 250.9 \text{ }^{\circ}\text{F.}$$

Given the circumferential temperature distribution of the outer tube surface, the circumferential temperature and heat flux distributions on the inner tube surface were calculated via the numerical solution described in Appendix A. The trial and error solution is complex and a full sample calculation would be difficult to show. The equations used in the computer solution are described in detail in Appendix A. The computer solution produced the following results for the inside wall temperature and heat flux for position 71:

$$(T_{\text{wall}})_{71} = 246.6 \text{ }^{\circ}\text{F.}$$

$$(Q/A)_{71} = 1.450 \times 10^4 \text{ Btu/(hr)(sq. ft.)}$$

The heat flux shown above is based on heat generation rates calculated as the square of the current flowing in a tube wall increment times the resistance of the increment. The total coil generation rate is the sum of all of the increment generation rates. The total coil heat generation rate calculated by the computer solution was:

$$Q_{\text{cal}} = 5132 \text{ watts}$$

The total coil heat generation rate can also be calculated as the product of the coil current and voltage, or:

$$\begin{aligned} Q_{\text{exp}} &= 400 \text{ amps} \times 12.7 \text{ volts} \\ &= 5080 \text{ watts} \end{aligned}$$

The ratio of experimental to calculated coil heat generation rates was used to correct the heat addition rate to the two-phase mixture. The ratio is:

$$\begin{aligned} R_Q &= Q_{\text{exp}}/Q_{\text{cal}} \\ &= 5080/5132 \\ &= 0.9899 \end{aligned}$$

The pressure of the two-phase mixture at station 7 was calculated by linear interpolation between the inlet and outlet pressures:

$$\begin{aligned} P_7 &= p_{\text{in}} - 7/10 (p_{\text{in}} - p_{\text{out}}) \\ &= 30.5 - 7/10 (30.5 - 21.1) \\ &= 23.9 \text{ psia} \end{aligned}$$

The saturation temperature at this pressure was calculated from the equation shown earlier:

$$\begin{aligned} (T_{\text{sat}})_7 &= 151.3 + 5.195 p - 0.07944 p^2 \\ &\quad + 0.5498 \times 10^{-3} p^3 \\ &= 237.6 \text{ }^\circ\text{F.} \end{aligned}$$

The heat flow with the two-phase mixture at station 7 is the heat flow of the inlet two-phase mixture plus the coil heat addition rate up to station 7. The heat flow of the inlet two-phase mixture was calculated as:

$$Q_{\text{in}} = w_{\text{total}} (1 - x_{\text{in}}) h_l + w_{\text{total}} x_{\text{in}} h_g$$

The enthalpies of the liquid and vapor in the inlet two-phase mixture

were calculated from the following equations derived from the steam tables of Keenan and Keys (12):

$$\begin{aligned} h_l &= 26.34 + 0.942 T + 0.147 \times 10^{-3} T^2 \\ &= 258.5 \text{ Btu/lb} \end{aligned}$$

$$\begin{aligned} h_g &= 1056 + 0.519 T - 0.353 \times 10^{-3} T^2 \\ &= 1159 \text{ Btu/lb} \end{aligned}$$

The heat flow of the inlet two-phase mixture is:

$$\begin{aligned} Q_{in} &= 1.76 \text{ lb/min} \times (1 - 0.657) \times 258.5 \text{ Btu/lb} \\ &\quad + 1.76 \text{ lb/min} \times 0.657 \times 1159 \text{ Btu/lb} \\ &= 1496 \text{ Btu/min} \times 60 \text{ min/hr} \\ &= 89,760 \text{ Btu/hr} \end{aligned}$$

The heat addition rate up to station 7 is the summation of the products of each inner surface increment heat flux times the inner surface area of the increment, i.e.,

$$(Q_{coil})_7 = \sum_{i=1}^7 \sum_{j=1}^8 (Q/A)_{i,j} \times A_{i,j}$$

$$(Q_{coil})_7 = 12,020 \text{ Btu/hr}$$

The heat flow with the two-phase mixture at station 7 is:

$$\begin{aligned} Q_7 &= Q_{in} + (Q_{coil})_7 \\ &= 89,760 + 12,020 \\ &= 101,800 \text{ Btu/hr} \end{aligned}$$

The quality of the two-phase mixture at station 7 was calculated from a heat balance at that point:

$$Q_7 = w_{\text{total}} \times (1 - x_7) \times h_1 \times 60 + w_{\text{total}} \times x_7 \times h_g \times 60$$

Solving for x_7 :

$$\begin{aligned} x_7 &= \frac{(Q_7/w_{\text{total}} \times 60) - h_1}{h_g - h_1} \\ &= \frac{(101,800/1.76 \times 60) - 258.5}{1159 - 258.5} \\ &= 0.784 = 78.4\% \end{aligned}$$

The heat transfer coefficient at position 71 is the heat flux at this position divided by the temperature difference between the inner tube wall and the two-phase mixture. The temperature difference between the inner tube wall and the two-phase mixture is:

$$\begin{aligned} \Delta T_{71} &= (T_{\text{wall}})_{71} - (T_{\text{sat}})_7 \\ &= 246.6 - 237.6 \\ &= 9.0 \text{ } ^\circ\text{F.} \end{aligned}$$

The heat transfer coefficient at position 71 is:

$$\begin{aligned} h_{71} &= (Q/A)_{71} / \Delta T_{71} \\ &= \frac{1.450 \times 10^4 \text{ Btu/(hr)(sq. ft.)}}{9.0 \text{ } ^\circ\text{F.}} \\ &= 1.61 \times 10^3 \text{ Btu/(hr)(sq. ft.)(} ^\circ\text{F.)} \end{aligned}$$

The data were correlated as the ratio of the heat transfer coefficient to a heat transfer coefficient calculated as if the gas phase were

flowing alone in the coil, h_{71}/h_{gc} . Values of h_{gc} were calculated from the Seban-McLaughlin equation (29):

$$h_{gc} = 0.023 \left(\frac{k_g}{d}\right) Re^{0.85} Pr^{0.4} \left(\frac{d}{D}\right)^{0.1}$$

The Reynolds number for the gas phase flowing alone is:

$$Re_g = \frac{dG_g}{\mu_g}$$

where:

$$\begin{aligned} G_g &= x_7 \times w_{total} \times 60/A_{xs} \\ &= 0.784 \times 1.76 \times 60/0.00133 \\ &= 62,250 \text{ lb/(hr)(sq. ft.)} \end{aligned}$$

The viscosity of the gas phase was calculated from the following relationship reported by Owhadi (22):

$$\begin{aligned} \mu_g &= \left[8.54 + \frac{0.49}{36} (T_{sat} - 224)\right] 3600 \times 10^{-6} \\ &= \left[8.54 + \frac{0.49}{36} (237.6 - 224)\right] 3600 \times 10^{-6} \\ &= 0.03141 \text{ lb/(ft)(hr)} \end{aligned}$$

The superficial gas phase Reynolds number is:

$$\begin{aligned} Re_g &= \frac{(0.495/12) \times 62,250}{0.03141} \\ &= 81,750 \end{aligned}$$

The Prandtl number for the gas phase is:

$$Pr_g = \frac{c_{pg} \mu_g}{k_g}$$

The heat capacity of the gas phase was calculated from the following polynomial fit of data from Perry's handbook (25):

$$\begin{aligned} c_{pg} &= 0.46621 - 0.33054 \times 10^{-3} T_{\text{sat}} \\ &\quad + 0.20982 \times 10^{-5} T_{\text{sat}}^2 \\ &= 0.5061 \text{ Btu/(lb)(}^\circ\text{F.)} \end{aligned}$$

The thermal conductivity of the gas phase was calculated from the following polynomial fit of data from Perry's handbook (25):

$$\begin{aligned} k_g &= 0.011257 + 0.13214 \times 10^{-5} T_{\text{sat}} \\ &\quad + 0.625 \times 10^{-7} T_{\text{sat}}^2 \\ &= 0.0151 \text{ (Btu)(ft)/(hr)(sq. ft.)(}^\circ\text{F.)} \end{aligned}$$

The Prandtl number for the gas phase is:

$$\begin{aligned} Pr_g &= \frac{0.5061 \times 0.03141}{0.0151} \\ &= 1.053 \end{aligned}$$

The heat transfer coefficient calculated as if the gas phase were flowing alone in the coil is:

$$\begin{aligned} h_{gc} &= 0.023 \left(\frac{0.0151}{0.495/12} \right) (81,750)^{0.85} \\ &\quad (1.053)^{0.4} (0.495/9.99)^{0.1} \\ &= 95.36 \text{ Btu/(hr)(sq. ft.)(}^\circ\text{F.)} \end{aligned}$$

The Lockhart-Martinelli parameter was calculated as:

$$X_{tt} = \left(\frac{1 - x_7}{x_7} \right)^{0.9} \left(\frac{\rho_g}{\rho_l} \right)^{0.5} \left(\frac{\mu_l}{\mu_g} \right)^{0.1}$$

The density of the gas phase was calculated from the following equation derived by Owhadi (22):

$$\begin{aligned}\rho_g &= 1.022 \left[\frac{18 p_7}{10.73 (T_{\text{sat}} + 460)} \right] \\ &= 1.022 \left[\frac{18 \times 23.9}{10.73 (237.6 + 460)} \right] \\ &= 0.5874 \text{ lb/ft}^3\end{aligned}$$

The density of the liquid phase was calculated from the following equation derived by Owhadi (22):

$$\begin{aligned}\rho_l &= 59.97 - \frac{0.96}{36} (T_{\text{sat}} - 212) \\ &= 59.97 - \frac{0.96}{36} (237.6 - 212) \\ &= 59.29 \text{ lb/ft}^3\end{aligned}$$

The viscosity of the liquid phase was calculated from the following equation reported by Owhadi (22):

$$\begin{aligned}\mu_l &= 241.9 \left\{ 2.148 \left(\frac{T_{\text{sat}} - 212}{1.8} \right) + 91.565 \right\} \\ &\quad + 2.1482 \left[8078.4 + \left(91.565 + \frac{T_{\text{sat}} - 212}{1.8} \right)^2 \right]^{\frac{1}{2}} - 120 \}^{-1} \\ &= 0.5966 \text{ lb/(ft)(hr)}\end{aligned}$$

The Lockhart-Martinelli parameter is:

$$\begin{aligned}X_{\text{tt}} &= \left(\frac{1 - 0.784}{0.784} \right)^{0.9} \left(\frac{0.05874}{59.29} \right)^{0.5} \left(\frac{0.5966}{0.03141} \right)^{0.1} \\ &= 0.01324\end{aligned}$$

APPENDIX D

HEAT TRANSFER DATA FOR SMALL COIL

TABLE X
 RUN 101, SINGLE-PHASE, LAMINAR FLOW

Water feed rate:	34,000 lb/(hr)(sq. ft.)							
Coil current:	198 amps							
Coil voltage:	5.9 volts							
Inlet temperature:	80 °F.							
Outlet temperature:	180 °F.							
Average heat flux:	3,080 Btu/(hr)(sq. ft.)							
Outside wall temperature, °F:								
Station	Circumferential Location							
	0°	45°	90°	135°	180°	225°	270°	315°
1	123.2		119.6		109.7		107.8	
2	133.2	134.0	126.6	120.7	117.2	114.9	116.5	123.8
3	140.0		134.0		127.5		127.7	
4	149.2		141.0		135.1		138.0	
5	158.8		150.8		143.7		145.9	
6	166.7		159.0		152.7		154.6	
7	176.8		168.6		160.4		163.0	
8	183.7		175.1		168.4		171.4	
9	192.0	191.8	184.7	180.0	178.1	178.6	181.3	185.5
10	200.0		190.8		182.3		184.5	

TABLE XI
 RUN 102, SINGLE-PHASE, LAMINAR FLOW

Water feed rate:	63,400 lb/(hr)(sq. ft.)							
Coil current:	256 amps							
Coil voltage:	7.6 volts							
Inlet temperature:	80 °F.							
Outlet temperature:	180 °F.							
Average heat flux:	5,120 Btu/(hr)(sq. ft.)							
Outside wall temperature, °F:								
Station	Circumferential Location							
	0°	45°	90°	135°	180°	225°	270°	315°
1	115.6		129.4		114.5		106.1	
2	131.6	142.5	137.4	129.4	122.9	119.1	117.9	121.3
3	142.0		143.6		132.7		125.7	
4	146.6		150.1		138.8		135.9	
5	154.0		157.1		144.7		142.8	
6	164.4		164.2		153.2		151.6	
7	173.4		172.6		160.3		158.8	
8	180.1		177.6		165.9		166.2	
9	186.4	192.9	185.8	179.0	174.5	172.7	175.1	178.8
10	191.7		191.3		179.6		178.8	

TABLE XII
 RUN 103, SINGLE-PHASE, TURBULENT FLOW

Water feed rate:	488,000	lb/(hr)(sq. ft.)						
Coil current:	496	amps						
Coil voltage:	15.0	volts						
Inlet temperature:	80	°F.						
Outlet temperature:	100	°F.						
Average heat flux:	19,500	Btu/(hr)(sq. ft.)						
Outside wall temperature, °F.:								
Station	Circumferential Location							
	0°	45°	90°	135°	180°	225°	270°	315°
1	118.2		141.3		121.5		111.8	
2	122.2	135.0	146.1	133.6	122.7	115.8	113.1	114.9
3	123.8		148.2		125.2		115.6	
4	127.1		150.2		128.1		119.8	
5	130.0		151.8		130.5		123.7	
6	132.9		154.4		134.5		126.8	
7	136.1		155.8		136.3		129.9	
8	139.7		158.6		138.2		132.9	
9	141.6	150.3	160.7	152.8	142.4	137.2	135.9	137.3
10	144.6		162.6		144.5		137.7	

TABLE XIII
 RUN 104, TWO-PHASE

Mass flow rate:	70,700	lb/(hr) (sq. ft.)
Coil current:	350	amps
Coil voltage:	11.1	volts
Average heat flux:	10,200	Btu/(hr) (sq. ft.)
	<u>Inlet</u>	<u>Outlet</u>
Temperature, °F.:	246.0	227.7
Pressure, psia:	27.8	19.9
Steam quality:	69.7	86.5
Outside wall temperature, °F.:		

Station	Circumferential Location							
	0°	45°	90°	135°	180°	225°	270°	315°
1	250.5		253.2		251.3		249.4	
2	249.7	251.3	252.7	251.8	250.4	248.4	248.9	248.7
3	248.5		251.6		249.3		247.9	
4	248.0		250.5		248.9		247.2	
5	246.9		250.0		247.2		246.3	
6	246.1		248.9		246.8		245.6	
7	245.0		247.6		245.5		244.8	
8	244.4		246.6		244.4		243.9	
9	243.4	244.7	245.9	245.2	243.7	242.9	242.5	243.2
10	242.7		245.5		243.0		242.4	

TABLE XIV
 RUN 105, TWO-PHASE

Mass flow rate:	70,900 lb/(hr)(sq. ft.)							
Coil current:	380 amps							
Coil voltage:	12.2 volts							
Average heat flux:	12,200 Btu/(hr)(sq. ft.)							
	<u>Inlet</u>	<u>Outlet</u>						
Temperature, °F.:	247.5	229.0						
Pressure, psia:	28.5	20.4						
Steam Quality:	69.7	89.4						
Outside wall temperature, °F.:								
Station	Circumferential Location							
	0°	45°	90°	135°	180°	225°	270°	315°
1	252.4		256.0		253.6		251.2	
2	251.8	253.8	255.1	254.4	252.6	250.5	250.7	250.8
3	251.2		254.7		251.9		250.4	
4	250.5		253.6		251.2		249.3	
5	249.2		252.7		249.4		248.5	
6	248.1		251.4		248.7		247.7	
7	247.2		250.2		247.6		246.7	
8	246.4		249.1		246.3		245.7	
9	245.1	246.8	248.2	247.6	245.4	244.8	244.4	245.1
10	245.5		247.9		246.3		244.3	

TABLE XV
 RUN 106, TWO-PHASE

Mass flow rate:	70,900 lb/(hr)(sq. ft.)							
Coil current:	250 amps							
Coil voltage:	7.9 volts							
Average heat flux:	5,200 Btu/(hr)(sq. ft.)							
	<u>Inlet</u>	<u>Outlet</u>						
Temperature, °F.:	242.6	222.3						
Pressure, psia:	26.1	18.0						
Steam quality:	80.5	90.0						
Outside wall temperature, °F.:								
Station	Circumferential Location							
	0°	45°	90°	135°	180°	225°	270°	315°
1	243.7		245.5		244.5		243.5	
2	243.0	243.9	244.8	244.3	243.5	242.6	243.1	243.2
3	242.5		243.9		242.5		241.9	
4	241.5		243.0		242.1		241.1	
5	240.6		242.4		240.7		240.4	
6	239.7		241.4		240.6		239.9	
7	239.0		240.5		239.3		238.9	
8	238.1		238.9		238.0		237.7	
9	237.3	237.9	238.8	238.0	237.4	237.2	236.5	237.3
10	236.7		238.2		237.4		236.8	

TABLE XVI
 RUN 107, TWO-PHASE

Mass flow rate:	71,300 lb/(hr)(sq. ft.)							
Coil current:	200 amps							
Coil voltage:	6.3 volts							
Average heat flux:	3,320 Btu/(hr)(sq. ft.)							
	<u>Inlet</u>	<u>Outlet</u>						
Temperature, °F.:	248.5	229.2						
Pressure, psia:	29.1	20.5						
Steam quality:	80.8	87.6						
Outside wall temperature, °F.:								
Station	Circumferential Location							
	0°	45°	90°	135°	180°	225°	270°	315°
1	249.8		251.0		250.5		250.0	
2	249.4	249.7	250.7	250.0	249.8	248.9	249.6	249.6
3	249.0		250.0		249.1		248.8	
4	248.5		249.3		248.8		248.1	
5	247.2		248.3		247.1		247.1	
6	246.5		247.5		247.0		246.4	
7	245.4		246.4		245.9		245.7	
8	245.1		245.5		245.1		244.9	
9	244.0	244.1	244.7	244.3	244.1	243.8	243.2	244.0
10	243.3		244.1		243.6		243.2	

TABLE XVII
 RUN 108, TWO-PHASE

Mass flow rate:	73,500 lb/(hr)(sq. ft.)							
Coil current:	150 amps							
Coil voltage:	4.8 volts							
Average heat flux:	1,900 Btu/(hr)(sq. ft.)							
	<u>Inlet</u>	<u>Outlet</u>						
Temperature, °F.:	248.1	229.0						
Pressure, psia:	28.8	20.5						
Steam quality:	81.4	86.1						
Outside wall temperature, °F.:								
Station	Circumferential Location							
	0°	45°	90°	135°	180°	225°	270°	315°
1	248.7		249.4		249.1		248.7	
2	248.2	248.1	248.7	248.6	248.4	247.4	248.2	248.3
3	247.4		248.0		247.5		247.3	
4	246.7		247.2		247.2		246.5	
5	245.9		246.8		245.9		245.9	
6	245.2		245.8		245.5		245.2	
7	244.0		244.7		244.2		244.0	
8	243.1		243.2		243.6		243.5	
9	242.5	242.6	242.8	242.6	242.4	242.2	241.5	242.5
10	242.0		242.4		242.1		242.0	

TABLE XVIII
 RUN 109, TWO-PHASE

Mass flow rate:	79,200 lb/(hr)(sq. ft.)							
Coil current:	400 amps							
Coil voltage:	12.7 volts							
Average heat flux:	13,400 Btu/(hr)(sq. ft.)							
	<u>Inlet</u>	<u>Outlet</u>						
Temperature, °F.:	251.0	230.3						
Pressure, psia:	30.4	21.0						
Steam quality:	65.7	85.1						
Outside wall temperature, °F.:								
Station	Circumferential Location							
	0°	45°	90°	135°	180°	225°	270°	315°
1	256.3		259.8		257.5		256.6	
2	255.5	257.1	258.7	257.6	255.8	253.7	253.8	254.5
3	254.5		257.8		255.2		253.5	
4	253.8		256.7		254.4		252.3	
5	252.5		256.1		253.0		251.9	
6	252.2		255.2		252.7		251.0	
7	250.9		254.1		251.7		250.6	
8	250.0		252.4		249.7		249.0	
9	248.6	250.4	251.7	250.9	249.0	248.4	247.5	248.6
10	248.3		251.3		246.9		247.6	

TABLE XIX
 RUN 110, TWO-PHASE

Mass flow rate:	84,000	lb/(hr) (sq. ft.)
Coil current:	550	amps
Coil voltage:	18.0	volts
Average heat flux:	26,100	Btu/(hr) (sq. ft.)
	<u>Inlet</u>	<u>Outlet</u>
Temperature, °F.:	257.7	238.5
Pressure, psia:	34.1	23.3
Steam quality:	67.6	100.0 (2.4 °F. superheated)
Outside wall temperature, °F.:		

Station	Circumferential Location							
	0°	45°	90°	135°	180°	225°	270°	315°
1	269.3		275.0		270.3		266.2	
2	268.1	271.7	274.3	272.4	268.7	265.5	265.6	266.1
3	266.9		273.6		268.6		265.2	
4	266.2		171.5		267.7		264.5	
5	265.0		271.6		265.2		263.6	
6	267.3		270.0		267.3		262.2	
7	305.1		268.9		301.7		262.0	
8	357.8		270.6		372.5		344.1	
9	426.2	353.0	276.5	294.9	403.4	431.8	426.5	437.0
10	459.5		284.7		444.1		464.6	

TABLE XX
 RUN 111, TWO-PHASE

Mass flow rate:	84,500 lb/(hr)(sq. ft.)							
Coil current:	550 amps							
Coil voltage:	17.8 volts							
Average heat flux:	25,800 Btu/(hr)(sq. ft.)							
	<u>Inlet</u>	<u>Outlet</u>						
Temperature, °F.:	261.6	236.3						
Pressure, psia:	36.5	23.4						
Steam quality:	49.5	83.5						
Outside wall temperature, °F.:								
Station	Circumferential Location							
	0°	45°	90°	135°	180°	225°	270°	315°
1	273.2		278.7		274.6		270.4	
2	272.0	274.7	277.1	275.3	272.3	269.6	268.9	269.5
3	270.2		275.8		271.4		268.0	
4	269.2		274.5		270.6		267.1	
5	267.5		273.1		268.5		266.2	
6	267.0		271.7		267.6		265.1	
7	265.2		269.8		265.7		263.9	
8	264.3		268.2		264.0		262.9	
9	262.8	265.6	267.8	266.8	263.3	262.2	261.2	261.4
10	261.9		267.2		262.0		260.6	

TABLE XXI
 RUN 113, TWO-PHASE

Mass flow rate:	80,500 lb/(hr) (sq. ft.)							
Coil current:	600 amps							
Coil voltage:	19.3 volts							
Average heat flux:	30,500 Btu/(hr) (sq. ft.)							
	<u>Inlet</u>	<u>Outlet</u>						
Temperature, °F.:	264.9	239.7						
Pressure, psia:	38.6	24.8						
Steam quality:	46.8	88.5						
Outside wall temperature, °F.:								
Station	Circumferential Location							
	0°	45°	90°	135°	180°	225°	270°	315°
1	278.3		284.8		279.8		275.2	
2	277.5	281.1	283.9	281.9	278.4	275.2	274.5	275.2
3	276.0		282.1		277.1		273.4	
4	275.0		280.8		276.4		272.3	
5	272.9		279.2		273.6		271.2	
6	271.5		277.4		272.6		270.0	
7	270.2		276.1		270.8		269.2	
8	269.3		274.6		269.2		268.0	
9	267.5	271.0	273.9	272.1	268.0	266.8	265.4	267.3
10	272.1		272.8		276.6		265.3	

TABLE XXII
 RUN 114, TWO-PHASE

Mass flow rate:	41,700 lb/(hr) (sq. ft.)							
Coil current:	300 amps							
Coil voltage:	9.6 volts							
Average heat flux:	7,550 Btu/(hr) (sq. ft.)							
	<u>Inlet</u>		<u>Outlet</u>					
Temperature, °F.:	227.6		218.0					
Pressure, psia:	19.8		16.6					
Steam quality:	67.6		88.3					
Outside wall temperature, °F.:								
Station	Circumferential Location							
	0°	45°	90°	135°	180°	225°	270°	315°
1	262.5		234.8		235.5		265.6	
2	245.7	233.7	234.1	233.1	231.7	234.7	237.8	251.2
3	245.9		233.5		230.7		242.1	
4	247.6		232.7		232.5		246.7	
5	256.7		232.4		235.0		254.0	
6	258.0		232.1		236.9		255.1	
7	266.4		231.1		243.8		280.5	
8	271.6		230.5		249.2		266.2	
9	282.7	242.5	230.9	230.5	250.9	280.0	280.7	289.2
10	278.9		230.9		260.3		303.3	

TABLE XXIII
 RUN 116, TWO-PHASE

Mass flow rate:	73,700 lb/(hr)(sq. ft.)							
Coil current:	400 amps							
Coil voltage:	12.7 volts							
Average heat flux:	13,400 Btu/(hr)(sq. ft.)							
	<u>Inlet</u>	<u>Outlet</u>						
Temperature, °F.:	248.7	226.2						
Pressure, psia:	29.2	19.4						
Steam quality:	63.3	84.2						
Outside wall temperature, °F.:								
Station	Circumferential Location							
	0°	45°	90°	135°	180°	225°	270°	315°
1	254.1		257.7		255.1		253.1	
2	253.3	255.1	256.6	255.4	253.9	251.5	251.9	252.2
3	251.8		255.4		252.2		251.0	
4	250.9		254.2		252.2		250.2	
5	249.7		253.8		250.4		249.1	
6	249.3		252.4		249.6		250.1	
7	249.9		252.9		248.2		249.2	
8	249.0		249.4		249.0		246.6	
9	245.6	249.5	248.8	248.5	246.3	245.2	244.4	246.1
10	245.3		248.5		245.5		245.1	

TABLE XXIV
 RUN 117, TWO-PHASE

Mass flow rate:	76,200 lb/(hr)(sq. ft.)							
Coil current:	550 amps							
Coil voltage:	18.0 volts							
Average heat flux:	26,100 Btu/(hr)(sq. ft.)							
	<u>Inlet</u>	<u>Outlet</u>						
Temperature, °F.:	257.4	237.3						
Pressure, psia:	33.9	23.2						
Steam quality	64.1	100.0 (1.4 °F. superheated)						
Outside wall temperature, °F.:								
Station	Circumferential Location							
	0°	45°	90°	135°	180°	225°	270°	315°
1	268.1		274.5		269.9		265.9	
2	268.0	271.4	274.1	272.1	268.3	266.7	264.8	265.3
3	266.0		272.5		267.1		264.1	
4	265.2		271.3		266.5		263.2	
5	263.6		270.7		264.3		262.9	
6	272.1		272.3		267.3		262.4	
7	298.2		268.9		292.6		261.7	
8	360.9		264.7		355.3		335.0	
9	419.9	345.4	274.8	291.7	400.5	432.7	431.4	440.7
10	443.7		278.0		427.9		448.3	

TABLE XXV
 RUN 118, TWO-PHASE

Mass flow rate:	67,800 lb/(hr)(sq. ft.)							
Coil current:	590 amps							
Coil voltage:	19.4 volts							
Average heat flux:	30,200 Btu/(hr)(sq. ft.)							
	<u>Inlet</u>	<u>Outlet</u>						
Temperature, °F.:	261.0	359.0						
Pressure, psia:	36.1	24.4						
Steam quality:	59.3	100.0 (120°F. super-heated)						
Outside wall temperature, °F.:								
Station	Circumferential Location							
	0°	45°	90°	135°	180°	225°	270°	315°
1	274.3		281.2		275.7		271.2	
2	273.3	277.2	280.3	277.9	273.7	270.0	270.4	270.8
3	271.4		279.0		272.8		269.5	
4	270.5		278.0		271.9		268.8	
5	272.8		278.3		271.3		268.1	
6	310.8		277.2		308.6		268.9	
7	415.5		279.0		402.5		444.1	
8	454.2		283.7		453.7		467.2	
9	530.1	458.8	319.4	374.3	487.9	506.4	499.6	515.6
10	671.8		757.4		677.0		596.5	

TABLE XXVI
 RUN 119, TWO-PHASE

Mass flow rate:	43,000 lb/(hr)(sq. ft.)							
Coil current:	400 amps							
Coil voltage:	13.0 volts							
Average heat flux:	13,700 Btu/(hr)(sq. ft.)							
	<u>Inlet</u>		<u>Outlet</u>					
Temperature, °F.:	232.5		221.9					
Pressure, psia:	21.7		17.3					
Steam quality:	68.2		100.0 (1.7 °F. superheated)					
Outside wall temperature, °F.:								
Station	Circumferential Location							
	0°	45°	90°	135°	180°	225°	270°	315°
1	318.4		245.5		244.7		260.5	
2	284.3	249.0	244.8	243.2	241.1	249.1	291.5	289.6
3	293.2		244.4		241.7		303.0	
4	316.2		243.9		273.6		355.5	
5	360.1		246.6		308.8		372.7	
6	362.3		245.2		326.9		377.1	
7	384.8		250.9		350.3		394.9	
8	397.2		254.8		375.4		416.1	
9	425.3	383.5	285.3	272.4	368.4	410.9	419.5	431.4
10	436.8		289.3		389.0		438.2	

TABLE XXVII
 RUN 120, TWO-PHASE

Mass flow rate:	33,300 lb/(hr)(sq. ft.)							
Coil current:	400 amps							
Coil voltage:	12.9 volts							
Average heat flux:	13,600 Btu/(hr)(sq. ft.)							
	<u>Inlet</u>	<u>Outlet</u>						
Temperature, °F.:	221.2	215.4						
Pressure, psia:	17.6	15.7						
Steam quality:	43.7	87.9						
Outside wall temperature, °F.:								
Station	Circumferential Location							
	0°	45°	90°	135°	180°	225°	270°	315°
1	228.2		235.7		232.8		227.9	
2	240.7	236.4	235.8	234.3	231.9	228.5	227.3	229.2
3	299.1		237.9		231.4		268.6	
4	359.2		241.3		233.8		327.8	
5	365.8		240.8		233.3		339.0	
6	369.6		239.5		236.3		357.7	
7	375.0		240.6		249.2		375.8	
8	324.2		236.5		238.7		291.6	
9	314.4	296.5	238.5	232.9	258.8	297.3	297.2	374.5
10	381.1		238.2		273.6		391.0	

TABLE XXVIII
 RUN 121, TWO-PHASE

Mass flow rate:	72,700 lb/(hr)(sq. ft.)							
Coil current:	250 amps							
Coil voltage:	7.9 volts							
Average heat flux:	5,200 Btu/(hr)(sq. ft.)							
	<u>Inlet</u>	<u>Outlet</u>						
Temperature, °F.:	256.0	235.0						
Pressure, psia:	33.1	22.8						
Steam quality:	84.7	94.1						
Outside wall temperature, °F.:								
Station	Circumferential Location							
	0°	45°	90°	135°	180°	225°	270°	315°
1	257.1		259.0		257.8		257.2	
2	256.7	257.2	258.2	257.7	256.9	256.0	256.8	256.7
3	255.9		257.6		255.3		256.2	
4	255.7		257.1		256.3		255.2	
5	256.3		256.4		254.5		254.6	
6	253.9		253.9		254.1		253.5	
7	253.3		254.0		253.8		252.0	
8	254.2		252.8		255.2		251.9	
9	256.4	253.7	252.3	252.4	257.8	253.6	250.0	251.8
10	260.0		252.4		263.4		251.2	

TABLE XXIX
 RUN 122, TWO-PHASE

Mass flow rate:	80,700 lb/(hr) (sq. ft.)							
Coil current:	300 amps							
Coil voltage:	9.6 volts							
Average heat flux:	7,580 Btu/(hr) (sq. ft.)							
	<u>Inlet</u>	<u>Outlet</u>						
Temperature, °F.:	257.3	236.9						
Pressure, psia:	33.9	23.6						
Steam quality:	86.4	98.1						
Outside wall temperature, °F.:								
Station	Circumferential Location							
	0°	45°	90°	135°	180°	225°	270°	315°
1	259.9		262.0		260.3		259.6	
2	259.1	260.0	261.3	260.4	259.2	258.1	258.9	258.9
3	258.6		260.4		257.6		257.8	
4	259.6		259.7		259.9		257.1	
5	259.0		259.4		262.2		256.9	
6	269.5		258.9		270.2		255.8	
7	276.2		257.5		279.5		261.1	
8	290.2		257.0		289.9		282.1	
9	300.4	276.7	257.6	261.7	293.4	300.9	295.5	301.8
10	304.1		257.8		300.0		301.5	

APPENDIX E

HEAT TRANSFER DATA FOR LARGE COIL

TABLE XXX
 RUN 201, TWO-PHASE

Mass flow rate:	67,200 lb/(hr) (sq. ft.)							
Coil current:	380 amps							
Coil voltage:	12.0 volts							
Average heat flux:	12,100 Btu/(hr) (sq. ft.)							
	<u>Inlet</u>	<u>Outlet</u>						
Temperature, °F.:	236.7	221.7						
Pressure, psia:	23.5	17.8						
Steam quality:	68.3	88.5						
Outside wall temperature, °F.:								
Station	Circumferential Location							
	0°	45°	90°	135°	180°	225°	270°	315°
1	241.8		243.8		242.1		242.1	
2	241.5	242.9	243.3	242.7	241.3	240.0	239.7	240.0
3	240.5		242.5		240.1		239.0	
4	239.3		241.8		239.9		238.1	
5	238.0		240.7		238.8		237.4	
6	237.6		240.5		238.3		236.5	
7	236.7		238.9		237.0		235.5	
8	237.4		237.9		237.2		234.1	
9	249.5	236.9	237.5	237.1	239.1	236.2	234.0	238.7
10	247.9		236.4		243.9		233.9	

TABLE XXXI
 RUN 202, TWO-PHASE

Mass flow rate:	91,600 lb/(hr)(sq. ft.)							
Coil current:	600 aamps							
Coil voltage:	19.2 volts							
Average heat flux:	30,300 Btu/(hr)(sq. ft.)							
	<u>Inlet</u>		<u>Outlet</u>					
Temperature, °F.:	254.1		233.9					
Pressure, psia	32.1		22.4					
Steam quality	53.5		89.6					
Outside wall temperature, °F.:								
Station	Circumferential Location							
	0°	45°	90°	135°	180°	225°	270°	315°
1	267.7		271.7		267.4		264.9	
2	267.4	269.8	270.7	269.0	266.3	264.5	264.1	265.4
3	266.4		270.4		265.9		263.5	
4	264.9		269.3		265.4		262.0	
5	262.9		267.7		263.7		260.3	
6	260.9		266.9		263.2		259.6	
7	261.3		265.8		262.1		259.3	
8	259.3		264.1		259.0		257.3	
9	259.4	260.7	262.9	262.9	259.3	257.4	256.2	256.3
10	294.0		261.5		264.8		254.8	

TABLE XXXII
 RUN 203, TWO-PHASE

Mass flow rate:	80,700 lb/(hr)(sq. ft.)							
Coil current:	250 amps							
Coil voltage:	7.9 volts							
Average heat flux:	5,200 But/(hr)(sq. ft.)							
	<u>Inlet</u>		<u>Outlet</u>					
Temperature, °F.:	247.9		230.7					
Pressure, psia:	28.7		21.1					
Steam quality:	86.2		94.6					
Outside wall temperature, °F.:								
Station	Circumferential Location							
	0°	45°	90°	135°	180°	225°	270°	315°
1	248.8		250.0		247.6		248.6	
2	248.0	248.6	248.9	248.8	248.2	247.8	247.8	248.0
3	247.3		248.3		247.3		247.0	
4	246.4		247.4		246.2		246.1	
5	245.4		246.6		245.7		247.2	
6	247.1		246.2		246.7		244.9	
7	248.6		245.2		251.7		243.4	
8	250.0		244.0		253.8		243.2	
9	256.4	243.9	242.7	243.7	254.3	254.1	243.2	253.0
10	256.1		243.1		257.5		244.8	

TABLE XXXIII
 RUN 205, TWO-PHASE

Mass flow rate:	78,900 lb/(hr) (sq. ft.)							
Coil current:	550 amps							
Coil voltage:	18.0 volts							
Average heat flux:	26,100 Btu/(hr) (sq. ft.)							
	<u>Inlet</u>	<u>Outlet</u>						
Temperature, °F.:	252.1	238.0						
Pressure, psia:	31.0	23.1						
Steam quality:	65.6	100.0 (2.4 °F. superheated)						
Outside wall temperature, °F.:								
Station	Circumferential Location							
	0°	45°	90°	135°	180°	225°	270°	315°
1	263.9		267.3		263.4		260.7	
2	263.3	265.9	266.6	265.2	262.2	260.2	259.8	260.5
3	261.2		265.6		261.3		258.6	
4	259.5		264.9		260.5		257.2	
5	259.8		263.4		258.3		255.9	
6	278.6		263.1		267.3		254.7	
7	318.2		263.0		323.0		381.5	
8	355.4		363.2		368.7		273.2	
9	430.9	331.0	270.8	293.9	412.8	450.5	461.6	457.0
10	456.6		278.5		456.4		480.0	

TABLE XXXIV
 RUN 206, TWO-PHASE

Mass flow rate:	42,200 lb/(hr)(sq. ft.)							
Coil current:	400 amps							
Coil voltage:	13.0 volts							
Average heat flux:	13,700 Btu/(hr)(sq. ft.)							
	<u>Inlet</u>	<u>Outlet</u>						
Temperature, °F.:	230.7	223.6						
Pressure, psia:	21.0	17.5						
Steam quality:	68.5	100.0 (2.7 °F. superheated)						
Outside wall temperature, °F.:								
Station	Circumferential Location							
	0°	45°	90°	135°	180°	225°	270°	315°
1	299.2		242.3		244.2		335.4	
2	296.8	245.3	242.0	240.7	245.9	300.2	345.9	336.1
3	307.9		242.0		242.7		351.7	
4	332.6		243.0		255.2		360.5	
5	343.5		241.6		276.8		373.8	
6	368.3		243.2		298.5		384.7	
7	379.5		244.2		341.0		407.5	
8	385.1		244.9		365.8		421.4	
9	422.1	363.6	266.5	267.9	368.2	419.2	436.9	442.3
10	451.4		300.4		398.1		455.3	

APPENDIX F

ERROR ANALYSIS

ERROR ANALYSIS

The three variations which are used in calculating the heat transfer coefficients all have some degree of uncertainty associated with them. These three variables are the inner surface heat flux, the inner surface temperature, and the temperature of the two-phase mixture. The heat transfer coefficient is calculated as:

$$h = f(Q/A, T_w, T_f) = \frac{Q/A}{(T_w - T_f)} = \frac{Q/A}{\Delta T} \quad (\text{F-1})$$

The uncertainty in the heat transfer coefficient is:

$$dh = \frac{\partial f}{\partial (Q/A)} d(Q/A) + \frac{\partial f}{\partial (\Delta T)} d(\Delta T) \quad (\text{F-2})$$

or:

$$dh = \frac{d(Q/A)}{\Delta T} - \frac{(Q/A)}{\Delta T^2} d(\Delta T) \quad (\text{F-3})$$

Dividing by the expression for the heat transfer coefficient:

$$\frac{dh}{h} = \frac{d(Q/A)}{(Q/A)} - \frac{d(\Delta T)}{\Delta T} \quad (\text{F-4})$$

The maximum error will occur when errors are such that all of the terms in the above expression are positive. The uncertainty in the heat flux is due to uncertainties in several measured experimental variables, namely coil current, coil voltage, outside tube wall temperature profile, and room temperature. In addition, any calculational uncertainties in the numerical solution for wall temperature profile and heat

flux add to the uncertainty. The coil current and voltage were measured on Weston meters having an accuracy of 1% of the full scale readings of 750 amps and 50 volts respectively. The outside tube wall temperatures were measured with iron-constantan thermocouples which were calibrated in place on the coil. The uncertainty in these measurements for temperatures below 300 °F. is estimated to be less than 0.5°F. For higher temperatures the uncertainty could be as high as 2°F. The room temperature was measured within 0.5°F. by a calibrated mercury thermometer. The uncertainty in the heat flux due to the uncertainties named above is estimated to be no greater than 5%.

The uncertainty in the temperature difference between the inner tube surface and the two-phase mixture is produced by uncertainties in a number of measured variables. These variables are:

- 1) coil current--7.5 amps;
- 2) coil voltage--0.5 amps;
- 3) outside tube wall temperature--0.5-2.0 °F.;
- 4) room temperature--0.5 °F.;
- 5) coil inlet temperature--0.5 °F.;
- 6) coil outlet temperature--0.5 °F.;
- 7) coil inlet pressure--0.3 psi;
- 8) coil outlet pressure--0.1 psi;
- 9) atmospheric pressure--0.1 psi;
- 10) liquid makeup flow rate--0.5%; and
- 11) total coil flow rate--0.2%.

The uncertainties in each of the variables are shown in the list above. The combined effect of these uncertainties is estimated to be 10%. The maximum uncertainty in the heat transfer coefficient is:

$$\begin{aligned}\left(\frac{dh}{h}\right)_{\max} &= \frac{d(Q/A)}{(Q/A)} + \frac{d(\Delta T)}{\Delta T} \\ &= 0.05 + 0.1 = 0.15 \\ &= 15\%\end{aligned}$$

APPENDIX G

CALIBRATION OF THERMOCOUPLES, ROTAMETERS, AND
COIL HEAT LOSS

TABLE XXXV
 CALIBRATION OF THERMOCOUPLES FOR SMALL COIL

Station	Circumferential Location							
	0°	45°	90°	135°	180°	225°	270°	135°
1	-0.013		-0.020		-0.015		-0.027	
2	-0.022	-0.021	-0.022	-0.017	-0.015	-0.024	-0.035	-0.024
3	-0.030		-0.025		-0.020		-0.011	
4	-0.018		-0.006		-0.040		-0.021	
5	-0.026		-0.029		-0.027		-0.007	
6	-0.016		-0.013		-0.017		-0.018	
7	-0.012		-0.010		-0.011		-0.005	
8	-0.010		-0.003		-0.004		-0.011	
9	-0.010	-0.011	-0.015	-0.007	-0.011	-0.008	-0.024	-0.010
10	-0.015		-0.015		-0.018		-0.004	

Note: The numbers in this table are thermocouple emf's in millivolts. Readings were taken with steam bleeding through the coil and with a steam bath reference junction at atmospheric pressure.

TABLE XXXVI
 CALIBRATION OF THERMOCOUPLES FOR LARGE COIL

Station	Circumferential Location							
	0°	45°	90°	135°	180°	225°	270°	135°
1	-0.025		-0.025		-0.035		-0.028	
2	-0.030	-0.037	-0.031	-0.030	-0.035	-0.032	-0.029	-0.029
3	-0.029		-0.030		-0.030		-0.033	
4	-0.031		-0.032		-0.028		-0.033	
5	-0.049		-0.026		-0.031		-0.036	
6	-0.027		-0.028		-0.031		-0.030	
7	-0.025		-0.030		-0.035		-0.030	
8	-0.030		-0.023		00.034		-0.028	
9	-0.025	-0.026	-0.030	-0.030	-0.031	-0.034	-0.035	-0.030
10	-0.026		-0.032		-0.035		-0.033	

Note: The numbers in this table are thermocouple emf's in millivolts. Readings were taken with steam bleeding through the coil and with a steam bath reference junction at atmospheric pressure.

TABLE XXXVII
 CALIBRATION OF ROTAMETER NO. 3
 (Water Temperature = 180°F.)

Scale Reading	Flow, lb/min
20	2.76
19	2.58
18	2.40
17	2.24
16	2.09
15	1.90
14	1.76
13	1.61
12	1.47
11	1.33
10	1.19
9	1.05
8	0.898
7	0.782
6	0.661
5	0.550

Results of Regression:

$$\text{Flow, lb/min} = 0.00554 + 0.0977(\text{Scale}) \\ + 0.00197(\text{Scale})^2 + 0.00000108(\text{Scale})^3$$

Average error of experimental points = 0.488%

TABLE XXXVIII
CALIBRATION OF ROTAMETER NO. 4
(Water temperature = 180°F.)

Scale Reading	Flow, lb/min
7	0.379
6	0.321
5	0.270
4	0.216
3	0.166

Results of Regression:

$$\text{Flow, lb/min} = 0.00291 + 0.0591(\text{Scale}) \\ + 0.00222(\text{Scale})^2 - 0.000205(\text{Scale})^3$$

Average error of experimental points = 0.381%

TABLE XXXIX
CALIBRATION OF HEAT LOSS FOR SMALL COIL

Atmospheric pressure = 14.3 psia
Room temperature = 76°F.
Water effluent from coil = 0.0146 lb/min
Steam effluent from coil = 0.101 lb/min

Saturation temperature at 14.3 psig = 211°F.
Water enthalpy at 14.3 psia = 179 Btu/lb
Steam enthalpy at 14.3 psia = 1150 Btu/lb

Heat balance:

$$\begin{aligned}\text{Heat loss} &= \text{Heat in} - \text{Heat out} \\ &= (0.101 + 0.0146)(1150) - [(0.101)(1150) \\ &\quad + (0.0146)(179)] \\ &= 14.2 \text{ Btu/min}\end{aligned}$$

$$\begin{aligned}\Delta T (\text{coil to ambient}) \text{ for heat loss} &= 211 - 76 \\ &= 135^\circ\text{F.}\end{aligned}$$

TABLE XL
CALIBRATION OF HEAT LOSS FOR LARGE COIL

Atmospheric pressure = 14.3 psia

Room temperature = 78°F.

Water effluent from coil = 0.0148 lb/min

Steam effluent from coil = 0.113 lb/min

Saturation temperature at 14.3 psia - 211°F.

Water enthalpy at 14.3 psia = 179 Btu/lb

Steam enthalpy at 14.3 psia = 1150 Btu/lb

Heat balance:

Heat loss = Heat in - Heat out

$$= (0.113 + 0.0148)(1150) - (0.113)(1150)$$

$$+ (0.0148)(179)$$

$$= 14.4 \text{ Btu/min}$$

ΔT (coil to ambient) for heat loss = 211 - 78

$$= 133^\circ\text{F.}$$

NOMENCLATURE

A	area, ft^2
a	area for heat conduction in numerical solution, ft^2
C_p	heat capacity, $\text{Btu}/(\text{lb})(^\circ\text{F.})$
D	helix diameter, ft.
d	tube diameter, ft.
d	distance for heat conduction in numerical solution, ft.
EMF	thermocouple reading, mv
f	friction factor, dimensionless
f	arbitrary function
G	mass velocity, $\text{lb}/(\text{hr})(\text{sq. ft.})$
g_c	dimensional constant, $(\text{lb}/\text{lb}_f)(\text{ft}/\text{sec}^2)$
h	heat transfer coefficient, $\text{Btu}/(\text{hr})(\text{sq. ft.})(^\circ\text{F.})$
\bar{h}	circumferential average heat transfer coefficient, $\text{Btu}/(\text{hr})(\text{sq. ft.})(^\circ\text{F.})$
i	indexing number
I	electric current intensity, amps
j	indexing number
k	thermal conductivity, $(\text{Btu})(\text{ft})/(\text{hr})(\text{sq. ft.})(^\circ\text{F.})$
\bar{k}	average thermal conductivity, $(\text{Btu})(\text{ft})/(\text{hr})(\text{sq. ft.})(^\circ\text{F.})$
l	coil axial distance, ft.
Nu	Nusselt number, $(\frac{hd}{k})$, dimensionless
n	number of radial slices in tube wall

Pr	Prandtl number, $(C_p \mu / k)$, dimensionless
p	pressure, psia or psig
Δp	pressure drop, psi
Q	heat flow, Btu/hr
Q/A	heat flux, Btu/(hr)(sq. ft.)
Re	Reynolds number, (dG/μ) , dimensionless
Re _g	Superficial Reynolds number of gas phase, dimensionless
R	helix radius, ft.
R _Q	ratio of measured coil heat generation rate to calculated coil heat generation rate, dimensionless
r _m	radius of unbent tube, ft.
\bar{r}	mean radius of two adjacent increments, ft.
T	temperature, °F.
ΔT	temperature difference, °F.
TCF	thermocouple correction factor, mv
w	mass flow rate, lb/hr
X	Lockhart-Martinelli parameter, dimensionless
x	steam quality, dimensionless
δ	local value of tube wall thickness, ft.
δ_m	tube wall thickness of unbent tube, ft.
μ	viscosity, lb/(ft)(hr)
ρ	density, lb/ft ³
ρ_e	electrical resistivity, (ohm)(sq. ft.)/ft
ϕ	angle measured clockwise from vertical, radian
θ	angle which subtends a one foot length of the coil, radian

Subscripts

acc	accelerational
cal	calculated
cr	critical
est	estimated
exp	experimental
f	fluid
f	frictional
g	gas or vapor phase
gc	gas phase flowing alone in coil
H ₂ O	liquid phase
i	index
in	coil inlet
j	index
l	liquid phase
lc	liquid phase flowing alone in coil
max	maximum
out	coil exit
r	radial direction
s	single-phase liquid
sat	saturation
steam	vapor phase
t	total
tt	both vapor and liquid phases turbulent
total	total
w	wall
xs	cross-sectional

z axial direction
 ϕ circumferential direction
0 top of tube
90 inside wall of tube
180 bottom of tube
270 outside wall of tube
7 axial position 7
71 axial position 7, thermocouple position 1

VITA

Berry Crain, Jr.

Candidate for the Degree of

Doctor of Philosophy

Thesis: FORCED CONVECTION HEAT TRANSFER TO A TWO-PHASE MIXTURE OF
WATER AND STEAM IN A HELICAL COIL

Major Field: Chemical Engineering

Biographical:

Personal Data: Born in Memphis, Tennessee, August 11, 1941, the
son of Berry and Inez Crain.

Education: Attended elementary school in Brandon, Mississippi;
graduated from Brandon High School in 1959; received the
Bachelor of Science degree from Mississippi State University
in 1963 with a major in Chemical Engineering; received the
Master of Science degree from Oklahoma State University in
1965 with a major in Chemical Engineering.

Professional Experience: Served as research engineer at U. S.
Army Natick Laboratories while on active duty in U. S. Army,
1969-1970; employed as research engineer at Savannah River
Laboratory, E. I. du Pont de Nemours and Co., Aiken, S. C.,
1970-1973.